IMMUNOPATHOLOGY IN HETEROLOGOUS PULMONARY INFECTION

MECHANISMS UNDERLYING THE IMMUNOPATHOLOGY IN HETEROLOGOUS PULMONARY INFECTION

By ELENA PRETUS YAGÜE, B.Sc.

A Thesis Submitted to the School of Graduate Studies in Partial Fulfilment of the Requirements for the Degree Master of Sciences

McMaster University
Hamilton, Ontario, Canada

MASTER OF SCIENCES (2012) McMaster University (Medical Sciences)
Hamilton, Ontario

TITLE: Mechanisms Underlying the Immunopathology of Heterologous Pulmonary Infection

AUTHOR: Elena Pretus Yagüe, B.Sc.

SUPERVISOR: Dr. Martin R. Stampfli

NUMBER OF PAGES: xii, 135

Abstract

Despite the advanced knowledge of the mechanisms of influenza infection and improved vaccines, Influenza A Virus still causes a life-threatening respiratory disease, especially during pandemics. Past investigations have proposed a synergism between Influenza A virus and a simultaneous or subsequent bacterial superinfection as the predominant cause of death. The recent development of animal models to study these heterologous infections has shed light onto the diverse mechanisms by which Influenza A Virus may increase the susceptibility to contract a secondary bacterial infection. These studies suggested an important role for the innate immune system in mediating such disease. We developed a model of heterologous infection combining Influenza A Virus and *Bordetella parapertussis* that demonstrated a critical role for MIP-2 to drive pulmonary neutrophilia in the pathology associated with bacterial superinfection of influenza. However, the origin of this increased MIP-2 production and the mechanisms underlying the immunopathology remained to be elucidated. The present studies proposed IL-1β overproduction as the upstream cause of the increased MIP-2 production observed in heterologous infection. This exaggerated IL-1β production was likely related to the increased bacterial burden observed in heterologously infected mice. This study also demonstrated that reduction in IL-1β production by blockade of the inflammasome seemed to provide an improvement in the clinical symptoms and the immunopathology of the disease. Thus, interventions to attenuate the exacerbated bacterial burden and the inflammatory responses derived from the subsequent IL-1β overproduction should be further investigate as possible therapeutic approaches to treat bacterial superinfections.

Acknowledgements

First of all, I want to thank **Martin Stampfli, Mark McDermott** and **Manel Jordana,** supervisor and committee members, for being the three guardian angels that walked beside me throughout the 3 years of my stay at McMaster and for being the best mentors I could have ever asked for, easing the bumps I found throughout my way and teaching me many important lessons academically and personally.

I want to give special thanks to **Cale Zavitz** and **Mathieu Morissette**, our postdocs, for being my trainers in the lab and whose wisdom and patience made me learn pretty much every lab technique I am taking with me. Thank you for being such good teachers.
Thank you to my other labmates – **Jake Nikota, Pam Shen, Kim Fernandes, Kristen Lambert, 'Jordanians' and 'Bowdishes'**– for their generous help in those never-ending days of work and for all the laughs and chilling moments we spent at the Phoenix.
Also, thank to **Sussan Kianpour** and **Joanna Kasinska** for providing the technical support I required at any time and for behaving like "second moms" whenever I needed them.

To **Terry McCurdy** for letting me experience the Teaching Assistantship and caring about the TAs' success as much as she cares for her students. I really enjoyed working together.

To the Spanish/Latin crew found at McMaster University –**David, Carla, Leti, Rami, Andres, Michael,** etc. as well as **Alba and Katherine & co.**– for making my life so enjoyable during my time in Hamilton and being my Canadian family and support day after day, sharing and understanding how tough surviving is when being so far away from home.

Thank you so much to **Laura Ramsingh** and **Maple Liu** for being amazing co-presidents of the HSGSF in 2012 and sharing the long summer days in the library and the painful moments that writing our theses accounted for (except for the distraction and fun of seeing Spain winning the Eurocup together!).

I am grateful to my **Soccer team mates** for letting me enjoy my favorite activity and release the stress from Graduate studies. I am taking so many good memories from all those games with me.

And finally, THANK to **Trini** (Mom), **Diego** (Dad) and **Miguel** (brother) because despite the 6000 km that kept us away from each other during these 3 years, there was not a single day that I did not count with your support, understanding and strength from the other side of the Atlantic Ocean. Also, thank to my Spanish friends –mi "**Biolokas**" and **Yoli, Ro, Antelo y compañía**– for keeping our lasting friendship up and running despite the long periods of time without sharing experiences.

My Graduate experience would not have been a success if it was not for you all and for the other numerous faculty, staff, students and friends that I am forced to omit here. I can just say *Gracias*.

Table of Contents

List of Figures

List of Abbreviations

AEC	3-amino-9-ethylcarbazole
AIM2	absent in melanoma 2
AMs	alveolar macrophages
ANOVA	analysis of variance
ASC	apoptosis-associated speck-like protein containing a CARD
$ASC^{-/-}$	ASC-deficient
BAL	broncho-alveolar lavage
BCR	B-cell receptor
B. parapertussis	*Bordetella parapertussis*
B. pp.	*Bordetella parapertussis*
BSA	bovine serum albumin
CARD	caspase-activating and recruiting domain
CFU	colony forming unit
CXCL	cystine-X-cystine chemokine ligand
CXCR	cystine-X-cystine chemokine receptor
D	day
DAMPs	danger-associated molecular patterns
DCs	dendritic cells
DTT	dithiothreitol
ELISA	enzyme-linked immunosorbent assay
FDC	follicular dendritic cells
G-CSF	granulocyte-colony stimulating factor
HA	hemagglutinin
H&E	hematoxylin and eosin
H. influenzae	*Haemophilus influenzae*
H_2O	water
HRP	horseradish-peroxidase
IAV	Influenza A Virus
IFN	interferon
Ig	immunoglobulin
IL	interleukin
IL-1RI	IL-1 receptor type I
IL-1Ra	IL-1 receptor antagonist
KC	keratinocyte-derived chemokine
LIX	LPS-induced CXC chemokine
LPS	lipopolysaccharide
MDCK	Madin-Darby canine kidney

MEM	minimum essential medium
MHC	major histocompatibility complex
MIP	macrophage inflammatory protein
MIRC	McMaster Immunology Research Centre
MMP9	matrix metalloprotease-9
MNC	mononuclear cells
MWs	molecular weights
NA	neuraminidase
NEU	neutrophils
NF-κB	nuclear factor-κB
NK	natural killer
NLR	NOD-like receptor
NLRC4	NLR family CARD domain-containing protein 4
NLRP3	NOD-like receptor protein 3
NOD	nucleotide-binding oligomerization domain
NS	not significant
OD	optical density
PAMPs	pathogen-associated molecular patterns
PBS	phosphate-buffered saline
PFU	plaque forming unit
PMN	polymorphonuclear
PRRs	pattern recognition receptors
PYD	pyrin domain
RIG-I	retinoic acid inducible gene-I
rpm	revolutions per minute
S. aureus	*Staphylococcus aureus*
SEM	standard error of the mean
S. pneumoniae	*Streptococcus pneumonia*
S. pyogenes	*Streptococcus pyogenes*
ssRNA	single stranded ribonucleic acid
TBS	Tris(hydroxymethyl)aminomethane-buffered saline
TCR	T-cell receptor
TCN	total cell number
Th	T helper lymphocyte
TLR	Toll-like receptor
TNF	tumor necrosis factor
WT	wild-type
YVAD-AFC	Tyr-Val-Ala-Asp-AFC

Chapter 1: Introduction

The lungs are internal organs that are in direct contact with the external environment since their main function is the respiration process and gas exchange (1). The volume of air breathed daily is considered to be 12 m^3/day which represents the average for males (14 m^3/day) and females (10 m^3/day) (2). This enormous amount of inspired air not only contains oxygen vital for survival but also many hazardous air pollutants and pathogens. The diameter of these respiratory aerosols is usually less than 10 μm and can easily reach the alveolar region, thus increasing the risk of contracting respiratory tract infections, especially after prolonged exposure in close proximity to the infectious source (3). Mucosal membranes are easy sites of entry for many virus and bacteria, particularly as a result of the huge absorptive area of the lungs (4).

In order to successfully establish an infection in the respiratory tract, most of these inhaled pathogens need to overcome a complex system of physical, chemical as well as immunological barriers in the respiratory tract that are effective at retaining most of these airborne infectious agents (1, 4). Despite this, a few of these pathogens escape these defense mechanisms and infect the epithelial and innate cells present in the alveoli, thereby initiating an immune response against the specific pathogen.

1. Pulmonary host defenses

Various pulmonary defense mechanisms have evolved to prevent the development of lung disease by resisting the invasion of microbes and noxious contaminants during respiration. These defenses must constantly distinguish potential pathogens from harmless agents inhaled in each breath, as well as minimize unnecessary inflammation and damage

to self-tissue (1). To accomplish this, the mammalian immune system consists of two interrelated arms: the evolutionarily ancient and immediate innate immune system, and the highly specific, but temporally delayed, adaptive immune system.

1.1. Innate defense mechanisms in the upper and lower respiratory tract

Innate defenses consist of intrinsic structural defenses, antimicrobial molecules produced in the airways, and phagocytic defenses provided by resident alveolar macrophages and polymorphonuclear leukocytes recruited into the lung in response to pulmonary infection (4, 5).

a. Structural defenses:

The first line of defense begins in the upper airway with filtration of large particles (>10 μm in diameter) by nasal hairs. In addition, the airflow becomes turbulent once it passes through the nasal turbinates in the nasopharynx and particles impact on the walls of the conducted airway, being retained in mucus and cleared by retrograde flow of mucus upon sneezing and coughing (4). Particles from 5 to 10 μm can escape from this defensive mechanism and access the further down respiratory airways (3). However, most of these will be trapped by adhesive mucus secreted by globet cells and submucosal glands intercalated between airway epithelial cells, and then transported out to the pharynx by cilia and either swallowed or ejected by sneezing and coughing. Thus, only particles less than 5 μm can reach the alveolar space and contact the phagocytic defenses residing there. This is particularly relevant as most bacteria and viruses are within this size range (4). Therefore, additional defense mechanisms are required in order to maintain homeostasis and sterility in the lower respiratory tract.

The airway epithelium also plays an important role in host defense against viral infection and bacterial adherence, in addition to its function as a physical barrier to the entry of microbes and mucocilliary clearance. Interaction between virus and epithelial cells activates signaling pathways that results in production of type I interferons (IFN), nitric oxide and a range of cytokines and chemokines that induce activation of innate and adaptive immune responses (6). Although this facilitates viral clearance from the respiratory tract, the production of proinflammatory mediators, the recruitment of inflammatory cells and the induction of apoptosis in viral-infected epithelial cells results in a degree of immunopathology or even worsening of pre-existing airway inflammation in patients suffering from asthma or chronic obstructive pulmonary disease (7, 8).

b. Antimicrobial molecules:

A wide range of antimicrobial molecules are available in the airways including lysozyme, complement factors, immunoglobulins (Ig) A and G, fibronectin, defensins or collectins, among others (9, 10). The most important antimicrobial innate defense is the pulmonary surfactant, a lipoprotein complex synthesized and secreted by alveolar type II epithelial cells and Clara cells to form a thin liquid layer that lines the epithelium (11). Surfactant has two different functions: first, it reduces surface tension at the air-liquid interface of the lung and, second, it plays a role in host defense against infection and inflammation (12). Surfactant proteins A and D are members of the collectin protein family (10, 13), and bind lipopolysaccharide (LPS), opsonise bacteria and viruses, facilitate phagocytosis by innate immune cells and regulate the production of inflammatory mediators (12, 14).

c. Phagocytic defenses:

Cellular phagocytic/inflammatory defense mechanisms are needed in the alveoli due to the absence of the mucociliary apparatus and the cough reflex which does not clear material from the alveoli unless it has moved up into the larger airways. The small particles that overcome the previously described mechanisms are phagocytosed by mononuclear cells (MNC) (monocytes, macrophages) and polymorphonuclear (PMN) cells (neutrophils), and eosinophils.

i. Resident alveolar macrophages

Alveolar macrophages (AMs) have evolved to clear the debris generated by the above mentioned antimicrobial defenses and to provide host defense in the terminal airways. AMs actively phagocytose both opsonised and non-opsonised bacteria and kill ingested microorganisms with proteolytic enzymes in order to guarantee homeostasis and effective gas exchange (15). However, certain microorganisms are resistant to the microbicidal activities of AMs and are capable of replicating intracellularly. To eradicate these pathogens, or when the load of the invading pathogens is excessive, AMs require additional cell-mediated immunity (16). Also, during antiviral and antibacterial responses, AMs produce mediators that recruit effectors cells such as natural killer (NK) cells, T-cells or B-cells (17).

The recognition of pathogens by AMs relies on a group of germ-line encoded of pattern recognition receptors (PRRs) that bind to pathogen-associated molecular patterns (PAMPs) which are highly conserved between infectious agents. Some of the well-characterized PPRs are i) Toll-like receptors (TLRs), which recognize extracellular or

endosomal PAMPs, and ii) cytoplasmic caspase-activating and recruiting domain (CARD) helicases –such as retinoic acid inducible gene-I (RIG-I) or nucleotide-binding oligomerization domain (NOD)-like receptor (NLR)–, which recognize cytoplasmic PAMPs. Activation of these PPRs leads to the activation of the IFN regulatory factor (IRF)-3 and/or 7 as well as the nuclear factor (NF)-κB, which translocate to the nucleus and induce the production of IFNs and proinflammatory cytokines such as tumor necrosis factor (TNF)-α and interleukin (IL)-1β (18, 19).

AMs release a variety of microbicidal molecules to enable killing of pulmonary pathogens, such as nitric oxide and other reactive oxygen species (20). Furthermore, AMs produce different cytokines that are known to participate in pulmonary host defense, including TNF-α, IL-10, IL-12, the chemokines, IFN-γ, and granulocyte colony-stimulating factor (G-CSF) (reviewed in (21)). Some of these secreted mediators elicit migration of a large number of PMN cells from the blood stream into the alveolar space (16, 22, 23). TNF-α and IL-1 are thought to affect PMN chemotaxis in an indirect manner through the induction of cystine-X-cystine (CXC) chemokines by AMs, neutrophils, type II epithelial cells and other cells of the airways (24, 25).

CXC chemokines are considered the most potent chemoattractants in the lung (26-28). In mice, four members of the CXC chemokine family have been identified to have neutrophil chemoattractant activities, but whether they provide distinct or redundant roles in inflammation and infection is still unknown. The four chemokines, keratinocyte-derived chemokines (KC, also named CXCL1), macrophage inflammatory protein-2 (MIP-2, also named CXCL2), LPS-induced CXC chemokine (LIX, also named CXCL5),

and lungkine (also named CXCL15) all interact with CXCR2, the only functional receptor mediating their chemotactic activity in mice. CXCL1 and CXCL2 have previously been suggested to be the two most important chemokines for neutrophil recruitment into the lung in rodents (29-31). CXCL5 has been shown to be produced by alveolar epithelial type II cells in the lung exposed to LPS (32). CXCL15 secretion is restricted to bronchial epithelial cells (33) and may play a role in pulmonary host defense against *Klebsiella pneumoniae* infection (34). CXCL7, a platelet-derived chemokine, is produced as a precursor peptide named platelet basic protein that is sequentially cleaved to produce connective tissue activating peptide III, β-thromboglobulin and finally CXCL7. It targets basophils, eosinophils, fibroblasts, NK cells, megakaryotes and endothelial cells as well as neutrophils (35). In conclusion, this gradient of chemokine production is essential for localization and direct migration of PMNs to the infected tissue site.

ii. Recruited neutrophils

Neutrophil recruitment must be highly regulated to avoid tissue damage due to their destructive potential when releasing reactive oxygen species and proteases to destroy the invading pathogens (21). There are various decision points in the migration cascade of neutrophils from the bone marrow to transport and recruitment into the site of infection; all regulated by chemokines. CXCL1 and CXCL2, among others, can act both distantly to induce the neutrophil mobilization from bone marrow into the peripheral blood and locally at the site of infection to induce recruitment of neutrophils from the circulation into the peripherally-infected tissue. This latter process requires the activation

of adhesion molecules such as selectins and β_2-integrins on the endothelium of postcapillary venules close to the inflammation or injury site, leading to interactions with circulating neutrophils (reviewed in 21). When rolling over the endothelium, neutrophils become activated by chemokines bound to the epithelial cells via glycoaminoglycans (36). Transmigration of neutrophils occurs through junctions between endothelial cells or intracellularly and alters the expression of proteins and receptors in the neutrophil surface, thereby priming them for their cytotoxic and phagocytotic function in the infection site.

Furthermore, neutrophils can also release more chemokines, cytokines and lipid mediators that self-perpetuate their recruitment. However, neutrophils are short-lived cells and undergo apoptosis once they accomplished their function. If not removed *in situ* by AMs through efferocytosis, dying neutrophils disintegrate and release their toxic content in the tissue, contributing to further inflammation, tissue destruction or autoimmunity (37).

1.2. Adaptive immunity

Despite the extremely well-organized innate immune system, clearance of invading pathogens (or their toxic molecules) frequently requires the participation of adaptive immunity. The main goal of this type of immunity is not only help the innate immunity to fight the infection more efficiently with pathogen-specificity, but also to generate immunological memory so that a more robust and rapid response takes place following the next encounter with the same agent (38). Both the innate and adaptive

immune systems cooperate closely with each other, and activation of the adaptive responses is elicited upon contact with innate immune cells. The adaptive immune system has been continuously modified throughout evolution, from being absent in some invertebrate species such as bivalves to becoming highly complex in jawed vertebrates (39). The adaptive immune system is comprised of two different type of response: the cellular-mediated adaptive immunity and the humoral (or antibody-mediated) adaptive immunity.

a. Cellular immunity

During the steady state, tissue-resident dendritic cells (DCs) –mononuclear phagoctyes of similar lineage as macrophages– play a crucial role in maintaining tolerance, not only to self antigens, but also to harmless environmental antigens and commensal organisms. DCs internalize antigens and process them into proteolytic peptides, which are loaded onto their major histocompatibility complex (MHC) class I and II molecules. This process of antigen uptake, degradation, and loading is called antigen presentation (40). Following infection, DCs function as sensors of microbial invaders and integrate multiple signals from the environment in order to initiate an appropriate adaptive immune response. DCs are specialized to engulf pathogens, process antigens and present these to T-cells via their MHC, since T-cells cannot recognize pathogens in the native conformation. Upon antigen capture, DCs undergo maturation and migrate to the secondary lymphoid organs where they prime naive T-cells. Pathogen-specific T-cells identify the presented antigen through their T-cell receptor (TCR) and become activated upon contact with a co-stimulatory signal. These effector T-cells then

initiate cellular division and differentiation, and migrate to the periphery to participate locally in immune responses. Effector functions of T-cell include either killing the pathogen directly or activating macrophages to kill the intracellular pathogen more efficiently (if $CD8^+$ or cytotoxic T-cells were activated) or secreting cytokine mediators that will elicit the humoral response (if $CD4^+$ or helper T (Th)-cells were activated) (41).

b. Humoral immunity

B-cells are the lymphocytes charged with providing humoral immunity by secreting antibodies specific for the invading pathogen. To become activated, mature naive B-cells enter the lymph nodes from the blood through the high endothelial venules, and migrate into a primary lymphoid follicle through networks of follicular DCs (FDC). Follicular DCs are a non-migratory population found in primary and secondary follicles of the B-cell areas of the lymphoid tissues (42). B-cell activation requires 2 signals: firstly, the recognition of the antigen through their surface-bound Ig (also known as B-cell receptor (BCR)) and, secondly, via the direct contact with an activated pathogen-specific T-cell (43). Upon binding and uptake of the soluble antigen by pinocytosis, B-cells expressing antigen-specific Ig molecules migrate to the border between the follicle and T-cell area, where they present antigen-derived peptides via MHC-II molecules to antigen-specific helper T-cells (44-46). The antigen-specific B-cells then receive signals from the helper T-cell, becoming activated (47-49). Antigen-activated B-cells are intercepted by the FDC and undergo clonal expansion, generating germinal centers. Activated B-cells undergo many rounds of somatic hypermutation, affinity maturation for positive and negative selection, isotype switching and differentiation into high-affinity antibody-

secreting plasma cells and memory B-cells (50, 51). Activated B-cells with low-affinity to antigen captured on FDCs surface as well as autoreactive B-cells undergo apoptosis, whereas high-affinity B-cells bound to FDCs through the antigen complex, survive due to apoptosis blockage caused by interaction with FDCs. Plasma cell-secreted antibodies contribute to immune protection against the corresponding pathogens in 3 different ways:

i. Neutralization of the corresponding virus or bacteria, preventing them from adhering to specific receptors on the host cell surface. In addition, neutralization by antibodies can block bacterial toxins from binding to and entering cells.

ii. Opsonization of bacteria by coating their surface facilitating the uptake of the pathogen by phagocytic cells, either through recognition of the Fc portion of the antibody or through activation of proteins of the complement system.

iii. Antibody-dependent cell-mediated cytotoxicity by NK cells, which recognize antibodies bound to intracellularly-infected cells through their Fc receptor. NK cells then release cytoplasmic granules containing perforin and granzymes that lyse the pathogens. Also, tissue mast cells, blood basophils and activated eosinophils can lyse large parasites like helminthes through their degranulation of their intracellular content.

The type of effector mechanisms take place in each immune response is determined by the isotype of antibody produced by the plasma cells (42).

2. Presentation of the clinical problem

Regardless of the efficacy of the host defense mechanisms and the widespread availability of vaccine and antibiotics, respiratory infections still represent a leading cause of mortality worldwide. The World Health Organization estimates that 4 millions of people die per year due to lower respiratory tract infections (52). Both virus and bacteria, and to a lesser extent, fungi, are responsible for most of these respiratory diseases.

Four viruses are the main causes of human respiratory infections: Influenza Virus, Adenovirus, Rhinovirus and Respiratory Syncytial Virus. For this study, focus will be given to Influenza Virus.

Influenza Virus is an enveloped, negative single-stranded ribonucleic acid (ssRNA) virus belonging to the family *Orthomyxoviridae*. Three different types of Influenza Virus have been described based on the composition of antigenic core proteins: A, B and C. Even though all of them can infect humans, only Influenza A Virus (IAV) has been seen to cause severe symptoms and pandemics (53). IAV is the etiological agent of a highly contagious acute respiratory disease (54) and is transmitted via aerosols and droplets from the respiratory tract of infected persons or by direct contact with skin contaminated with respiratory secretions. Inhalation of as few as three infective particles can transmit infection, and the majority of infected persons have symptoms of disease (55). Contagion of IAV varies inversely with the level of immunity in the population, which is determined largely by the presence or absence of antibodies against hemagglutinin (HA), neuraminidase (NA) –which are viral surface proteins–, or both (54).

Epidemics and outbreaks of influenza usually occur in a seasonal pattern, being more common during late autumn and winter in areas with temperate climate. However, in tropical regions where temperatures fluctuate little between seasons, IAV may cause disease all year-round (56). The average global burden of seasonal influenza is currently estimated to be around 600 million cases, 3 million cases of severe illness and up to 500,000 deaths per year, particularly afflicting to young children (57), the elderly and immunocompromised individuals.

This elevated prevalence is consequence of the ability of IAV to develop strategies that evade the adaptive immune responses previously mounted against other strains. IAV has numerous mechanisms to utilize the host cell machinery for its own replication (58), as well as a high rate of mutation. Errors introduced by the viral RNA polymerase or the incorporation of RNA fragments from different IAV strains that had previously infected the same host can accumulate mutations in the genes encoding for HA and NA. These mutations lead to constant emergence of new virus variants to which there was little or no pre-existing protection in the population (59). Antigenic drift, a minor change, usually results in the population partially protected by cross-reacting antibodies whereas antigenic shift can lead to epidemic or pandemic infections (54), being most of them unpredictable.

Four influenza pandemics have been reported from the 20th century to present: 1918, 1957, 1968, and 2009. The most devastating pandemic was in 1918, when 50 million of people died within a year and the worldwide population growth was depressed for 10 years (60). The influenza virus had a profound virulence, with a mortality rate at

2.5% compared to the previous influenza epidemics which were less than 0.1% (61). Many healthy young adults succumbed to fatal influenza infection whereas in regular seasonal outbreaks. Fatal cases tended to afflict people suffering from chronic illnesses or at the extremes of age (62).

It has been demonstrated recently that the elevated mortality accounted during those IAV pandemics should be attributed mainly to secondary bacterial infections rather than the primary viral pneumonia *per se* (63, 64). Indeed, influenza and pneumonia death rates for those aged 15–34 years old in 1918 were greater than 20-fold higher than in previous years (65). Apart from pneumonia, the incidence of otitis media also increased during epidemics with influenza. The fact that vaccination against IAV effectively prevented bacterial otitis supports the hypothesis that viral infections predispose to bacterial disease (66). The most common bacterial pathogens associated with IAV pandemics are *Streptococcus (S.) pneumoniae* and *Haemophilus (H.) influenzae* (63). In addition, several other bacteria have been found in patients already virally-infected, such as *S. pyogenes*, *Staphylococcus (S.) aureus*, and *Mycoplasma pneumoniae* (67).

Currently, coinfection or superinfection with IAV and bacterial pneumonia are among the most deadly infectious diseases and are associated with elevated morbidity and mortality worldwide. A high rate of mortality is still observed in IAV-infected patients that contract secondary bacterial pneumonia despite treatment with antibiotics (68). No effective treatments for post-IAV bacterial superinfection are currently available. Why bacterial infection stays uncontrolled remains unknown. It has been suggested that mortality could result from the immunopathology elicited rather than the bacterial

infection *per se*, since once initiated, systemic sepsis and septic shock progress independently of the bacterial burden (67, 69, 70). Furthermore, an increase in multidrug-resistant bacteria and the aging populations have resulted in more individuals at risk of suffering from polymicrobial or "heterologous" infections (71, 72). In any case, the pathogenic mechanisms underlying these heterologous infections are still poorly understood. For those reasons, and under the constant threat of new influenza pandemics, the development of animal models that mimic what is seen in human have been required for the study of the disease.

3. Animal models of pulmonary disease

3.1. Overview

To date, several animal models have studied the interaction between a host and a specific given pathogen, thus helping expand the understanding of an individual infection. However, these models do not take into consideration that hosts are frequently infected with more than one pathogen, either concurrently or consecutively. Actually, those co- or heterologous infections have been considered the predominant cause of complications and influenza-attributed deaths during pandemics (63), but no effective treatments exist for them since the mechanisms underlying superinfections are unknown. The immune system elicits different types of immune responses against viral and bacterial pathogens, and it could well happen that these responses are exclusive. For example, while antibacterial immunity focuses on engulfment and destruction of bacteria, antiviral responses kill infected cells and neutralize free virus. Therefore, further investigations urge to be done

within this area. For the last three decades, new models combining two different infectious agents have been developed in order to mimic the main features of superinfections and investigate the mechanisms underlying the increased susceptibility observed in these cases. If successful, new molecules will be identified as potential therapeutic targets in the future.

The most common studied murine model combines IAV and *S. pneumoniae* (73), since this bacteria has been regularly isolated from many dual-infected patients. Some other models include *H. influenza (74), S. aureus (75), Neisseria meningitidis (76) or Bordetella (B.) parapertussis (28).* Findings from these studies propose numerous conditions and mechanisms that may facilitate the acquisition of polymicrobial diseases as well as mechanisms for each individual infection.

Once IAV reaches the lung, it infects the epithelial cells of the respiratory airway which produce large amounts of virus that can subsequently infect AMs and DCs. IAV is recognized through the spikes of HA on the viral membrane that attach to sialic acid on the surface of the host's cells membrane (58). Upon infection, the viral ssRNA is recognized in the endosome by TLR7 and in the cytoplasm by RIG-I, both leading to the activation of NF-κB and translocation into the nucleus. There, it activates the transcription of NLRP3, proinflammatory cytokines and the pro-forms of IL-1β and IL-18 (18, 19).

NLRP3 is one of the best characterized NLRs, an extensive family of PPRs that forms multiprotein complexes called inflammasomes that participate in the activation of caspase-1 (77, 78). IAV can also activate the NLRP3 inflammasome recruiting the

adaptor protein *apoptosis-associated speck-like protein containing a CARD* (ASC) and activating caspase-1, which mediates the processing of pro-IL-1β and pro-IL-18 to their mature forms and their successive release into the extracellular space (18, 19). Exposure to bacterial pore-forming toxins such *B. pertussis*' adenylate cyclase can also induce the formation of the NLRP3 inflammasome, leading to the activation of caspase-1. Active caspase-1 catalyzes the cleavage of pro-IL-1β, culminating in an increased secretion of active IL-1β (79). Thus, in response to viral and bacterial infections, IL-1β secretion is present in the lung of wild-type (WT) mice.

IL-1β is a potent pro-inflammatory cytokine belonging to the IL-1 family. It mediates its biological action by binding to the IL-1 receptor type I (IL-1RI), receptor that shares with IL-1α, another isoform of IL-1. The macrophage-monocyte is a primary source of IL-1, but many other cells, including neutrophils, fibroblasts, T-cells, and respiratory epithelial cells also produce IL-1 (reviewed in 77). IL-1β is synthesized as a 31 kDa precursor (pro-IL-1β) but lacks biological activity. Its cleavage by IL-1β-converting enzyme (ICE/caspase-1) or by other proteases releases the mature, active IL-1β form (80). Unlike other cytokine families, the IL-1 family exerts control over inflammation at both the receptor and nuclear levels.

Different mechanisms have been proposed to explain the increased susceptibility to IAV-induced bacterial superinfection. There is evidence that viral components such as neuraminidase and HA (81) or bacterial components such as staphyloccocal enterotoxin B (82) contribute to bacterial superinfection. Viruses can also lyse the epithelial cells lining the respiratory airways (83-85), exposing the underlying membrane and facilitating the

subsequent attachment of the bacteria to areas that were not previously in contact with the environment. Also, bacteria adherence can be increased by enhanced expression of pattern-recognition receptor (PRRs) in those epithelial cells that escape from viral lysis (86). Furthermore, virus could affect the recognition of bacteria through desensitization of TLRs, reducing NF-κB expression and chemokine production in AMs (87) and, consequently, cell recruitment post-IAV infection would be also decreased (87). The antibacterial function of AMs has also been suggested to be impaired (88), affecting the early bacterial clearance (89, 90). Influenza infections have been demonstrated to impair the innate and the adaptive immune responses. Small *et al.* (2010) demonstrated that IAV infections weaken NK cell response in the lung and increase the susceptibility to subsequent *S. aureus* infection (75). On the other hand, Kudva *et al.* (2011) showed that IAV inhibits the Th17-mediated host defense by expression of type I-IFN, which is required to combat bacterial pneumonia and this would also increase the susceptibility to secondary bacterial infections (91). All these findings suggest that a combination of multiple factors and complex mechanisms can be responsible for the IAV-increased susceptibility to secondary bacterial superinfection, and can differ greatly depending on the nature of the causative bacterial pathogen or on the interval between the viral and bacterial infections.

Few approaches have been proposed as useful treatments for IAV-bacterial superinfections. Besides the improvement of the current vaccine for IAV (92), the use of innate inhibitors, like collectins or defensins, are thought to inhibit both IAV and bacteria (59). However, further investigations to identify therapeutic targets are needed.

3.2. *Bordetella parapertussis* model

Dr. Martin Stämpfli's laboratory established a different murine model of heterologous infection, combining IAV and *Bordetella (B.) parapertussis*, as described in (28). The *Bordetellae,* Gram negative bacteria, are common respiratory pathogens with a wide host range. In humans, *B. pertussis* and *B. parapertussis* are the causative agents of whooping cough (93), a serious respiratory syndrome most frequently afflicting children. Consequently, vaccination programs against these pathogens have been established in most developed countries to reduce the incidence of the disease. Of interest, new cases of whooping cough have been reported in Canada, United States, Australia and Europe since 1980s (94).

B. parapertussis is a convenient model organism, since it infects both humans and mice. Zavitz *et al*. (2010) showed that *B. parapertussis* successfully established an infection in the murine respiratory tract for at least 14 days without inducing evident illness or body weight loss (28). In contrast, other bacterial pathogens frequently associated with bacterial superinfection in humans such as *S. pneumoniae*, *S. aureus,* and *H. influenza* (63) are typically cleared from the mouse without ever multiplying or causing elevated mortality rates early after infection. In addition, *B. parapertussis* exacerbates primary viral infection by acquiring a secondary bacterial pneumonia and increasing the mortality rate. Based on Zavitz's work (2010), superinfection of H1N1 IAV-infected mice with *B. parapertuss*is led to severe pulmonary inflammation, mainly characterized by an exaggerated neutrophilia in the lung. Analyses of the expression of inflammatory mediators showed that MIP-2 and KC especially were significantly

enhanced upon heterologous challenge, although only MIP-2 expression was exacerbated early after bacterial infection when neutrophils were already being recruited into the lung as the bacterial burden remained unchanged. This increased production was found to be exacerbated only in heterologously infected mice and was lacking in animals infected with either pathogen alone. Immunoneutralization of MIP-2 elicited a decrease in lung inflammation, weight loss and an improvement in the clinical presentation of the disease but did not affect the bacterial burden. In contrast, blockage of CXCR2, the receptor through which MIP-2 mediates its action, significantly worsened the clinical manifestations and eliminated the protection provided by neutralization of MIP-2. These data indicated that MIP-2 can drive the profound lung inflammation and neutrophil recruitment which occurs in heterologous infection independently of the bacterial burden (28).

4. Hypothesis and aims

Since exacerbated MIP-2 production is known to be involved somehow in the development of the disease upon pulmonary heterologous infection, we strongly hypothesize that other upstream factor(s) of the molecular cascade must be playing a major role and leading to the exacerbated production of chemokines.

As noted above, IL-1β is secreted in the lung upon viral and bacterial infections. Evidences in the literature suggest that IL-1β has the ability to induce CXC chemokines secretion and neutrophil recruitment *in vivo* (25) through enhanced expression of adhesion molecules such as intercellular adhesion molecule-1 on mesenchymal cells and

vascular cell adhesion molecules on endothelial cells (77). As a result, IL-1β promotes the infiltration of inflammatory cells from the circulation into the extravascular space and then into the infected tissues. Hence, the molecules involved in the IL-1β processing (such as ASC and caspase-1) or in the IL-1β signaling (such as IL-1RI) are crucial for the cellular infiltration seen upon infection (95). It has also been demonstrated that IL-1β is required to promote antigen-specific IL-17-producing CD4+ T (Th17) cells immunity and for the effective *B. parapertussis* clearance, thus providing protection against the infection (79).

Thus, deficiency of IL-1 or IL-1 signaling molecules compromises host defense and increases the susceptibility to viral (96) and bacterial infections (97-99). Alternatively, excessive production of IL-1 may also have negative effects in the outcome of the infections (100). A delicate balance between immunity and inflammation is required in order to resist pathogens effectively while limiting the tissue damage derived from inflammation (101). Since both IAV and *B. parapertussis* activate the inflammasome when subsequent infection occur within the same host, IL-1β levels can be over expressed causing exacerbation of the host inflammatory response against these pathogens.

Therefore, we hypothesize that exaggerated expression of IL-1β drives the severe neutrophilia and the immunopathology observed in bacterial superinfection of influenza. We further hypothesize that this exacerbated IL-1β production results from the induction of pro-IL-1β expression and activation of the inflammasome by both IAV and *B.*

parapertussis. Thus, the elevated levels of pro-IL-1β are subsequently processed into biologically active IL-1β, leading to exaggerated neutrophilia.

To test this hypothesis, 4 different aims have been undertaken:

I. Re-characterization of the heterologous infection model upon modification of the viral and bacterial doses;

II. Determination of the levels of IL-1β production and relevant chemokines that contribute to increased pulmonary inflammation;

III. Investigation of the mechanisms leading to IL-1β overproduction; and

IV. Analysis of the outcome of reduced IL-1β production on pulmonary inflammation.

Chapter 2: Materials and Methods

2.1. Animals

Adult female C57BL/6 mice, purchased from The Jackson Laboratories (Bar Harbor, Maine, USA), and $ASC^{-/-}$ mice (a kind gift from Dr. Gabriel Nuñez, University of Michigan Medical School, USA), were kept in a specific pathogen-free environment with 12 hour light/dark cycle and self-administration of autoclaved food and water *ad libitum*. Animals were handled in class II biosafety cabinets by gloved, masked and gowned staff.

2.2. Infectious agents

Two infectious agents were used in this study. Mouse-adapted H1N1 Influenza A strain (A/FM/1/47) (a kind gift from Dr. Earl Brown, University of Ottawa, Canada) had been genetically-sequenced, plaque-purified and biologically characterized in mouse lung infections (102, 103). *B. parapertussis* strain 12822 (American Type Culture Collection, Manassas, VA, USA) had also been genetically sequenced (104), microbiologically characterized (105) and studied in the murine respiratory tract (106). This strain was isolated in 1993 from a nasopharyngeal swab of a 16-month-old German boy by his pediatrician. *B. parapertussis* from a frozen stock was streaked onto Bordet-Gengou agar (Difco, Oakville, ON, Canada) plates containing 15% defibrinated sheep blood (Cedarlane, Burlington, ON, Canada) and grown at 37ºC for 4 days. Colonies were transferred into liquid Stainer-Scholte broth (107) and incubated for 24 hours at 37ºC on a shaking incubator. The optical density (OD) of the broth was measured at 600 nanometers (nm) and bacteria were collected for infection of animals when log-phase growth was

reached. Both the virus and the bacterial were diluted in phosphage-buffered saline (PBS) to the final concentration needed to infect the experimental animals.

2.3. Infection of experimental animals

Mice were anesthetized with Isoflurane® (Pharmaceutical Partners of Canada Inc., Richmond Hill, ON, Canada) and inoculated intranasally with $1x10^4$ plaque forming unit (PFU) of IAV in 35 µl of PBS. Five days post-infection, mice were challenged with $5x10^5$ colony forming unit (CFU) of *B. parapertussis* in 35 µl of PBS. Vehicle, IAV-only, and *B. parapertussis*-only infected groups were also included as controls. Additional hydration in the form of gel was provided upon succumbing to infection.

Mice were sacrificed at several time points after viral and/or bacterial challenge. Individual body weight and clinical status was monitored before inoculation with the infectious agents and daily throughout the course of experimentation. The clinical status of experimental animals was assessed based on appearance, provoked and unprovoked behaviour, hydration status, clinical signs, and breathing pattern.

The notation "Dx+y" (where D=day) denotes animals infected with IAV on day 0 of experimentation, followed by *x* days post-infection before superinfecting them with *B. parapertussis* and sacrificed *y* days after the bacterial challenge. For instance, D5+7 refers to mice infected with IAV at day 0, superinfected with *B. parapertussis* at day 5 and sacrificed 7 days after the bacterial challenge.

2.4. Tissue and cell collection

At sacrifice, mice were anaesthetized with Isoflurane® in a rodent anaesthetic machine inside of a level II biological safety cabinet. For dissection, the animals were maintained under full anesthesia with a nose cone containing Isoflurane®. Mice were euthanized by exsanguination, via severing the descending aorta.

The lungs were dissected and the trachea was cannulated with a polyethylene tube (Becton Dickinson, Sparks, MD, USA) of 0.58 mm of diameter. The multi-lobe was separated from the uni-lobe by a suture. The multi-lobe lung was cut off and collected for analyses of bacterial burden, inflammatory mediators and caspase-1 activation. The uni-lobe lung was lavaged twice with PBS (a first lavage of 250 µl followed by a second lavage of 200 µl), followed by aspiration of the broncho-alveolar lavage (BAL) through a 23G1 PrecisionGlide® needle (Becton Dickinson, Sparks, MD, USA). The BAL collected in the syringe was pooled for determination of local cellular inflammation and assessment of the inflammatory mediators. The BAL was diluted in Turk solution (Ricca Chemical Company, Arlington, Texas, USA) to hemolyze the red blood cells and stain the white blood cells for counting. Total cell counts were determined microscopically using a haemocytometer and expressed as cell/ml. The BAL supernatant was then separated from the cells by centrifugation for 10 seconds at 12,000 rpm and stored at -80ºC for later quantification of inflammatory mediators by enzyme-linked immunosorbent assays (ELISAs). Cell pellets were resuspended in PBS and centrifugal cell smears for differential cell counts were prepared by cytocentrifugation at 300 rpm for 2 minutes using a cytocentrifuge (CytoSpin* 4, Thermo Scientific, Burlington, ON,

Canada). Cells were fixed and stained with Hema 3 (Biochemical Sciences Inc., Swedesboro, NJ, USA) and differential counts were determined from at least 500 leukocytes using standard hemocytological procedures to classify mononuclear cells, neutrophils and eosinophils.

For histological analysis, the uni-lobe lung was inflated with 10% formalin at 30 cm H_2O pressure (28), embedded in paraffin, cut in 5 µm-thick sections and stained with hematoxylin and eosin (H&E) by the MIRC Core Histology Facility (Department of Pathology and Molecular Medicine, McMaster University). This method allowed study of the tissue pathology associated with heterologous infection. Images were captured with OpenLab software (Version 3.0.3; Improvision, Guelph, ON, Canada) using a Leica camera and microscope (Leica Microsystems, Richmond Hill, ON, Canada). The magnification of the images was 100 diameters.

2.5. Bacterial burden and viral titre

For determination of lung bacterial burden and viral titres, the multi-lobe lung was ligated with a suture from the uni-lobe and cut off prior to BAL acquisition. The caudal and middle lobes were snap-frozen in liquid nitrogen and stored at -80ºC for later analysis of proteins by western blot and biological activity assays, respectively. The upper lobe was immersed in 650 µl of cold PBS and homogenized with a Polytron PT 1200C (Kinematica, Littau-Lucerne, Switzerland). 25 µl of 10-fold serially-diluted fresh homogenates were plated onto Bordet-Gengou blood agar plates and incubated for 4 days at 37ºC. Viable colonies were then enumerated and expressed as CFU/ml.

Lung homogenates were stored at -80ºC until determination of viral titres on Madin-Darby canine kidney (MDCK) cell monolayers. MDCK cells were grown in 6-well tissue culture plates (BD Falcon®, Franklin Lakes, NJ, USA) until reaching 95-100% confluency and rinsed twice with warm PBS to remove culture medium. 200µl of serially-diluted samples of both non-infected and infected mice were added to each well. The plates were agitated by rocking and an overlay of 0.65% agarose (BioShop Canada, Burlington, ON, Canada) in 2x minimum essential medium (MEM) supplemented with 2% L-glutamine, 2% penicillin and streptomycin, and 1µg/ml trypsin were add on top. Once the agarose solidified, the plates were incubated for 48h at 37ºC. After removing the agarose overlays, cells were fixed with Carnoy's fixative and stained with Giemsa to reveal and enumerate the viral plaques.

2.6. Lung and BAL cytokine measurements

Cytokines levels for IL-1β, CXCL1, CXCL2, CXCL5, CXCL7 and CXCL15 were quantified in BAL and/or lung homogenates using DuoSet ELISA kits (R&D Systems, Minneapolis, MN, USA) according to the manufacturer's instructions. A 96-well plate was coated overnight with the specific capture antibody. The wells were blocked with 1% bovine serum albumin (BSA) in PBS to reduce non-specific protein binding. 100µl of lung homogenates or standards were then added to each well and incubated for 2 hours at room temperature to allow the corresponding cytokine to bind to the capture antibody. Next, a biotinylated detection antibody, specific for the cytokine of interest, was added to each well allowing its binding for 2 hours. Streptavidin covalently conjugated to horseradish-peroxidase (HRP) was then added into the plate. The colour of the

chromogenic substrate was detected by absorbance measured at 450 nm and cytokine concentrations of the different samples were calculated based on a standard curve.

2.7. Analysis of IL-1β and caspase-1 by western blot

Western blot analysis was carried out for those proteins that are expressed both as pro-form and as its proteolytically cleaved, active form. This is the case of the IL-1β cytokine and the protease responsible for its cleavage, caspase-1.

Lung lobes from WT and $ASC^{-/-}$ mice were homogenized in 600 µl of lysis buffer containing protease-inhibitor cocktail (cOmplete Mini, Roche Diagnostics, Indianapolis, IN, USA) for the inhibition of serine, cysteine and metalloproteases. Next, the protein concentration of each sample was quantified by using a dye-binding assay (*RC DC*™ Protein Assay, Bio-Rad, Mississauga, ON, Canada) and samples from each experimental group were pooled together into a single tube containing the same amount of protein from each sample, and lysis buffer containing the protease inhibitor cocktail and loading buffer were also added to each tube to make a final concentration of 80µg protein/50µl volume. Samples were then heated at 95ºC for 3 minutes in order to denature the proteins. The samples were applied to a 15% polyacrylamide gel, together with a prestain protein ladder (BenchMark™, Invitrogen™, Burlington, ON, Canada) to control for molecular weights (MW). Proteins were separated electrophoretically based on their MWs and transferred from the gel onto a nitrocellulose membrane using electric current. The membrane was stained later with Ponceau Red to control for protein transfer, followed by blocking of the membrane with 5% non-fat dry milk in Tris(hydroxymethyl)aminomethane-buffered saline (TBS) containing Tween 20 (Sigma-Aldrich, Oakville, ON, Canada). Finally, the

membrane was exposed at 4ºC overnight with the corresponding primary antibodies, followed by incubation with secondary IRDye® 800CW antibodies. For the detection of the different forms of IL-1β, polyclonal goat anti-mouse IL-1β IgG (R&D Systems, Minneapolis, MN, USA) diluted 1:100 and IRDye®-conjugated donkey anti-goat IgG antibodies (Li-Cor Biosciences, Guelph, ON, Canada) diluted 1:2500 were used. For the detection of caspase-1, rat anti-mouse caspase-1 antibodies (clone 5B10) (eBioscience, San Diego, CA, USA) and IRDye®-conjugated goat anti-rat IgG antibodies (Li-Cor Biosciences, Guelph, ON, Canada) were used. The membrane was finally scanned by infrared light to reveal the presence of the IRDye® using a Li-Cor Odyssey® infrared detector (Li-Cor Biosciences, Guelph, ON, Canada).

2.8. Immunohistochemistry

Lung lobes from WT mice that had been infected according to the experimental model were dissected at D5+7, inflated with 10% formalin, processed and embedded in paraffin by the MIRC Core Histology Facility (Department of Pathology and Molecular Medicine, McMaster University). 5µm-thick slices were cut and air dried overnight prior to perform immunohistochemistry in order to localize the cellular source of IL-1β expression. Tissue was washed in xylene to remove paraffin and washed sequentially in absolute ethanol to dehydrate. Endogenous peroxidase activity was blocked with methanolic hydrogen peroxide (EMD Inc., Mississauga, ON, Canada), the tissue was rinsed sequentially in 100%, 95% and 70% (v/v) ethanol and water. Antigen retrieval was performed by exposing tissue to citrate buffer for 45 minutes in a humid chamber and washed with TBS-Tween 20. Tissue was then blocked with Rodent block M (from Goat

HRP-Polymer Kit) (Biocare Medical, Markham, ON, Canada) and incubated with 4 µg/ml of primary antibodies (goat anti-mouse IL-1β IgG (R&D Systems, Minneapolis, MN, USA)) or the isotype control (normal goat IgG (R&D Systems, Minneapolis, MN, USA)) overnight at 4ºC. After washing, a goat probe that labeled the primary antibodies and a goat HRP-polymer that conjugated to the probe (from Goat HRP-Polymer Kit) (Biocare Medical, Markham, ON, Canada) were added for 15 minutes and slices were placed in 3-amino-9-ethylcarbazole (AEC) buffer and in AEC chromogenic substrate solution (dimethylformamide) (Acros Organics, NJ, USA) to reveal the stain. Finally, slices were place in distilled H_2O, Mayer's solution, rinsed again with tap water and washed in TBS before cover slipping the slides with glycerol gelatin.

2.9. Caspase-1 activity assay

Lung lobes from WT and $ASC^{-/-}$ mice were homogenized in 600 µl of chilled Cell Lysis Buffer (Abcam, Cambridge, MA, USA) to release the cellular content, including caspase-1 protease. Next, the protein concentration of each sample was quantified by a dye-binding assay (*RC DC*™ Protein Assay, Bio-Rad, Mississauga, ON, Canada). Samples from each experimental group were pooled to a final concentration of 50µg protein/50µl of lung homogenate. Caspase-1 activity in the lung homogenates was detected using a fluorometric assay kit (Abcam, Cambridge, MA, USA). A mix containing 2X Reaction Buffer, dithiothreitol **(**DTT) and the fluorometric peptide substrate YVAD-AFC (Tyr-Val-Ala-Asp-AFC) was prepared according to manufacturer's instructions and 55 µl were added to 50 µl of each sample. The samples containing active caspase-1 cleaved the substrate YVAD-AFC into free AFC, altering its

emission spectrum from blue to yellow-green. A kinetic curve for caspase-1 activity was quantified by fluorescent detection of free AFC at excitation wavelength of 400 nm and emission wavelength of 505 nm at 37ºC for 2 hours, using a fluorescence microplate reader Synergy 4 and the Software Gen5 v.1.08 (both from BioTek, Winooski, VT, United States). The slope of the kinetic curve for each experimental group was extracted and compared to the vehicle-treated group.

2.10. Data analyses

Data in this report were expressed as the mean ± standard error of the mean (SEM). Data were analyzed using Excel (Microsoft, Seattle, WA, USA) and Sigma Plot version 11 (Systat Software, Chicago, IL) for the generation of the standard curve and the statistical tests. Unpaired Student's t-tests were used for 1-factor, 2-group comparisons (Mann-U-Whitney rank sum test in cases where the data were not normally distributed), and 2-way ANOVA for 2-factor comparisons. Additional details and interpretation are indicated in the corresponding figure legends. Differences were considered statistically significant at $p<0.05$. Data were graphed using GraphPad Prism version 5 (GraphPad Software, LaJolla, CA).

Chapter 3: Results

Aim I: Re-characterization of the heterologous infection model upon adjustments of the viral and bacterial doses.

1. Effect of viral dose on mortality and body weight upon IAV infection.

A concern in the model previously established in Dr. Stampfli's laboratory was the elevated 25% mortality rate observed following infection of mice with $2.5x10^5$ PFU of IAV at day 0 and superinfection with 500,000 CFU of *B. parapertussis* 5 days later (28). In order to decrease mortality, the viral dose was reduced to $2.5x10^4$ PFU per mouse. Mortality was thus reduced to 15%, but still was considerably elevated. The viral dose was finally decreased to $1x10^4$ PFU IAV per mouse and mortality was as low as 2.5%. Therefore, this dosage was used for future experiments. Reducing the viral dose from $2.5x10^5$ PFU to $1x10^4$ PFU also had impact on body weight loss, which were less compared to the weight loss experienced by mice infected with the higher viral dose. In addition, differences in body weight loss and recovery between IAV alone-infected mice and heterologously-infected mice were narrowed compared to the high dose experiments. Thus, body weight loss and mortality were determined to be viral dose-dependent (Figure 1).

2. Re-establishment of the standard curve for B. parapertussis *growth.*

In addition, a new standard curve measuring the OD of the *B. parapertussis* growth had to be generated due to the use of a different spectrophotometer in order to maintain a constant bacterial dose of $5x10^5$ CFU per mouse (Figure 2A). The *B. parapertussis* culture remained in lag phase for approximately 20 hours, after which it

grew exponentially for 12 hours during the log phase until reaching the stationary and death phase. Serially-diluted samples of log phase bacterial broth were cultured onto Bordet-Gengou blood agar plates and incubated at 37ºC for 3 days. The OD of the broth at 600 nm (OD_{600}) was found to correlate linearly (via y = mx+b) with the number of viable bacterial colonies. Therefore, the new equation of the curve describing the bacterial concentration is:

$$[\text{bacteria}] = (OD_{600}-0.2852) \times (1.56\times10^{9}\ \text{CFU/ml})$$ (see Figure 2A).

It was determined that the current spectrophotometer underestimated the measurements compared to the previous instrument. Therefore, the modifications made in the viral and bacterial dosages might have modified the phenomenon characterized by Zavitz *et al*. (2010). Also, corroboration of my ability to reproduce the same experimental plan and results than previous labmates was also required before addressing any further experiment.

3. Analyses of the inflammatory processes upon heterologous infection.

C57BL/6 mice were infected with 1×10^{4} PFU IAV and 5×10^{5} CFU *B. parapertussis* in order to re-characterize the pulmonary inflammation and bacterial burden previously observed in the lung upon heterologous infection. IAV-infected mice lost up to 10-15% of their initial weight by day six or seven after infection, compared to vehicle-inoculated or *B. parapertussis* only-infected mice which did not lose any body weight. Bacterial superinfection of IAV-infected mice slightly enhanced the weight loss and the severity of the clinical symptoms and it retarded the recovery and gain of body weight (Figure 3A). Bacterial burden in heterologously-infected mice was significantly

higher than in *B. parapertussis* alone-infected mice. While *B. parapertussis*-infected mice were able to clear the bacteria seven days post-infection, heterologously-infected mice could not control the infection and bacterial burden in lung increased over time (Figure 3B).

The total cell number enumerated in the BAL showed that heterologously-infected mice had a higher cellular infiltration compared to control mice at the three time points of sacrifice, becoming appreciably different at D5+7. These differences were mainly due to a severe neutrophilia found in the lung of heterologous infected mice, which was not observed in either IAV or *B. parapertussis* infections alone. Mononuclear cells were not found to be increased in heterologously-infected mice compared to IAV-alone control group (Figure 3C).

Viral titers were measured at day 5 post-viral infection to elucidate the concentration of IAV at the peak of infection. Lung homogenates were applied to MDCK cell monolayers for 2 days. Vehicle-inoculated mice did not show any viral particles in their lungs, whereas IAV-infected WT animals showed approximately $3.7x10^5$ PFU/ml of viral particles. $1.2x10^5$ PFU/ml was recovered from IAV-infected $ASC^{-/-}$ mice. Thus, IAV was present in the lungs upon 5 days post-infection (Figure 2B).

Taken together, these results in Aim I demonstrated that the phenomenon previously observed upon heterologous infection persisted despite the modification in the viral dose and adjustment of the bacterial dose, thus indicating that the severe pulmonary inflammation and the impairment in the bacterial clearance upon heterologous infection are viral dose-independent. However, a lower viral dose did reduce the mortality and

body weight loss in IAV-infected mice. Thus, these two parameters are viral dose-dependent. In addition, these data validated this model as adequate to further study the immunopathology elicited upon bacterial superinfection of IAV.

Aim II: Determine levels of IL-1β production and relevant chemokines that contribute to the increased pulmonary inflammation.

IL-1β induces the production of CXC chemokines, and these chemokines are known to be potent neutrophil chemoattracts (25). Therefore, we investigated whether the dysregulated expression of IL-1β led to increased expression of CXC chemokines, consequently explaining the exaggerated neutrophilia observed in the lung of heterologous infected mice. Thus, levels of IL-1β and the main lung chemokines (CXCL1, CXCL2, CXCL5, CXCL7 and CXCL15) were quantified by ELISA in lung homogenates of heterologously-infected mice sacrificed at D5+7.

4. IL-1β production was exacerbated in heterologously-infected mice.

IL-1β levels were measured by ELISA in the BAL and lung homogenates of mice that had been infected with IAV at day 0, superinfected with *B. parapertussis* at day 5 and sacrificed at D5+7. The results in Figure 4A show that IL-1β were found to be significantly increased in both the BAL and lung homogenates of heterologously-infected mice compared to vehicle only-, *B. parapertussis* only-, or IAV only-infected mice. Furthermore, lower amounts of IL-1β were found in the BAL compared to the lung homogenates, thus suggesting that most of the IL-1β measured in lung homogenate was

not secreted into the BAL and, therefore, was expressed as the pro-form and not as the active form.

To investigate this, a western blot was prepared to evaluate the different forms of IL-1β contained in the homogenates (Figure 4B). At D5+7, levels of pro-IL-1β (31kDa) and active IL-1β (17kDa) in *B. parapertussis*-alone and heterologously-infected mice were found in high concentrations compared to vehicle-inoculated or IAV-infected mice. Also, levels of pro-IL-1β seemed to be more elevated (by visual judge) than the active form.

Levels of IL-1β were also measured in lung homogenates of IAV-infected mice at day 5 post-viral infection alone to determine whether IL-1β production was dysregulated at an earlier time point than D5+7 upon IAV infection. The results (Figure 4B) showed that IAV induced production of IL-1β; however, only a slight production of the pro-form could be detected and this was clearly not the active form. These data formulated the experiments noted in Aim III.

5. Exacerbated IL-1β levels corresponded with a simultaneous increase in the CXCL1 and CXCL2 chemokines production.

Since previous reports suggested that IL-1β regulates CXC chemokine induction (25, 108), experiments were conducted to determine whether the increased IL-1β levels observed in heterologously-infected animals coincided with an enhancement in the levels of the CXC chemokines that are known to be produced in the lung. Thus, CXCL1, CXCL2, CXCL5, CXCL7 and CXCL15 were quantified by ELISA.

Production of CXCL1, CXCL2, and to a lesser extent CXCL5, was found to be increased by D5+7 only in heterologously-infected mice compared to the low levels seen in animals infected with either pathogen alone (Figure 5). In contrast, no significant differences in CXCL7 and CXCL15 expression were found in heterologous infection. Indeed, only *B. parapertussis*-infected mice showed a significant decrease in CXCL7 levels. Therefore, CXCL7 and CXCL15 did not appear to have a determinant role in the immunopathology of superinfections. Therefore, the severe infiltration of neutrophils in the lung of heterologous infected mice was likely provoked by the exacerbated production of CXCL1 and CXCL2.

In conclusion from Aim II, IL-1β, CXCL1/KC and CXCL2/MIP-2 seem to play a major role in the immunopathology and the severe inflammation observed upon heterologous infection.

Aim III: Mechanisms leading to IL-1β overproduction.

Based on the foregoing findings, the detection of only pro-IL-1β by western blot at 5 days post-IAV infection (Figure 4B) provoked the proposal that IAV leads to major expression of pro-IL-1β and minor production of active IL-1β. Alternatively, *B. parapertussis* was shown to induce both pro- and active IL-1β seven days post-infection; however, IL-1β production by *B. parapertussis* at earlier time points had not been confirmed yet. Thus, we hypothesized that IAV induces activation of caspase-1 and production of active IL-1β during the first few days of infection. However, 5 days post-IAV infection only pro-IL-1β levels are detected, as seen in Figure 4B. Therefore, when

IAV-infected mice were superinfected with *B. paparapertussis*, the bacteria induces pro-IL-1β expression and high levels of pro-IL-1β accumulate intracellularly. Since *B. parapertussis* is known to activate the inflammasome, caspase-1 levels will be increased, and the high levels of pro-IL-1β will be processed into the active form and released from the cells.

To test this hypothesis, timeline experiments were conducted in C57BL/6 mice infected with either IAV or *B. parapertussis* alone. The results would help to finally understand how *B. parapertussis* infection influences a prior IAV infection.

6. IAV induces expression and activation of caspase-1 and IL-1β.

To investigate the time courses of IL-1β expression, mice were infected with $1x10^4$ PFU IAV and sacrificed at days 1, 3, 5 and 14 post-infection. Figure 7 shows the evolution of IAV infection in WT mice during a two week-period. IAV-infected mice lost up to 10% of their body weight by day 7, after which the recovery began. IAV had no evident effects on body weight or pulmonary inflammation at day 1 post-infection. However, by day 3, inflammation in the lung reached its highest point throughout the course of infection, reflected by a significant increase in the total cell number –both mononuclear cells and neutrophils– infiltrated into the lung. This neutrophilia was slightly decreased by day 5 post-infection and completely cleared by day 14, though the monocyte-derived macrophages remained elevated in the lung two weeks upon infection.

In addition, levels of IL-1β, CXCL1 and CXCL2 were quantified in lung homogenates by ELISA (Figure 8A). IAV-infected mice showed significantly increased IL-1β levels at day 3, 5 and 14 post infection compared to non-infected mice. Conversely,

no differences in CXCL1 or CXCL2 production were observed between infected and non-infected mice along the course of the infection.

IL-1β was further analyzed by western blot to determine whether IAV induces expression of the pro-form only or whether the active form is also induced at the early time points (Figure 8B). The western blot also showed that IL-1β production peaked at day 3 and 5 post-infection in IAV-infected mice whereas non-infected mice did not show any expression. Of note, expression of pro-IL-1β (31 kDa) appeared to be greater than the active form (17 kDa) at days 3 and 5.

In order to further investigate mechanisms of processing of pro-IL-1β into active IL-1β, caspase-1 expression was analyzed by western blot (Figure 9A). Pro-caspase-1 (42 kDa) was found to be expressed in both IAV-infected and non-infected mice. Expression appeared to be slightly higher (by judge visually) in infected mice at day 3 and 5 post-infection. No active form of caspase-1 (two subunits of 20 and 10 kDa, respectively) was detected by western blot. To further investigate whether IAV activated caspase-1, activation of caspase-1 was evaluated by an activity assay. Figure 9B shows that IAV did induce caspase-1 activation after 3 days post-infection. Caspase-1 activation increased over time and the protease remained activated even 14 days post-IAV infection.

Taken together, the results from the IAV infection alone suggest that IAV increased pulmonary inflammation which may be driven by an increased IL-1β expression. However, despite evidence of caspase-1 activation by IAV, IL-1β was mainly found as the pro-form and not as the cleaved, active form.

7. B. parapertussis *activates inflammasome and the subsequent IL-1β activation*

Similarly to IAV infection, a time course experiment was carried out for infection with *B. parapertussis*. Mice were infected with $5x10^5$ CFU *B. parapertussis* and sacrificed at days 1, 3, and 7 post-infection. Figure 10 shows body weights recorded during 7 days post-bacterial infection. In contrast to what was seen in IAV infection, *B. parapertussis*-infected mice did not experience weight loss and remained at their original weight for 5 days, at which time they began to gain weight. Pulmonary inflammation was first observed 3 days upon infection and increased over time, being highest at day 7. Neutrophilia in *B. parapertussis*-infected mice was observed from the beginning of the infection. Mononuclear cells were only found to be increased in infected mice 7 days post-infection, contributing to the increased inflammation (Figure 10). Remarkably, even though the highest pulmonary inflammation was observed 7 days post infection, bacterial burden was significantly decreased at this time point, indicating that *B. parapertussis* was being cleared within 1 week after infection.

IL-1β expression was next measured by ELISA. *B. parapertussis* induced IL-1β production significantly from the first day post-infection, peaking at day 3 (Figure 11A). By day 7, significant IL-1β levels were still detectable but production of this cytokine was returning to basal levels. No IL-1β was produced in vehicle-inoculated mice. CXCL1 and CXCL2 were also significantly increased early upon *B. parapertussis* infection, and lower production was detected by day 7 post-infection (Figure 11A).

IL-1β was also analyzed by western blot to determine whether there were differences in *B. parapertussis*-induced expression of the pro-IL-1β and active IL-1β.

Figure 11B shows that *B. parapertussis* activated the expression of both the pro-form and the active form of IL-1β at day 1 and 3 post-infection. As determined by ELISA, the western blot also showed lower expression of IL-1β at day 7 post-infection, although it was noticeably higher that non-infected mice (Figure 11B).

Next, we analyzed caspase-1 by western blot. Figure 12A showed that no evident differences were found in the levels of pro-caspase-1 expression at day 1 post-bacterial infection. However, at later time points, pro-caspase-1 was seen to be appreciably increased in *B. parapertussis*-infected mice compared to the constitutive levels of non-infected mice. Analysis of caspase-1 activation by an activity assay showed that active caspase-1 began to increase at day 3, reaching the maximum at day 7 or later (Figure 12B). No active caspase-1 was found at day 1, indicating that the inflammasome did not get activated immediately upon *B. parapertussis* infection despite IL-1β expression did.

Taken together, infection with *B. parapertussis* induced rapid expression of IL-1β, CXC chemokines and neutrophilia. Of note, caspase-1 activation occurred a few days post-bacterial infection. Interestingly, the reduction in the bacterial burden by day 7 post-infection coincided with a reduction in IL-1β and CXC chemokine levels whereas the neutrophilic inflammation and caspase-1 remained increased at that time point.

Collectively, the results from the individual *B. parapertussis* infection indicated that *B. parapertussis* induced neutrophilia early post-infection as well as rapid IL-1β production –both as the pro-form and the active form. *B. parapertussis* induced caspase-1 activation but at later time points post-infection.

8. Superinfection of IAV-infected mice with B. parapertussis *at day 5 implies elevated amounts of pro-IL-1β produced and processed into active IL-1β*

Based on the findings thus far, it was elucidated that levels of pro-IL-1β and caspase-1 were increased in IAV-infected mice 5 days post-infection. Additionally, *B. parapertussis* activated IL-1β production immediately after infection. Therefore, we hypothesized that upon superinfection of IAV-infected mice with *B. parapertussis* lead to dysregulation of IL-1β production and the subsequent induction of CXC chemokines in heterologously-infected mice.

Thus, IL-1β, CXCL1, and CXCL2 levels were quantified by ELISA at earlier and later time points post-superinfection (Figure 13A). All of these pro-inflammatory mediators were found to be significantly increased in the heterologously-infected group at D5+1 compared to IAV only- and *B. parapertussis* only-infected mice. By D5+3, *B. parapertussis* only-infected mice showed similar or slightly higher IL-1β, CXCL1 and CXCL2 production than heterologously-infected mice. At D5+7, levels of IL-1β and CXCL1 were significantly dysregulated compared to any control groups. However, no differences in CXCL2 production were observed between groups at this later time point.

Figure 13B demonstrated that both IAV and *B. parapertussis* activate IL-1β production, both its pro-form and its active form. Intense production of IL-1β was seen 1 day after *B. parapertussis* infection, either by this pathogen alone or in previously IAV-infected mice. However, IL-1β production was notably higher in heterologously-infected mice, as previously confirmed by ELISA. Similar results were observed at D5+3. The western blot also showed that vehicle only-, *B. parapertussis* only- or IAV only-infected

mice had low levels of IL-1β at D5+7 whereas heterologously-infected mice showed elevated levels of pro- and active IL-1β.

Caspase-1 levels were also analyzed by western blot (Figure 14A). Unexpectedly, pro-caspase-1 levels were seen to be slightly increased in IAV- and heterologously-infected mice at D5+1 and D5+3 whereas vehicle only- and *B. parapertussis* only-infected mice showed basal levels. At D5+7, pro-caspase-1 in heterologously-infected mice appeared increased compared to control groups. No active caspase-1 form was detected by western blot.

Next, caspase-1 activity assay was performed. Figure 14B shows that levels of active caspase-1 in *B. parapertussis*-infected mice at D5+3 were similar to the basal or constitutively expressed levels of vehicle-inoculated mice, indicating that inflammasome and caspase-1 activation occurred after day 3 post-bacterial infection. IAV- and heterologously-infected mice showed increased caspase-1 activity at D5+3 compared to vehicle- and *B. parapertussis*-infected mice. At D5+7, levels of active caspase-1 in IAV- and heterologously-infected mice are notably reduced compared to D5+3, in contrast to *B. parapertussis*-infected mice which showed an increase in caspase-1 activation from D5+3 to D5+7, although it was still lower than caspase-1 levels in IAV- and heterologously-infected mice.

Taking all these results together, superinfection of IAV-infected mice with *B. parapertussis* led to dysregulation of IL-1β production as well as significantly increased levels of CXCL1. Heterologous infection also induced enhanced expression of pro-caspase-1 and its subsequent processing to active caspase-1. Thus, these data suggested

higher activation of the inflammasome induced by a heterologous infection that led to increased IL-1β processing and induction of CXCL1.

9. Localization of the cellular source of IL-1β overproduction

Previous results demonstrated dysregulated levels of IL-1β upon heterologous infection. Next, we analyzed the localization of the IL-1β production by immunohistochemistry in order to elucidate the cellular source of this overproduction.

Figure 15A shows the localization of IL-1β in vehicle-treated and heterologously-infected mice at D5+7. Basal IL-1β levels were detected in vehicle-treated mice. IL-1β staining was seen mostly in the epithelium of the airways and in AMs. Some staining could also be detected in the endothelium of the vascular system, although to a lesser extent. An isotype control was included in the experiment to measure the background levels of non-specific binding of these antibodies to Fc receptors present on the surface of the tissue.

Expression of IL-1β was also assessed in IAV- and *B. parapertussis*-infected mice. Figure 15B showed that IAV-infected mice, after 12 days of infection, did not express IL-1β in the lung or these levels are back to basal, since no notable differences were seen when compared to the corresponding isotype control. *B. parapertussis* alone-infected mice did express high levels of IL-1β in their lungs, even seven days post-infection. IL-1β staining was localized mainly in the airway epithelium, in the alveolar macrophages and in the vascular epithelium.

AIM IV: Analyze the outcome of reduced IL-1β production on pulmonary inflammation.

According to the data obtained, IL-1β is a proinflammatory mediator that may play a critical role in the inflammatory immunopathology of heterologous pulmonary infection. Thus, interventions were pursued to elucidate whether decreased IL-1β levels could regulate the severe pulmonary inflammation observed in heterologously-infected mice and thereby improve the clinical outcome of the disease. The first approach was explored in *ASC*$^{-/-}$ mice.

10. Deficiency in ASC seems to reduce the inflammatory immunopathology in heterologous infection.

Processing of bioactive IL-1β mainly depends on activation of caspase-1 by multiprotein complexes termed inflammasomes (80). ASC is an adaptor protein required for the recruitment of caspase-1 in some inflammasomes. To investigate whether ASC and, by extension, IL-1β processing contributed to increased neutrophilia observed in heterologous infection, ASC$^{-/-}$ mice were infected with 1x10^4 PFU of IAV. Five days later, ASC$^{-/-}$ mice were superinfected with 5x10^5 CFU of *B. parapertussis* and sacrificed at D5(+0), D5+3 and D5+7 post-infection.

Initial experiments showed that ASC$^{-/-}$ mice had an improved clinical presentation after heterologous infection compared to WT mice (Figure 16). The body weight loss was lower in ASC$^{-/-}$ mice than WT mice and the recovery started earlier and was more rapid than control mice. Furthermore, cell inflammation in the BAL was also significantly lower in ASC$^{-/-}$ mice, with remarkably less mononuclear cell and neutrophilic infiltration

than WT mice. These differences became evident after D5+3 post-infection. Interestingly, $ASC^{-/-}$ mice did show a significant increase in bacterial burden in the lung compared to WT mice. Pulmonary inflammation and epithelium damage were also assessed by histological analysis. Tissue sections from WT and $ASC^{-/-}$ mice at D5+3 and D5+7 time points were stained with H&E and analyzed microscopically. The differences in cellular infiltration observed in $ASC^{-/-}$ mice could not be appreciated by this observation (Figure 17). Interestingly, the integrity of the airway epithelium in both WT and $ASC^{-/-}$ mice seemed to be intact by D5+3; however, damage of the epithelial cells could be appreciated at D5+7, being more severe in WT mice than in $ASC^{-/-}$ mice. The epithelium had lost its integrity and cells had a squamous appearance, although this was more evident in WT mice (Figure 18).

IL-1β and CXCL2 levels were quantified by ELISA to determine whether the reduced neutrophilia also corresponded with a decrease in these cytokine levels (Figure 19). No differences were observed at D5+3, but a significant reduction was seen in both IL-1β and CXCL2 between $ASC^{-/-}$ and WT mice at D5+7. However, when this experiment was repeated it could not be completely replicated and validated (Figure 20). $ASC^{-/-}$ mice had a similar body weight loss than WT mice, although recovery was faster in the $ASC^{-/-}$ mice. The bacterial burden was again seen to be significantly higher at D5+7 in $ASC^{-/-}$ mice than in WT mice. No differences in pulmonary cell infiltration were observed at D5(+0) or D5+3; however, a small reduction was seen at D5+7, especially in the number of neutrophils recruited into the lung, although these differences did not reach significance in the statistical analysis.

Quantification of the inflammatory mediators was then performed (Figure 21A) at the aforementioned time points. As seen before, IL-1β levels increased overtime upon heterologous infection. However, no statistically significant differences were found between $ASC^{-/-}$ and WT mice at any of the time points, although a slight reduction was observed in IL-1β, CXCL1 and CXCL2 at D5+7, that could partially explain the reduction in neutrophilia observed as well. IL-1β was further analyzed by western blot (Figure 21B). As determined by ELISA, levels of IL-1β seem to increase over time, but no significant differences are seen between $ASC^{-/-}$ and WT mice.

Consequently, the expression of caspase-1 was assessed to determine if the reduction seen in IL-1β levels correspond with a decrease in caspase-1 activation. Figure 22A showed that an increase in pro-caspase-1 was induced over time upon heterologous infection, similarly to what had been seen in IL-1β production. Again, no active caspase-1 could be detected. The evaluation of caspase-1 activation by an activity assay showed no significant difference in caspase-1 activation at D5+0 and D5+3, and unexpectedly, higher caspase-1 activation in $ASC^{-/-}$ mice compared to WT mice (Figure 22B).

In conclusion, there is some incongruence in the results between the first and second repetition of the experiment in $ASC^{-/-}$ mice. According to the first set of results, $ASC^{-/-}$ mice showed a beneficial outcome upon heterologous infection as well as reduced immunopathology; however, these results could not be reproduced in the second experiment. Further investigations will be carried out to determine whether deficiency in ASC can resolve the severe inflammation occurring in heterologous pulmonary infections.

Chapter 4: Discussion

Despite the advanced knowledge concerning the mechanisms of IAV infection and the improved vaccines raised against it, IAV still causes a life-threatening respiratory disease, especially during pandemics (52). Investigations from past years have elucidated that many IAV-attributable deaths are mainly due to bacterial superinfections, rather than the primary viral infection (63, 109). The immunopathology triggered by these heterologous infections has been suggested as the major cause of death independent of the bacterial burden. However, the mechanisms underlying this immunopathology are still poorly understood and, thus, this is the focus of this thesis.

Several studies in animal models of bacterial superinfection of IAV have proposed different factors involved in the viral-bacterial synergy. These factors include increased bacterial adherence to the airway epithelium due to upregulation of platelet-activating factor receptor expression (110), impaired neutrophil and AMs function (111, 112), and dysregulated cytokine responses (73, 113). Our laboratory established a novel model combining IAV and *B. parapertussis* and determined that the chemokine CXCL2/MIP-2 plays a major role in the immunopathology of the disease (28). This project aimed to deepen our understanding of the inflammatory immunopathology caused by heterologous infections and elucidate the origin of that overproduction of MIP-2. Evidence in the literature suggests that IL-1β induces and regulates CXC chemokines production. Thus, we hypothesized that dyregulated IL-1β production is involved in the outcome of the disease, playing a major role and leading to the MIP-2 overproduction. The proposed aims tried to first confirm exacerbated IL-1β production in heterologously-infected mice

by studying how individual infections contribute to inflammasome activation and IL-1β expression independently. Secondly, inhibition of the main pathway that leads to IL-1β processing was pursued as an attempt to regulate IL-1β overproduction and elucidate whether this has a beneficial outcome in the disease. The results from this study provide support to the hypothesis.

4.1. Decreased mortality in heterologous infection by reduction of viral dose.

The parameters most commonly used to assess IAV pathogenicity in mice are body weight loss and mortality (114). Our study demonstrated that the elevated mortality rate seen in previous experiments using a higher dose of IAV was successfully reduced by decreasing the viral dose administered intranasally (Figure 1). The reduction of the viral dose also had an impact on the body weight loss but did not affect the exacerbated pulmonary inflammation and the impairment in the bacterial clearance occurring upon heterologous infection (Figure 3). Furthermore, a model using lower IAV infectious dose is more likely to mimic what actually occurs in humans in influenza epidemics, since a lower IAV dose is needed for humans to become infected.

Different strategies have been attempted in order to reduce the mortality in patients suffering from heterologous infections; most of them included antibacterial therapies, such treatment with sterilizing antibiotics to reduce the uncontrolled lung bacterial burden found in these patients (68, 69). Unfortunately, many of these therapies failed to prevent progression to septic shock and mortality. Patients eventually succumbed to the inflammatory immunopathology triggered by the combination of both the virus and the bacteria. Antiviral therapy has been ignored because viral infections usually resolve

by the time bacterial pneumonia is present. However, IAV produces a long-term impact in the host and activated pathways remain altered even several weeks after the resolution of the virus. For example, IAV infection has been shown to impair the host antibacterial functions provided by AMs and neutrophils (88). Sun and Metzger (2008) demonstrated that the IFN-γ produced by T-cells during the recovery phase of IAV infection suppresses the initial bacterial clearance by AMs (112). McNamee and Harmsen (2006) showed that neutrophil dysfunction in IAV-infected mice in the form of decreased phagocytosis and intracellular reactive oxygen species generation in response to *S. pneumoniae* (111). These alterations of the host's innate immunity affects not only in processes of superinfections but also in delayed bacterial infections. Zavitz *et al.* (data not published) have demonstrated that IAV-infected mice induced significantly increased pulmonary inflammation when superinfecting mice with *B. parapertussis* 14 or even 90 days post-IAV infection, time points at which viral load has been already cleared.

Therefore, since IAV impairs the manner the host responds to subsequent infections even long time after clearance, antiviral therapies should be considered for the treatment of bacterial superinfections of IAV. Firstly, prophylactic measures such vaccination of the population against IAV, especially in high risk groups like children and the elderly, are strongly recommended. Replication of IAV in vaccinated individuals is contained and viral load remains low, being easily cleared by the host's immune system. Secondly, in the cases where IAV establishes a successful infection, our data suggest that antiviral therapies directed to decrease the viral load may help to reduce mortality upon IAV infection or the subsequent bacterial superinfection (Figure 1). However, providing

antiviral drugs to infected patients early post-IAV infection is difficult to carry out since in many occasions patients do not seek for professional medical care. The risk of contracting secondary bacterial infections is increased in these patients. For them, a combination of antiviral and antibacterial drugs could be recommended. As McCullers (2004) (68) demonstrated, treatment of mice suffering from secondary pneumococcal pneumonia after IAV with oseltamivir showed remarkably improved survival, even when therapy was administered up to 5 days post-IAV infection. In contrast, treatment with ampicillin cleared the bacterial infection but did not improve survival in the absence of treatment with oseltamivir. Of note, only 7 of the 22 mice receiving oseltamivir developed pneumonia, and subsequent treatment with ampicillin resulted in 100% survival and recovery.

In conclusion, treatment of the predisposing IAV infection with inhibitors specific for the viral neuraminidase may improve the efficacy of antibiotics and increase survival in people who are at high risk for complications and mortality during IAV infection. Therefore, mortality in heterologous infections is likely due to a combination of different factors involving the virus, the bacteria, and the inflammatory profile produced by both pathogens.

4.2. MIP-2 dysregulation could be driven by IL-1β overproduction.

CXCL2/MIP-2 is a potent neutrophil chemoattractant that was found to be overproduced in heterologous infections (28). Our laboratory previously showed that immunoneutralization of MIP-2 significantly regulated the clinical and pathological manifestations in heterologously-infected mice. Thus, MIP-2 accounted for part of the

profound lung inflammation and neutrophil recruitment occurring in heterologous infection (28). However, the origin of the MIP-2 dysregulation was unknown. The main goal of this project was to elucidate the mechanisms that lead to the inflammatory immunopathology in bacterial superinfections of IAV, including that MIP-2 overproduction. Based on the evidence in the literature, we proposed IL-1β as the principal cytokine involved in the signaling cascade that eventually induces MIP-2 overproduction. Sensitization of the pathogens such IAV and *B. parapertussis* through TLR on the innate immune cells induces expression of IL-1β and activation of the inflammasome, leading to the subsequent caspase-1 activation, which is a protease critically involved in the processing of pro-IL-1β into active IL-1β (115, 116). Active IL-1β, in turn, activates production of CXC chemokines such as CXCL1/KC or CXCL2/MIP-2 (25). According to this, heterologous infection was seen to significantly increase IL-1β production compared to infections with either pathogen alone, and even as early as day 1 after superinfection (Figure 13A). This increase in IL-1β induced a similar pattern of expression for CXCL1. However, production of CXCL2 was not found to be overproduced in heterologously-infected mice, particularly at the D5+7 time point. These data contradict the results from Zavitz *et al.* (28), where CXCL2 was found highly expressed in heterologously-infected mice, even at an earlier time point than CXCL1. Of note, the difference between both experiments relies on a different viral dose used to infect mice: in Zavitz *et al.* (2010), mice were infected with $2.5x10^5$ PFU of IAV whereas in the present studies the viral dose used was $1x10^4$ PFU of IAV. In addition, these two chemokines were also measured in lung homogenates of mice infected with the

intermediate dose of $2.5x10^4$ PFU of IAV (Figure 5). Significant increased expression of CXCL1 and CXCL2 was seen. Taken together, these data indicate that at higher doses of IAV CXCL2/MIP-2 could play a more relevant role than CXCL1; however, at lower doses of IAV the phenomenon could be reverted and CXCL1/KC could play a more important role than MIP-2.

Furthermore, Figure 8 shows that even though IAV induced significantly higher levels of IL-1β than vehicle-treated mice, these levels were not high enough to induce expression of CXCL1 and CXCL2. In contrast, Figure 11 shows that *B. parapertussis*-induced IL-1β levels are higher than IAV-induced levels, and that led to subsequent production of CXCL1 and CXCL2. Interestingly, *B. parapertussis*-induced IL-1β levels at day 7 post-infection are similar to those induced by IAV, and at that time point no increased production of CXC chemokines were observed. Therefore, these data suggest that a threshold of IL-1β expression must be achieved in order to induce CXCL1 and CXCL2, and at the lower dose of IAV this threshold was not reached whereas at higher levels of IAV it did. If this were correct, CXCL1 and CXCL2 production would be expected since IL-1β levels induced in heterologously-infected mice at D5+7 reached that threshold. However, CXCL2 was found not to be induced. In addition, both CXCL1 and CXCL2 productions were expected to increase over time from D5+1 to D5+7 and be responsible for the severe neutrophilia observed in the lung. Therefore, some inconsistencies have been observed in these results compared to previous experiments and it is thought that some technical issues might have interfered in the results. In addition, these data are difficult to interpret because background levels were considerably

elevated in some of the ELISAs, as estimated in vehicle-inoculated mice which showed extremely elevated levels of CXC chemokines where no expression was expected. It is unlikely that these mice became naturally infected and CXC chemokine expression increased, since the room that housed the animals was specific-pathogen free. Thus, samples should be re-assayed by ELISA. Troubleshooting of this enzymatic assay is currently being performed in order to determine whether the results obtained are reliable or not. A commercial reagent diluent has been purchased to reduce the elevated background levels obtained. Otherwise, a repeat of the *in vivo* experiment would be required to elucidate whether these data are reproducible and determine whether IAV does increase CXC chemokine production in heterologous infection when mice are infected with $1x10^4$ PFU of IAV.

4.3. Contribution of each individual infection to the IL-1β dysregulation seen in heterologous infection

IL-1β protein is expressed as an inactive pro-form that requires post-translational processing into a cleaved form in order to achieve potent inflammatory activity. In many inflammatory systems, this processing is caspase-1-dependent as consequence of the inflammasome activation (80). We detected significantly increased IL-1β levels in heterologously-infected mice compared to single-pathogen infections (Figure 4 and 13). The study of the individual contribution of each pathogen to IL-1β production and caspase-1 activation suggested that IAV-induced IL-1β production peaked at day 3 and 5 post-infection and was reduced by day 14. We observed mainly expression of inactive pro-IL-1β rather than the active form (Figure 8). IAV-induced caspase-1 activation was

observed by day 3 but peaked at day 14 or later (Figure 9). These data indicated that IAV-induced IL-1β expression peaked during the first week of infection whereas caspase-1 activation peaked 2 weeks post-infection or later. Likewise, *B. parapertussis*-induced IL-1β production peaked at day 3 and was reduced by day 7. We observed increased expression of the pro-form and the active form (Figure 11). However, caspase-1 activation persisted increased at day 7 (Figure 12). These data, together, indicated that despite a delayed and prolonged inflammasome activation, the resolution of the IL-1β production and the neutrophilic inflammation was the result of a decrease in the levels of total IL-1β, implying that the transcriptional or translational regulation of IL-1β is crucial for the resolution of the inflammatory response, as opposed to regulation of IL-1β production through its processing via the inflammasome. Of note, IAV-induced IL-1β levels were lower than *B. parapertussis*-induced levels, thus suggesting that *B. parapertussis* could induce higher transcription and translation of IL-1β than IAV.

In addition, *B. parapertussis* has been demonstrated to induce caspase-1 activation later than day 1, but interestingly, IL-1β expression had been already detected significantly increased compared to non-infected mice at this time point (Figure 11 and 12, respectively). The data indicated that at the early stages of *B. parapertussis* infection, alternative caspase-1-independent mechanisms might trigger the induction of mature IL-1β. For instance, there is evidence that *casp-1*$^{-/-}$ mice, although reduced, still express mature form of IL-1β upon injection with monosodium urate monohydrate crystals –a danger-associated molecular pattern (DAMP). Thus, production of active IL-1β is also triggered by caspase-1-independent mechanisms (117). Furthermore, it has been shown

that pro-IL-1β can be cleaved by different proteases in addition to caspase-1, such as neutrophil elastase, proteinase-3, matrix metalloprotease-9 (MMP9), and cathepsin-G, which are produced by neutrophils recruited to sites of tissue damage (117-119). Moreover, it is also known that in macrophages enhanced pro-IL-1β processing depends on caspase-1, whereas in neutrophils IL-1β secretion is caspase-1 independent and depends on serine proteases (120). It is thought that activation of pro-IL-1β occurs in an inflammasome-independent fashion in situations where neutrophils are the major cell population in the inflammatory infiltrate (80).

Taken together, the data discussed here suggest that superinfection of IAV-infected mice with *B. parapertussis* at day 5 involves elevated levels of pro-IL-1β induced by both IAV and *B. parapertussis* that are processed by IAV-induced active caspase-1 as well as other caspase-1 independent mechanisms induced by the bacteria. Consequently, a considerably high pool of active IL-1β levels is being produced in heterologously-infected mice, subsequently leading to the increased neutrophil recruitment observed. In fact, analysis of IL-1β expression in heterologously-infected mice showed that these mice express higher levels of pro- and active IL-1β at any time point (Figure 13). Importantly, while IAV only- or *B. parapertussis* only-infected mice were able to control IL-1β production by D5+7, heterologously-infected mice showed an exacerbated IL-1β dysregulation. The reason why heterologously-infected mice cannot regulate and decrease the transcription and translation of IL-1β needs to be elucidated.

4.4. IL-1β dysregulation in heterologously-infected mice may be consequence of their impairment in bacterial clearance

IL-1β is a potent cytokine that drives the host inflammatory response and plays an essential role in innate as well as adaptive immunity (77). Therefore, its production and activity needs to be tightly regulated at the levels of expression, synthesis and secretion (121). IL-1β is synthesized as a precursor molecule (31 kDa) that can be cleaved into its mature and active form (17 kDa) by the protease caspase-1. This activation occurs when the cells receive an activator signal, either a PAMP or a DAMP, which triggers the assembly of a large molecular complex called inflammasome where caspase-1 activity is regulated (122). In this study, we demonstrated that both IAV and *B. parapertussis* were able to activate the inflammasome and induce caspase-1 activation (Figure 9 and 12, respectively). However, analysis of IL-1β by immunoblotting showed not only bands at the 31 kDa and 17 kDa, but also a pattern of several intermediate bands with different MWs (Figure 11B, 13B). While other studies in the literature showed two clearly separated bands for the pro-form and the cleaved form, our results always showed the same similar pattern of bands whenever IL-1β was expressed, whether it was in bacterial- or viral-infected lung homogenates. The difference between many of those published studies and ours relies on the fact that the IL-1β assessed was secreted in *in vitro* supernatants whereas we assayed IL-1β from *in vivo* lung homogenates. Many proteins, including proteases, are contained in these homogenates that might interfere with the proper cleavage of IL-1β. Moreover, it has been shown that pro-IL-1β can be cleaved by different proteases in addition to caspase-1, such as elastase, proteinase-3 and MMP9

which are produced by neutrophils recruited to sites of tissue damage (117-119). It could be that these other proteases act on different sites of the pro-IL-1β molecule, generating active forms of diverse MWs. However, further analysis is required to ensure that the bands different to 31 and 17 kDa are also IL-1β-derived and not unspecific binding of the anti-IL-1β antibody to other proteins. To test this, anti-IL-1β antibodies will be pre-treated with recombinant IL-1β prior incubation with the membrane in the immunoblotting. Thus, if the intermediate bands are absent from the analysis, it will become clear that they were processed IL-1β as well.

Inflammation is the response of the innate immune system to tissue injury caused by pathogens, cellular stress or environmental insults. Most viral and bacterial PAMPS are known to induce inflammatory responses upon recognition by PRRs such TLRs in the host immune cells (116). TLR activation triggers different signalling cascades that result in NF-κB activation and the synthesis of various pro-inflammatory molecules, including IL-1β. Interestingly, in the results presented in this report, the profile of IL-1β production observed upon *B. parapertussis* infection coincided with the profile found in bacterial burden in the lung (Figure 10 and 11). IL-1β production in *B. parapertussis*-infected mice initially increased at the same time that lung bacterial burden did. There is also a correlation between the time points when both bacterial burden and IL-1β production peaked. Eventually, levels of IL-1β were reduced by day 7 when clearance of *B. parapertussis* seemed to be under control. It is believed that IL-1β production in IAV-infected mice also correlated with the viral load in the lung, and that reduction of IL-1β production by day 14 is due to clearance of the virus from the lung. However, this

hypothesis cannot be verified here since viral titres were not measured at those time points. Therefore, these data suggest that viral and bacterial burden could be driving IL-1β expression and its regulation at the transcriptional and translational levels, as discussed earlier. Similarly, the dysregulated IL-1β production observed in heterologously-infected mice (Figure 13) coincided with the exaggerated bacterial burden found in the lung of these mice (Figure 3). According to the previous discussion, the inability of heterologously-infected mice to clear the *B. parapertussis* infection could be preventing the regulation of IL-1β production at the transcriptional level. Thus, as long as *B. parapertussis* keep replicating in the lung, and the AMs and neutrophils are incapable of clearing the bacteria, expression of pro-IL-1β via NF-κB will still be induced. Since levels of active caspase-1 have been shown to be significantly increased in these mice (Figure 14), pro-IL-1β will be cleaved into active IL-1β, exerting its biological activity by inducing CXC chemokines and the subsequent neutrophil recruitment. However, our laboratory previously established that the immunopathology of heterologous infection was independent of the bacterial burden (28). The hypothesis discussed here disagrees with this statement, since according to the data presented here, IL-1β production and the subsequent inflammatory mediators seem to be dependent on the bacterial burden. In conclusion, in order to diminish the inflammatory immunopathology observed in heterologous infection, it is crucial to elucidate why the intense and prolonged inflammatory response is incapable of clearing the pulmonary bacterial burden.

Previous studies indicated that neutrophils are required for *B. parapertussis* clearance (106). Nevertheless, it has been reported that infection with IAV impairs

neutrophil function to the extent that partial depletion of neutrophils from IAV-infected mice does not have a further detrimental effect on the antibacterial defence (111). Impairment of the antibacterial function of AMs by IAV has also been reported (88, 112). At the time of superinfection of IAV-infected mice with *B. parapertussis* (day 5), a large number of neutrophils were recruited in the lung adding additional antiviral defences to AMs to fight the infection. Neutrophils are short-lived and undergo apoptosis shortly after they phagocytose a target, being removed by AMs and DCs by efferocytosis (37). Efferocytosis has been shown to compromise the AMs antibacterial function by inducing the release and autocrine activity of prostaglandin E2 (37). Thus, the availability and efficiency of AMs to combat the bacterial superinfection after IAV-infection is very limited while they are clearing the IAV-induced neutrophilia. Consequently, the host antibacterial defences are impaired, allowing *B. parapertussis* to replicate within the lung and inducing activation and release of IL-1β and emphasizing the ever-increasing neutrophil recruitment. It is recommended to study the function of neutrophils and AMs isolated from heterologously-infected mice in order to shed light on this hypothesis. Eventually, the resolution of the inflammation several days or weeks after the bacterial superinfection of IAV is likely to occur through the intervention of the adaptive immunity. Zavitz *et al.* (28) demonstrated that the adaptive immune responses were not substantially affected in this model of heterologous infection. This hypothesis is consistent with the fact that survivors from the 1918 influenza pandemic who suffered from secondary bacterial superinfections presented a robust B-cell response against IAV antigens even 80 years later (123).

Collectively, the data suggest a mechanism involving IL-1β that is likely to play a critical role in the induction of the immunopathology emerged upon heterologous infection. Thus, different strategies could be pursued to intervene in the proposed cascade that leads to the severe pulmonary inflammation. Since the use of antibiotics to reduce of the lung bacterial burden apparently seemed to not have a beneficial outcome and people suffering from bacterial superinfection still succumbed, we elected to investigate whether inhibition of the signaling cascade leading to IL-1β activation would attenuate the inflammatory response. To do so, three different approaches are being pursued: two of them –*ASC*-gene deficiency and *caspase-1*-gene deficiency– avoided the formation of the inflammasome complex and inhibited the processing of pro-IL-1β into its mature active form. The third one –*IL-1β*-gene deficiency– attempted to identify the suggested essential role of the cytokine IL-1β in the induction of the inflammatory immunopathology.

4.5. Importance of the inflammasome in the immunopathology of heterologous infections

Processing of bioactive IL-1β mainly depends on activation of caspase-1 by multiprotein complexes termed inflammasomes (80). Several inflammasomes have been described for the activation of caspase-1, which occurs after oligomerization of caspase-1 with the NLRs or absent in melanoma 2 (AIM2) proteins. This interaction takes place through CARD-CARD domain interactions. While NLRC4 and NLRP1 can interact directly with caspase-1 through their CARD domains, NLRP3 and AIM2 need the presence of the adaptor protein ASC to recruit caspase-1 into the complex through pyrin

domains (PYD)-PYD interactions (122). Therefore, deficiency in ASC inhibits the formation of NLRP3 inflammasome, affecting caspase-1 activation and the subsequent processing of IL-1β. For that reason, $ASC^{-/-}$ mice were considered a good tool/approach to study whether inhibition of the inflammasome and a reduction in IL-1β production attenuates the inflammatory response, improving the clinical symptoms upon heterologous infection. Indeed, $ASC^{-/-}$ mice showed a beneficial effect –in terms of lower body weight loss and reduced pulmonary inflammation– compared to WT mice upon heterologous infection (Figure 16). This reduction could be related to the significantly decreased production of IL-1β and CXC chemokines observed in $ASC^{-/-}$ mice (Figure 19). These data corresponded to two independent experiments. However, these significant differences between $ASC^{-/-}$ and WT mice could not be entirely reproduced a third time, neither at the level of body weight, pulmonary inflammation nor cytokine production (Figure 20 and 21). Unfortunately, the reason why the divergences between $ASC^{-/-}$ and WT mice did not reach statistical significance in the last experiment are unknown. The fact that $ASC^{-/-}$ mice showed higher caspase-1 activation than WT mice –when a considerably reduction was expected (Figure 22) – led us to suspect that $ASC^{-/-}$ mice might have been mixed by mistake in the breeding room of the Animal Facility and experiments were conducted in a different strain than $ASC^{-/-}$ mice. Therefore, genotyping of $ASC^{-/-}$ mice will be carried out to clarify whether or not these mice were *ASC*-gene deficient. Assuming that these mice were not *ASC*-deficient and, thus, only the initial results obtained are reliable, the reduction of IL-1β production by inflammasome inhibition allows regulation of IL-1β overproduction and improves the inflammatory

immunopathology. However, the bacterial burden in $ASC^{-/-}$ mice was still uncontrolled, being even significantly higher than in WT mice, thus suggesting that IL-1β may be involved in the control of the bacterial burden. Despite the promising data resulted from $ASC^{-/-}$ mice, further investigations need to be carried out before addressing any therapeutic approach. Future experiments will involve caspase-$1^{-/-}$ mice (purchased from The Jackson Laboratories) and IL-$1\beta^{-/-}$ mice (a kind gift from Yoichiro Iwakura, Center for Experimental Medicine and Systems Biology, Institute of Medical Science, University of Tokyo, Tokyo, Japan) to assess, in a more direct manner, the outcome in heterologous infection upon IL-1β reduction. Differences in body weight, pulmonary inflammation and cytokine production (IL-1β, CXCL1 and CXCL2) will be assessed as aforementioned for previous experiments. If the results indicate that IL-1β is playing the major role in the immunopathology, a caspase-1 inhibitor or anti-IL-1β antibodies would be tested as therapeutic approach to treat heterologous infections. Diverse anti-IL-1 therapies such as use of recombinant IL-1Ra (called Anakinra) or immunoneutralization of IL-1β using a monoclonal anti-IL-1β antibodies (called Canakinumab) has been reported to have beneficial consequences in patients suffering from pro-inflammatory diseases such rheumatoid arthritis or cryopyrin-associated periodic syndromes (124, 125).

4.6. Relevance of these findings in the field of heterologous infection

To date, many clinical studies have confirmed increased morbidity and mortality of IAV-infected patients caused by secondary bacterial infections. Thus, a synergism between IAV infections and bacterial pneumonia has been suggested. Different animal models of post-influenza bacterial pneumonia have been developed in order to study the

mechanisms by which IAV predisposes to bacterial superinfection. To date, the mechanisms suggested could be summarized into 3 different categories: 1) Altered bacterial adherence to respiratory epithelium after viral infection, 2) impaired leukocyte recruitment and/or activation, and 3) dysregulated cytokine responses (reviewed in (126)).

IAV has a tropism to infect alveolar epithelial cells which results in phenotypic changes that alter the cellular characteristics of the epithelial cells (127). Infected epithelial cells expose or modify their surface molecules and cell receptors that promote the adherence of bacterial pathogens such as *S. pneumoniae* (110). Lysis of the infected epithelial cells by innate immune cells exposes the basal basement membrane, facilitating the adherence of bacteria to fibronectin or glycoproteins (128). In addition, IAV also impairs the mechanical clearance of bacteria from the airway by reducing the mucociliary velocity in the trachea (129).

Most studies showed an increased neutrophil recruitment at 24 hours post-secondary bacterial challenge (73, 130). However, defects in their functionality, including decreased phagocytic activity, myeloperoxidase production, respiratory burst and lysozyme secretion has been suggested (111, 130, 131). Engelich *et al.* (2001) suggested that increased apoptosis and reduced survival in neutrophils coinfected with IAV and *S. pneumoniae* (132). In addition, impaired function of both resident and recruited AMs has been described. Early after IAV infection the phagocytic capacity of AMs is enhanced, whereas at later time points the ability to phagocytose and kill bacteria is markedly reduced (112, 133). Small *et al.* (2010) proposed that the impaired AM function is due to

a reduction in the accumulation of NK cells and their production of TNF-α in mice coinfected with IAV and *S. aureus* (75).

Furthermore, dysregulated cytokine and chemokine production promotes deleterious tissue damage and impairs innate responses required for effective clearance of bacterial pathogens, as shown in the present studies. However, some controversy remains in this area. While some studies showed enhanced production of proinflammatory cytokines (such as TNF-α, IL-6, IL-1β, and chemokines) post-IAV infection (130), others stated that IAV-infected macrophages produced decreased levels of neutrophil chemoattractants (such KC and MIP-2) (134). Moreover, reduced IL-15 production by AMs has been shown to be involved in the reduced recruitment of NK cells and NK-derived TNF-α production, which in turn impaired activation of AM phagoctyic activity (75). Conversely, IAV was shown to induce immunosuppressive cytokines such IL-10 (135), as well as *B. parapertussis* (136), inhibiting leukocytes and impairing the antibacterial host defense by limiting a protective IFN-γ response. Type I and type II IFNs are released by the host for antiviral defense and to induce the adaptive immunity. Interestingly, these IFNs suppress host response to secondary bacterial challenge (112). IAV has evolved mechanisms to combat these IFN responses. IAV expresses non-structural protein 1 (NS1) protein, a potent virulence factor that inhibits IFN synthesis and induction of antiviral responses in DCs and airway epithelial cells, thus, allowing the virus to overcome host defenses and replicate efficiently (137).

Not only impairment of the innate immune defenses has been proposed, other mechanisms involving the adaptive immune response have been studied also. Th17 cells

have been recognized for their role mediating as a link between the innate and the adaptive immunity. Th17 cells release IL-17, which induce the NF-κB and mitogen-activated protein kinase (MAPK) pathways leading to release of proinflammatory mediators (138). Additionally, Th17 cells release IL-22 and IL-21, which induces neutrophil activation, tissue remodeling and repair, and production of antimicrobial proteins (139). Infection of mice with *Klebsiella pneumoniae*, *B. pertussis*, and *S. pneumoniae* elicited a robust Th17 response, and inhibition of the IL-17 pathway enhanced susceptibility to these pathogens. This was demonstrated by Tilg *et al.* (2009), who suggested that type I IFN suppress IL-17 expression and Th17 differentiation (140). Kudva *et al.* (2011) also showed that IAV inhibits the Th17-mediated host defense by expression of type I-IFN, which is required to combat bacterial pneumonia and this would increase the susceptibility to secondary bacterial infections (91).

Together, all these proposed mechanisms help to build a general idea of how IAV actually increases the susceptibility to secondary bacterial infections. There is likely not just a unique mechanisms responsible for this phenomenon, but a combination of many of them, if not all. Further investigation needs to be elucidated in order to determine which pathways may be more critical and determine a therapeutic approach that attenuates the increased morbidity and mortality in bacterial pneumonia post-IAV infection. Our findings, although focused on the dysregulation of the pro-inflammatory cytokine IL-1β, attempt to link the impairment in bacterial clearance and the related uncontrolled bacterial burden caused by IAV infection with the subsequent exaggerated production of IL-1β and the severe neutrophil and macrophage recruitment into the lung, the function of which is

likely to be altered. We hypothesize that by targeting the IL-1β pathway and re-establishing the adequate levels of IL-1β, the subsequent release of chemokines and increased neutrophilia may be contained. However, we believe that the IL-1β dysregulation is consequence of the continuous sensitization of *B. parapertussis* that persists in the lung due to inability of AMs and neutrophils to clear it. Therefore, therapies directed to reduce the bacterial burden of the lung may interrupt the proinflammatory cascades initiated upon sensitization. β-lactam antibiotics such ampicillin has been shown to cause lysis of bacteria, releasing their intracellular components and causing subsequent recruitment of neutrophils into the lungs, resulting in a consolidative pneumonia, necrotic lung damage, and significant mortality (141). In contrast, treatment with macrolide antibiotics such as azithromycin prevented neutrophil influx and decreased subsequent mortality of mice. However, combined treatment with ampicillin and azithromycin to clear an azithromycin-resistant strain also cured secondary pneumonia (141). These finding suggest that strategies for eliminating bacteria without induction of lysis, together with immunomodulation of inflammation, could be a successful therapy to reduce the immunopathology in heterologous pulmonary infections.

4.7. Conclusions and future directions

The present studies demonstrated the increased susceptibility of IAV-infected mice to an otherwise subclinical bacterial infection by *B. parapertussis*. Here, we proposed that dysregulation in IL-1β production likely derived from the continuous sensitization of the bacteria as the upstream cause of the MIP-2 overproduction observed

in heterologous infection. The impairment in the antibacterial function of AMs and neutrophils upon IAV infection may be the cause of the exaggerated bacterial burden. This study also demonstrated that reduction in IL-1β production by blockade of the inflammasome seemed to provide an improvement in the clinical symptoms and the immunopathology of the disease. Thus, interventions to attenuate the uncontrolled bacterial burden and the inflammatory responses derived from the subsequent IL-1β overproduction should be further investigate as possible therapeutic approaches to treat bacterial superinfections in the future influenza pandemics.

Future directions will include experiments of bacterial superinfection post-IAV in caspase-$1^{-/-}$ and IL-$1\beta^{-/-}$ mice. We will further investigate whether a reduction in the IL-1β overproduction observed in heterologous infection can successfully control the proinflammatory profile observed in these mice. However, due to caspase-1-independent mechanisms of IL-1β activation, especially in situations where neutrophils are the major cell population in the inflammatory infiltrate, a beneficial outcome might not be achieved. Similarly, deficiency in IL-1β might cause impaired survival, higher bacterial burden and decreased neutrophilia in the lung, but enhanced tissue damage since IL-1β is required for eliciting innate and adaptive immune response against infections.

Finally, if reduction of IL-1β turned out to be promising to control the immunopathology of heterologous infection, therapeutic treatments such as caspase-1 inhibitor or anti-IL-1β antibody should be tested. Alternatively, beneficial therapeutic effects may be also achieved with the IL-1Ra, independent of the mechanisms involved in the processing of the pro-IL-1β.

Chapter 5: Figures and legends

Figure 1: Body weight loss and mortality rate are viral dose-dependent. C57BL/6 mice were infected with different doses of IAV at day 0 and superinfected with 500,000 CFU of *B. parapertussis* at day 5. Body weight and mortality was recorded during the course of infection. Each experimental group had a sample size (n) = 5 animals.

A) Body weight and survival of mice infected with 2.5 $x10^5$ PFU of IAV.

B) Body weight and survival of mice infected with 2.5 $x10^4$ PFU of IAV.

C) Body weight and survival of mice infected with 1 $x10^4$ PFU of IAV.

A

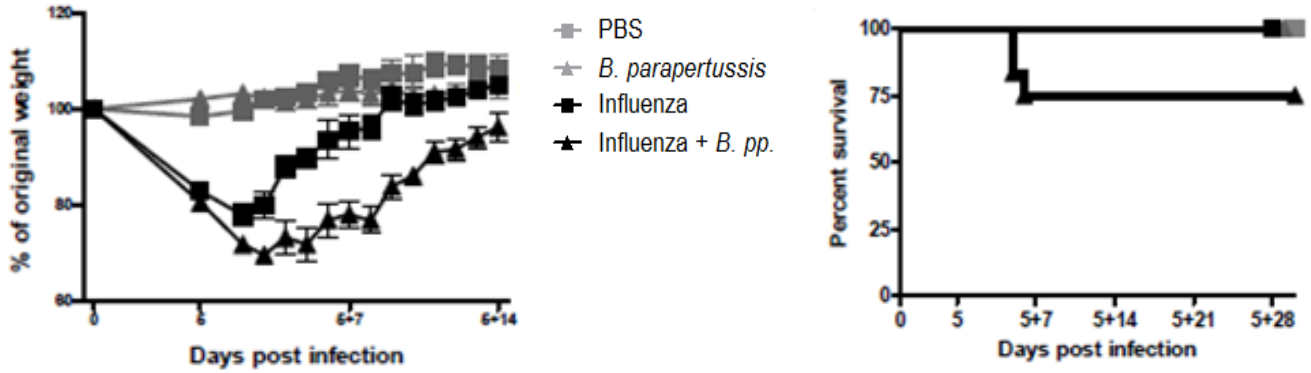
% of original weight
Days post infection
PBS
B. parapertussis
Influenza
Influenza + B. pp.
Percent survival
Days post infection

B

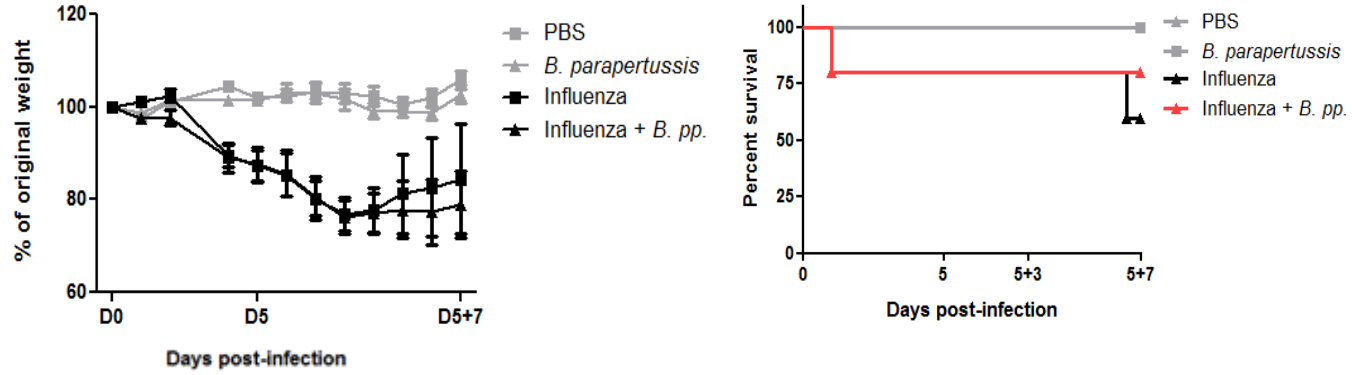
% of original weight
D0
D5
D5+7
Days post-infection
PBS
B. parapertussis
Influenza
Influenza + B. pp.
Percent survival
Days post-infection

C

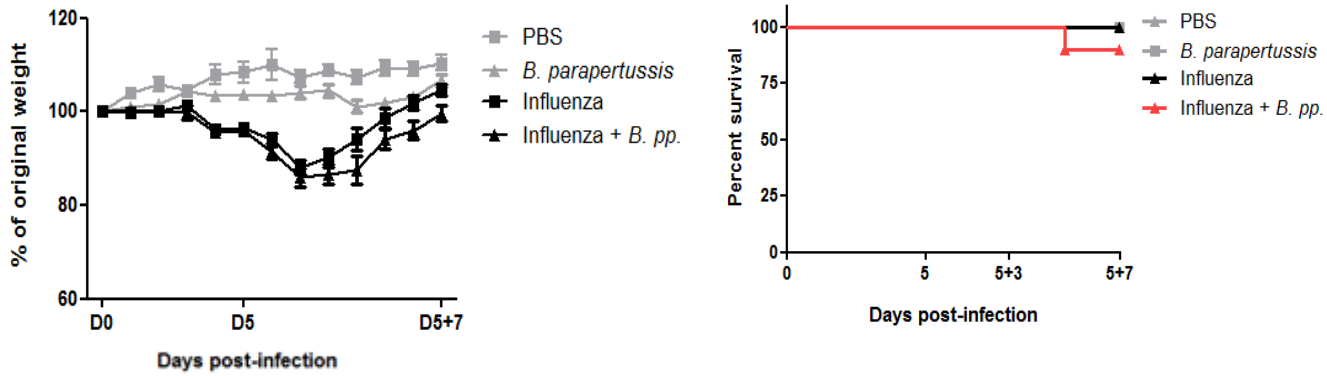
% of original weight
D0
D5
D5+7
Days post-infection
PBS
B. parapertussis
Influenza
Influenza + B. pp.
Percent survival
Days post-infection

Figure 2: Determination of bacterial and viral titres.

(A) New standard curve for *B. parapertussis* growth generated upon replacement of a spectophotometer. *B. parapertussis* was grown in blood agar for 3 days, isolated colonies were added into Scholte-Stainer broth and incubated at 37ºC in shaking incubator. The optical density of the broth at 600nm (OD_{600}) was taken at time 12, 20, 21, 22, 23, 24, 25 and 26 hours post incubation. 35µl from the broth were serially-diluted, plated onto Bordet-Gengou blood agar and incubated at 37ºC for 3 days, after which viable colonies were enumerated. The new equation of the curve that allows the calculation of the bacterial concentration (CFU/ml) based on the OD_{600} of the broth is:

$$[\text{bacteria}] = (OD_{600}-0.2852) \times (1.56\times10^{9}\ \text{CFU/ml}).$$

(B) Titre of the IAV in lung homogenates of mice at day 5 post-infection, using the plaque assay technique. Lung homogenates were incubated onto MDCK cell monolayers at 37ºC for 2 days. Viral particles infected and lysed cells, creating plaques that could be enumerated.

A

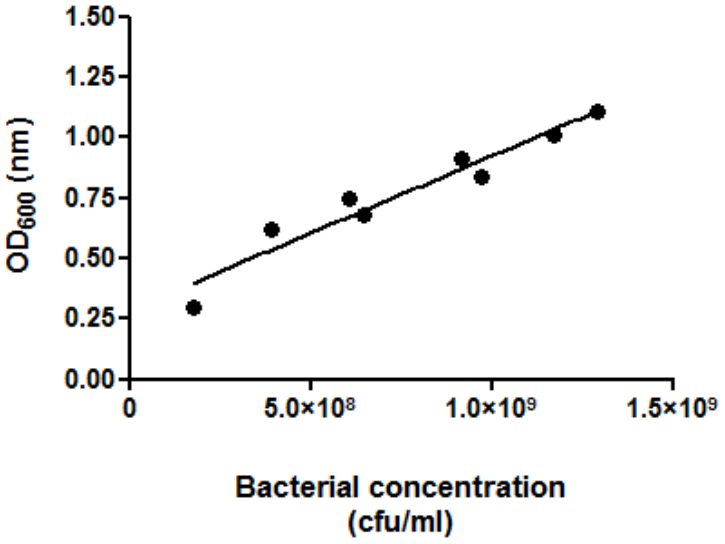

$$cfu/ml = (OD-0.2852) \times 1.56 \times 10^9$$

B

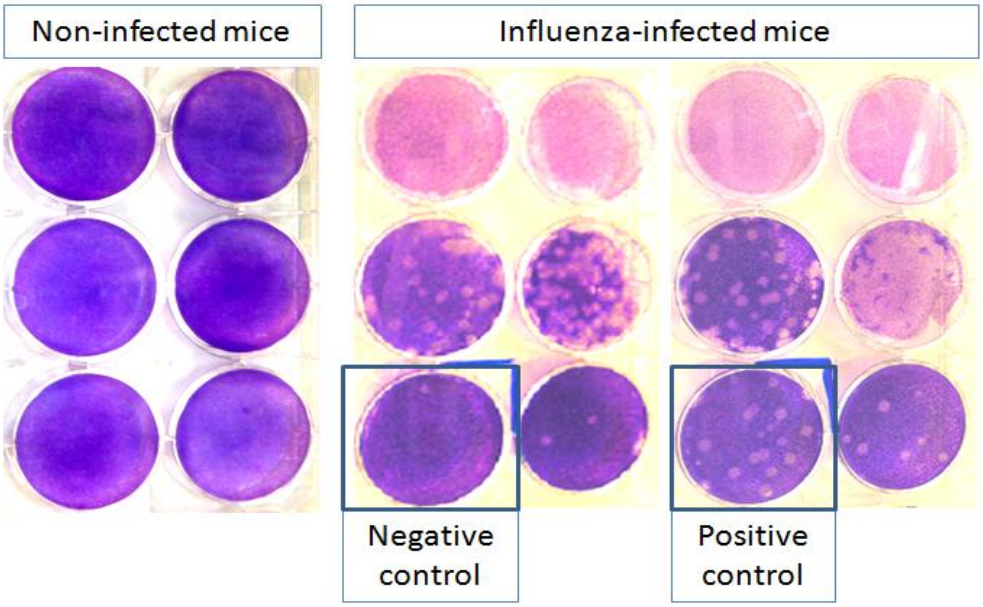

Figure 3: Effect of heterologous infection on body weight and pulmonary inflammation for a twelve day period. Mice were inoculated with PBS or IAV intranasally at day 0, and superinfected with sterile PBS or *B. parapertussis* at day 5. Mice were sacrificed at D5+1, D5+3, or D5+7 post infection. Vehicle-only, IAV-only, and *B. parapertussis*-only infected groups were used for control purposes. X axes represent days post-infection.

(A) Body weights recorded during the 12 days post infection.

(B) Bacterial burden in lung homogenates.

(C) Pulmonary cellular infiltration, measured by total cell number (TCN), mononuclear cells (MNC) and neutrophils (NEU) enumerated in the BAL at the mentioned time points. Each experimental group at each time point consisted of an n=5 mice. Data were expressed as the mean±SEM. No statistical analyses were required to be performed.

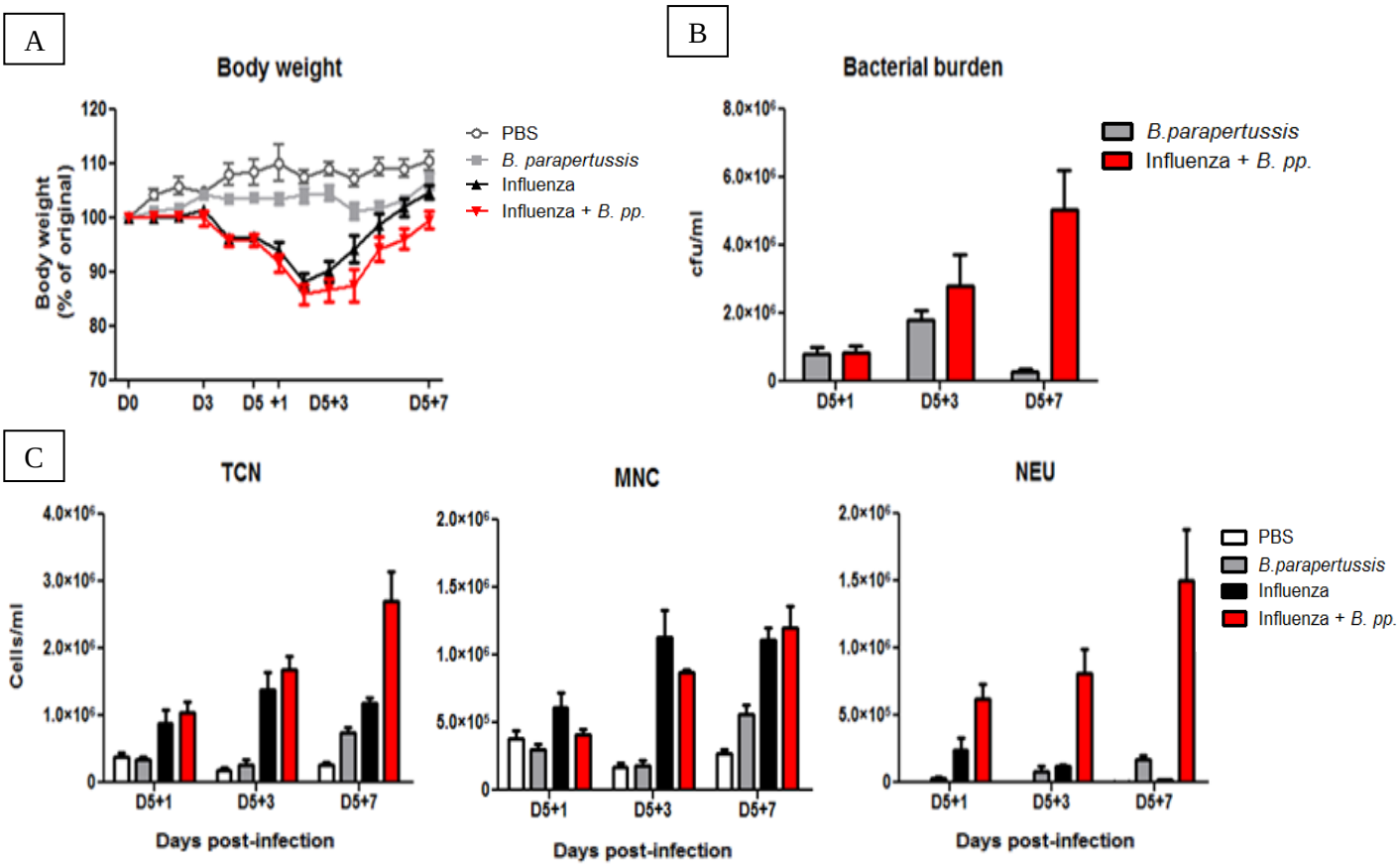
A
Body weight
Body weight (% of original)
120
110
100
90
80
70
D0
D3
D5 +1
D5+3
D5+7
PBS
B. parapertussis
Influenza
Influenza + B. pp.
B
Bacterial burden
cfu/ml
8.0×10⁶
6.0×10⁶
4.0×10⁶
2.0×10⁶
0
D5+1
D5+3
D5+7
B.parapertussis
Influenza + B. pp.
C
TCN
MNC
NEU
Cells/ml
4.0×10⁶
3.0×10⁶
2.0×10⁶
1.0×10⁶
0
2.0×10⁶
1.5×10⁶
1.0×10⁶
5.0×10⁵
0
D5+1
D5+3
D5+7
Days post-infection
PBS
B.parapertussis
Influenza
Influenza + B. pp.

Figure 4: Heterologous infection induces exacerbated IL-1β production in the BAL and lung homogenates.

A) **Quantification of IL-1β by ELISA** in the BAL and in lung homogenates. Mice were inoculated with PBS or IAV (X axis) intranasally at day 0, and superinfected with sterile PBS (open bars) or *B. parapertussis* (filled bars) at day 5. Mice were sacrificed at D5+7 post infection. Each experimental group at each time point consisted of an n=5 mice. Data were expressed as the mean±SEM and were analyzed by 2-way ANOVA. *, †, ‡ denote a significant difference at $p<0.05$ compared to PBS, *B. parapertussis*, and IAV-exposed mice, respectively.

B) **Determination of the IL-1β form by western blot** in lung homogenates 5 days post-IAV infection (non-infected *vs.* IAV-infected mice) and D5+7 post-heterologous infection (vehicle-inoculated mice, *B. parapertussis* only-, IAV only- and heterologously-infected mice). Lung lobes were homogenized in lysis buffer containing protease inhibitor cocktail. The protein concentration was quantified by a dye-binding assay. Samples from each experimental group were pooled together and lysis buffer and loading buffer were added to make a final concentration of 80µg protein/50µl volume. A prestain protein ladder and the samples were separated electrophoretically in a 15% polyacrylamide gel and transferred onto a nitrocellulose membrane. The membrane was blotted at 4ºC overnight with goat anti-mouse IL-1β antibodies, followed by incubation with secondary IRDye®-conjugated donkey anti-goat IgG antibodies. The membrane was finally scanned by infrared light to reveal the presence of the IRDye® using a Li-Cor Odyssey® infrared detector.

A

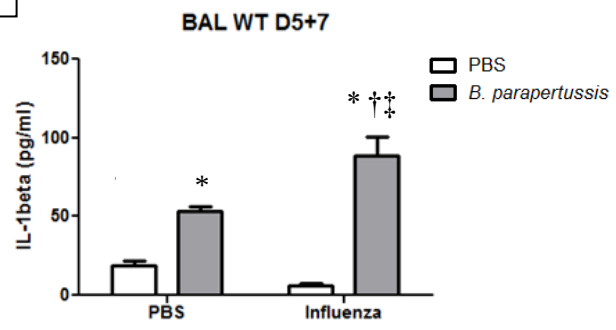
BAL WT D5+7
IL-1beta (pg/ml)
150
100
50
0
PBS
Influenza
* †‡
*
PBS
B. parapertussis

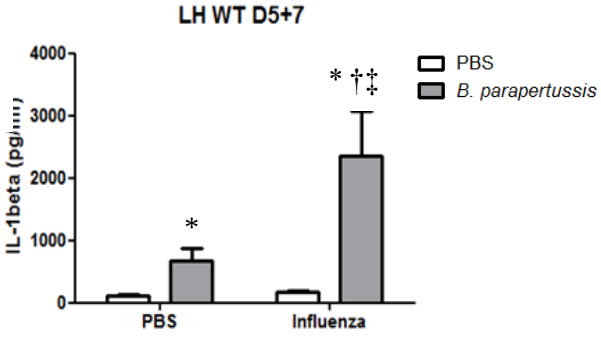
LH WT D5+7
4000
3000
2000
1000
0
PBS
Influenza
* †‡
*
PBS
B. parapertussis

B

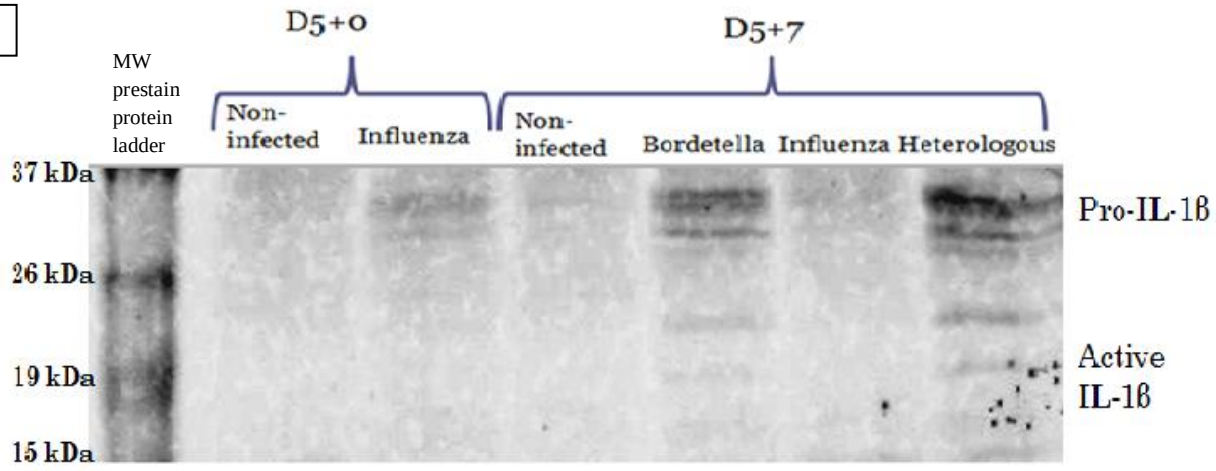
D5+0
D5+7
MW prestain protein ladder
Non-infected
Influenza
Non-infected
Bordetella
Influenza
Heterologous
37 kDa
26 kDa
19 kDa
15 kDa
Pro-IL-1ß
Active IL-1ß

Figure 5: Determination of relevant inflammatory mediators in lung during heterologous infection. Mice were inoculated with PBS or $2.5x10^4$ pfu of IAV (X axis) intranasally at day 0, and superinfected with sterile PBS (open bar) or *B. parapertussis* (filled bars) at day 5. Mice were sacrificed at D5+7 post infection. Levels of CXCL1/KC, CXCL2/MIP-2, CXCL5, CXCL7 and CXCL15 chemokines were quantified in lung homogenates by ELISA. Vehicle-only, IAV-only, and *B. parapertussis*-only infected groups were used for control purposes. Each experimental group at any time point consisted of an n=5 mice. Data were expressed as the mean±SEM and analyzed by 2-way ANOVA. *, †, ‡ denote a significant difference at $p<0.05$ compared to PBS, *B. parapertussis*, and IAV-exposed mice, respectively.

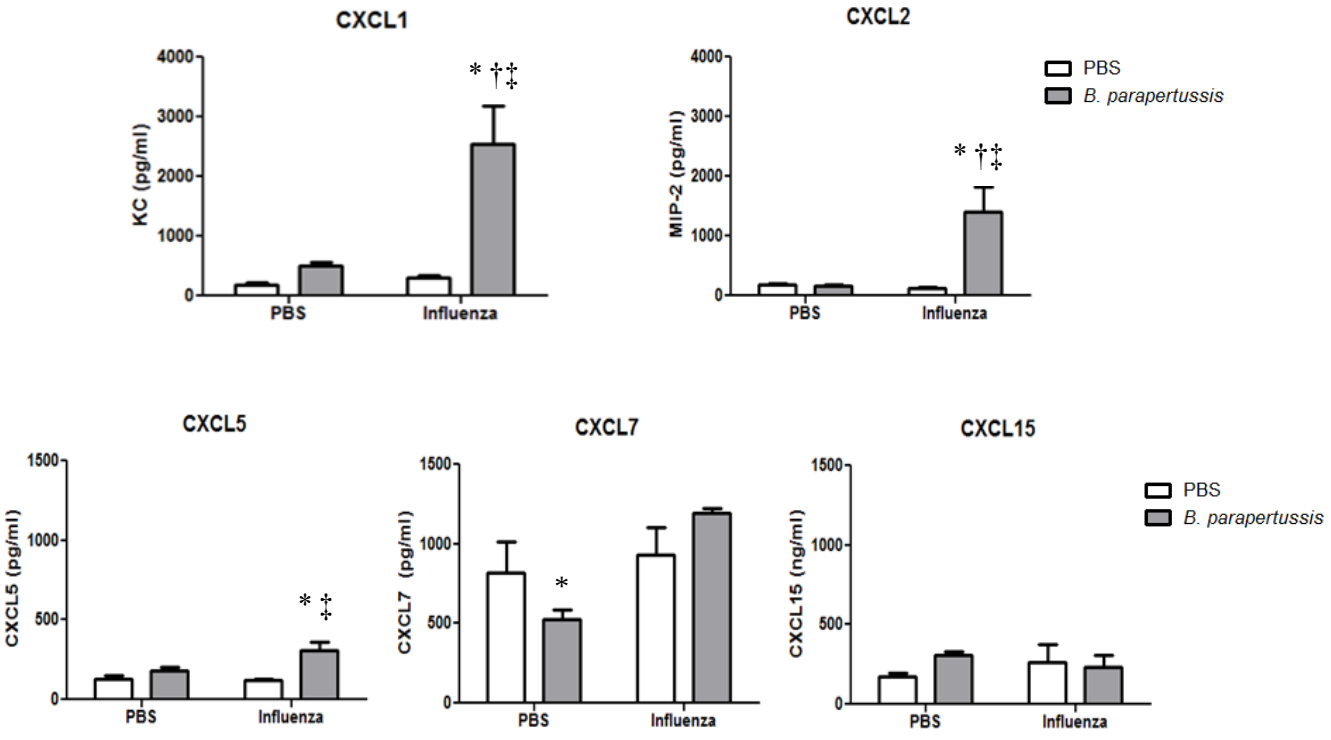
CXCL1
KC (pg/ml)
4000
3000
2000
1000
0
PBS
Influenza
* †‡
CXCL2
MIP-2 (pg/ml)
4000
3000
2000
1000
0
PBS
Influenza
* †‡
PBS
B. parapertussis
CXCL5
CXCL5 (pg/ml)
1500
1000
500
0
PBS
Influenza
* ‡
CXCL7
CXCL7 (pg/ml)
1500
1000
500
0
PBS
Influenza
*
CXCL15
CXCL15 (ng/ml)
1500
1000
500
0
PBS
Influenza
PBS
B. parapertussis

Figure 6: Hypothesis schema for the production of different forms of IL-1β and caspase-1 throughout the course of heterologous infection.

It was hypothesized that IAV does induce activation of caspase-1 and thus production of active IL-1β during the first days of infection. However, upon 5 post-infection only pro-IL-1β levels could be detected. Therefore, when IAV-infected mice were superinfected with *B. parapertussis*, the bacteria induces pro-IL-1β expression and high levels of pro-IL-1β accumulate inside the cells. Since *B. parapertussis* activates the inflammasome, caspase-1 levels will be increased, and the high levels of pro-IL-1β will be processed into the active form and released from the cells.

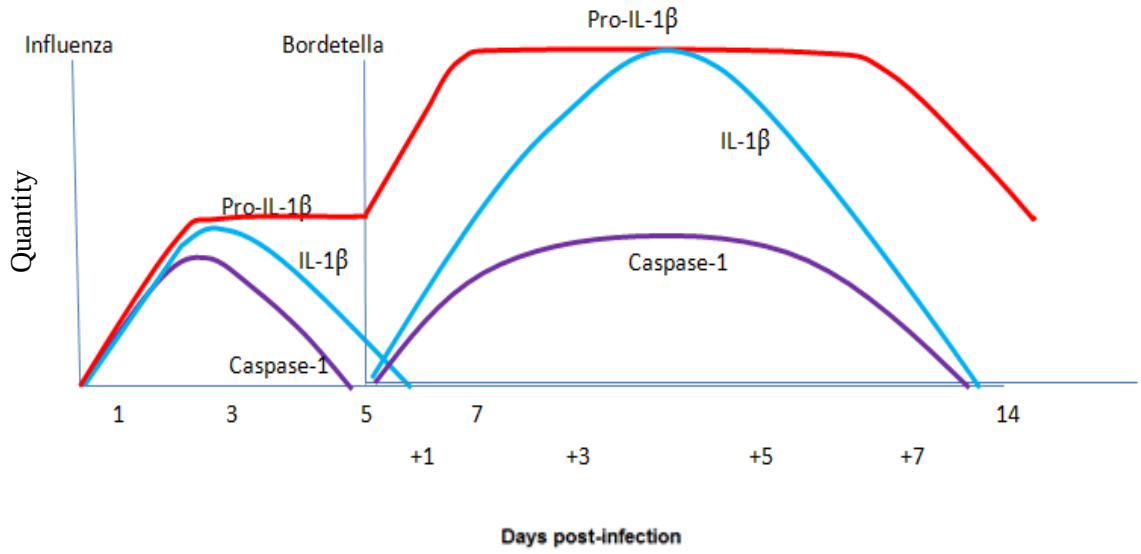
Influenza
Bordetella
Pro-IL-1β
IL-1β
Caspase-1
Quantity
1
3
5
7
14
+1
+3
+5
+7
Days post-infection

Figure 7: Effect of IAV infection on body weight and pulmonary inflammation for a 2 week period. Mice were infected with PBS (open bars) or IAV (filled bars) at day 0 and sacrificed at day 1, 3, 5 and 14 post-infection.

(A) Body weights recorded during the 14 days post infection.

(B) Total cell number, (C) mononuclear cells (MNC) and (D) neutrophils (NEU) were counted in the BAL at the time points mentioned above.

Each experimental group at any time point consisted of an n=5 mice. Data are shown as mean±SEM. No statistical analyses were required to be performed.

A

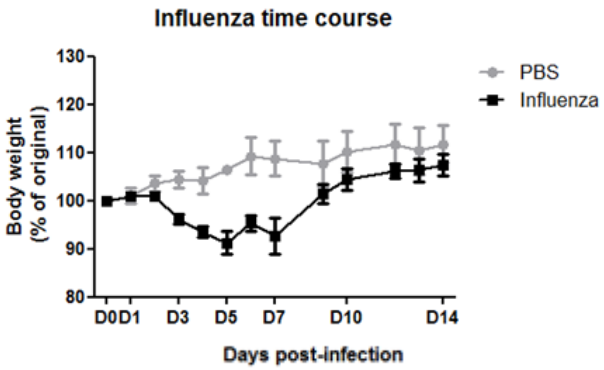
Influenza time course
Body weight (% of original)
130
120
110
100
90
80
D0D1 D3 D5 D7 D10 D14
Days post-infection
PBS
Influenza

B

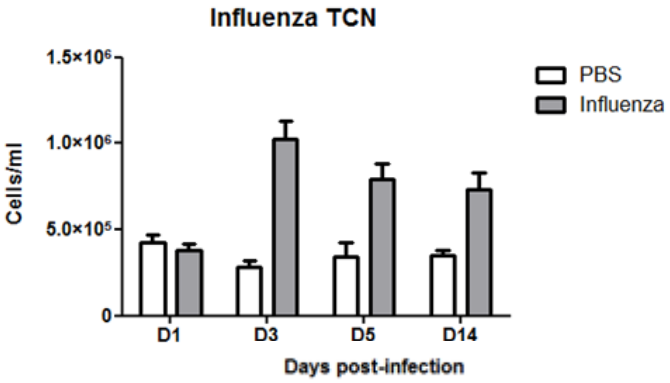
Influenza TCN
Cells/ml
1.5×10⁶
1.0×10⁶
5.0×10⁵
0
D1 D3 D5 D14
Days post-infection
PBS
Influenza

C

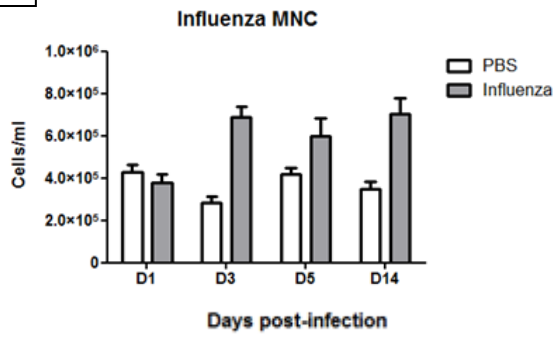
Influenza MNC
Cells/ml
1.0×10⁶
8.0×10⁵
6.0×10⁵
4.0×10⁵
2.0×10⁵
0
D1 D3 D5 D14
Days post-infection
PBS
Influenza

D

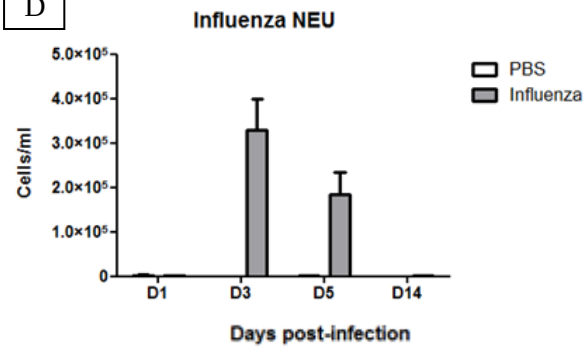
Influenza NEU
Cells/ml
5.0×10⁵
4.0×10⁵
3.0×10⁵
2.0×10⁵
1.0×10⁵
0
D1 D3 D5 D14
Days post-infection
PBS
Influenza

Figure 8: Analysis of IL-1β production and quantification of the main chemokines in lung homogenates at day 1, 3, 5 and 14 post-IAV infection. Mice were infected with PBS (open bars) or IAV (filled bars) at day 0 and sacrificed at the aforementioned time points. n=5 mice/group.

(A) Quantification of IL-1β, CXCL1 and CXCL2 levels by ELISA. Lung lobes were homogenized in PBS and cytokine levels were quantified by ELISA. Data were expressed as the mean±SEM of the concentration (pg/ml) for each cytokine. Data were analyzed by unpaired t-test. * denotes a significant difference at $p<0.05$ compared to PBS-exposed mice.

(B) Analysis of IL-1β processing by western blot. Lung lobes were homogenized in lysis buffer containing protease inhibitor cocktail. The protein concentration was quantified by a dye-binding assay. Samples from each experimental group were pooled together and lysis buffer and loading buffer were added to make a final concentration of 80µg protein/50µl volume. A prestain protein ladder and the samples were separated electrophoretically in a 15% polyacrylamide gel and transferred into a nitrocellulose membrane. The membrane was blot at 4ºC overnight with goat anti-mouse IL-1β antibodies, followed by incubation with secondary IRDye®-conjugated donkey anti-goat IgG antibodies. The membrane was finally scanned by infrared light to reveal the presence of the IRDye® using a Li-Cor Odyssey® infrared detector.

A

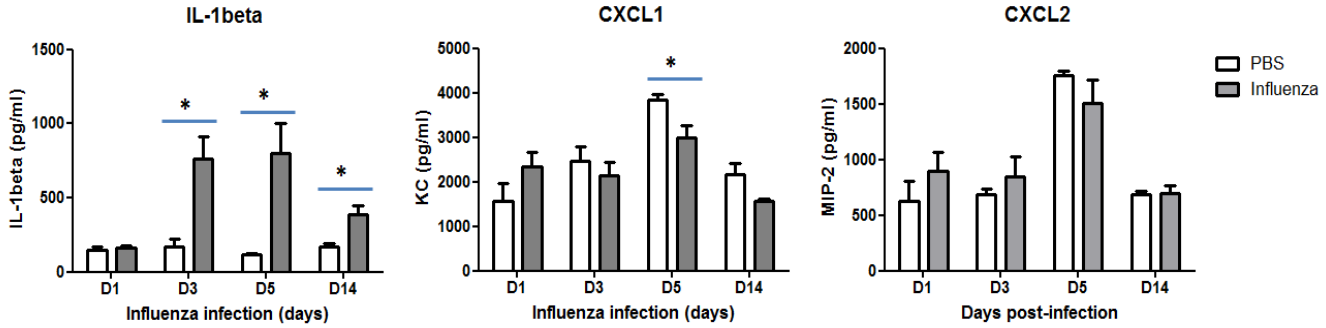
IL-1beta
IL-1beta (pg/ml)
1500
1000
500
0
D1
D3
D5
D14
Influenza infection (days)
CXCL1
KC (pg/ml)
5000
4000
3000
2000
1000
0
Influenza infection (days)
CXCL2
MIP-2 (pg/ml)
2000
1500
1000
500
0
Days post-infection
PBS
Influenza

B

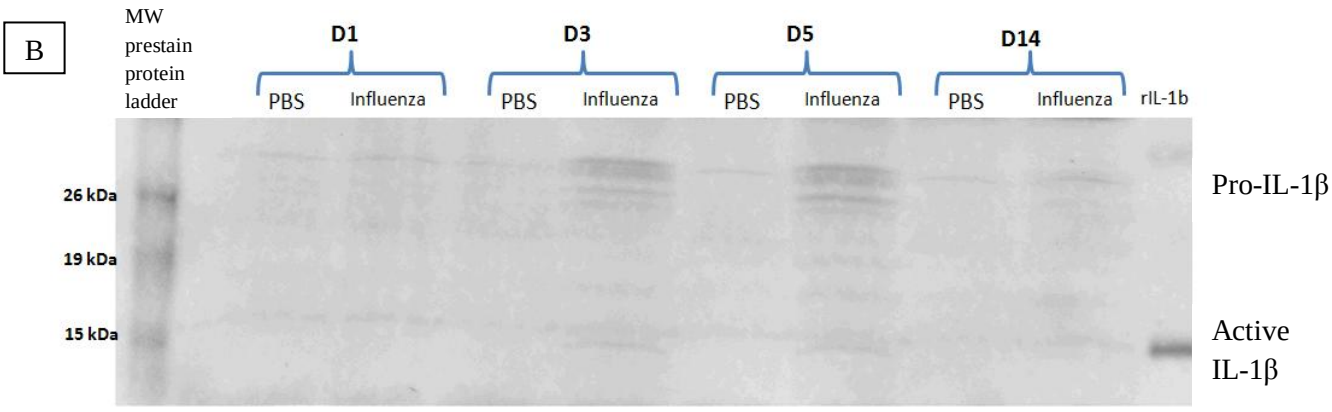
MW prestain protein ladder
D1
D3
D5
D14
PBS
Influenza
rIL-1b
26 kDa
19 kDa
15 kDa
Pro-IL-1β
Active IL-1β

Figure 9: Analysis of caspase-1 expression post-IAV infection. Mice were infected with PBS (open bars) or IAV (filled bars) at day 0 and sacrificed at the specified time points. n=5 mice/group

(A) **Caspase-1 western blot**. Lung lobes were homogenized in lysis buffer containing a protease inhibitor cocktail. The protein concentration was quantified by a dye-binding assay. Samples from each experimental group were pooled together and lysis buffer and loading buffer were added to make a final concentration of 80µg protein/50µl volume. A prestain protein ladder and the samples were separated electrophoretically in a 15% polyacrylamide gel and transferred onto a nitrocellulose membrane. The membrane was blotted at 4ºC overnight with rat anti-mouse caspase-1 antibodies, followed by incubation with secondary IRDye®-conjugated goat anti-rat IgG antibodies. The membrane was finally scanned by infrared light to reveal the presence of the IRDye® using a Li-Cor Odyssey® infrared detector.

(B) **Analysis of caspase-1 activity.** Lung lobes were homogenized in lysis buffer without protease inhibitor cocktail. The protein concentration was quantified by a dye-binding assay. Samples from each experimental group were pooled together containing the same amount of protein (50µg/50µl). Lung homogenates were mixed with reaction buffer, DTT, and the substrate YVAD-AFC. The plate was placed in a microplate reader at 37ºC. Samples containing active caspase-1 cleaved the substrate and free fluorescent AFC was measured every 10 minutes over a 2 hour period. The slope of the kinetic curve for each experimental group was extracted and compared to the vehicle-treated group.

A

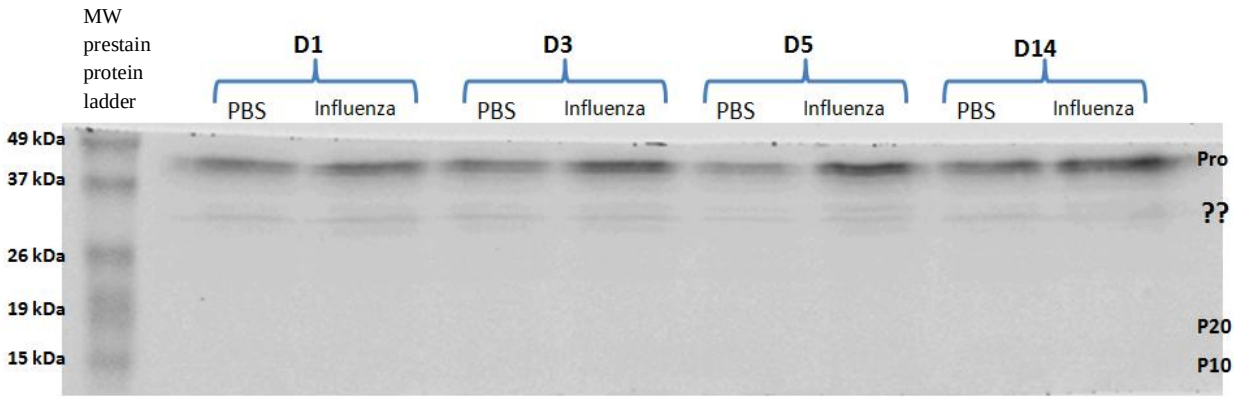
MW
prestain
protein
ladder
D1
D3
D5
D14
PBS
Influenza
PBS
Influenza
PBS
Influenza
PBS
Influenza
49 kDa
37 kDa
26 kDa
19 kDa
15 kDa
Pro
??
P20
P10

B

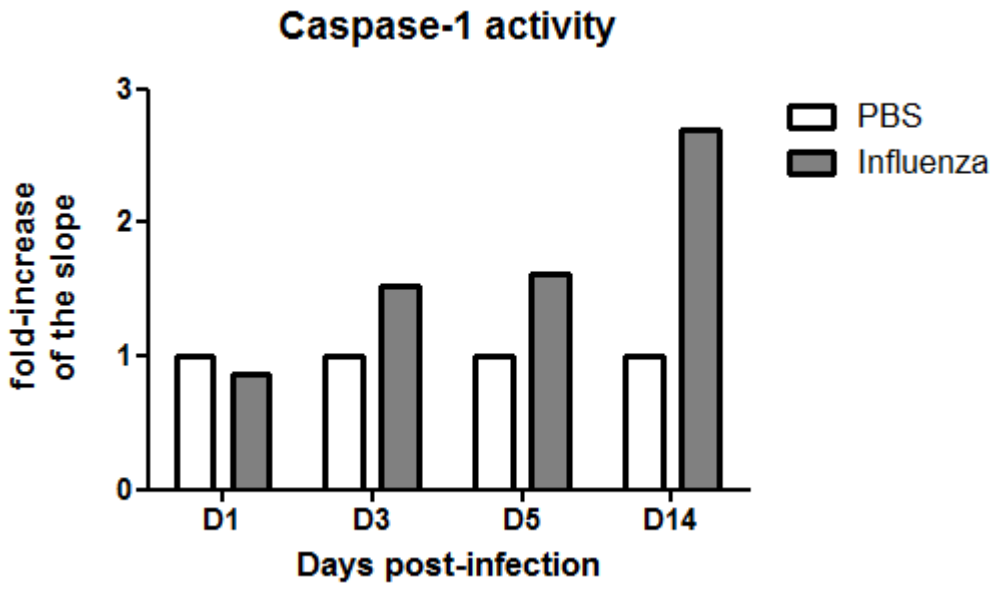
Caspase-1 activity
fold-increase of the slope
0
1
2
3
D1
D3
D5
D14
Days post-infection
PBS
Influenza

Figure 10: Effect of *B. parapertussis* infection on body weight and pulmonary inflammation for 1 week period. Mice were infected with PBS (open bars) or *B. parapertussis* (filled bars) at day 0 and sacrificed at day 1, 3, and 7 post-infection.

(A) Body weights were recorded during the 7 days post infection.

(B) Bacterial burden in lung homogenates.

(C) Total cell number (TCN), mononuclear cells (MNC) and neutrophils (NEU) in the BAL, were counted at the mentioned time points.

Each experimental group at any time point contains an n=5 mice. Data are expressed as the mean±SEM. No statistical analysis was required to be performed.

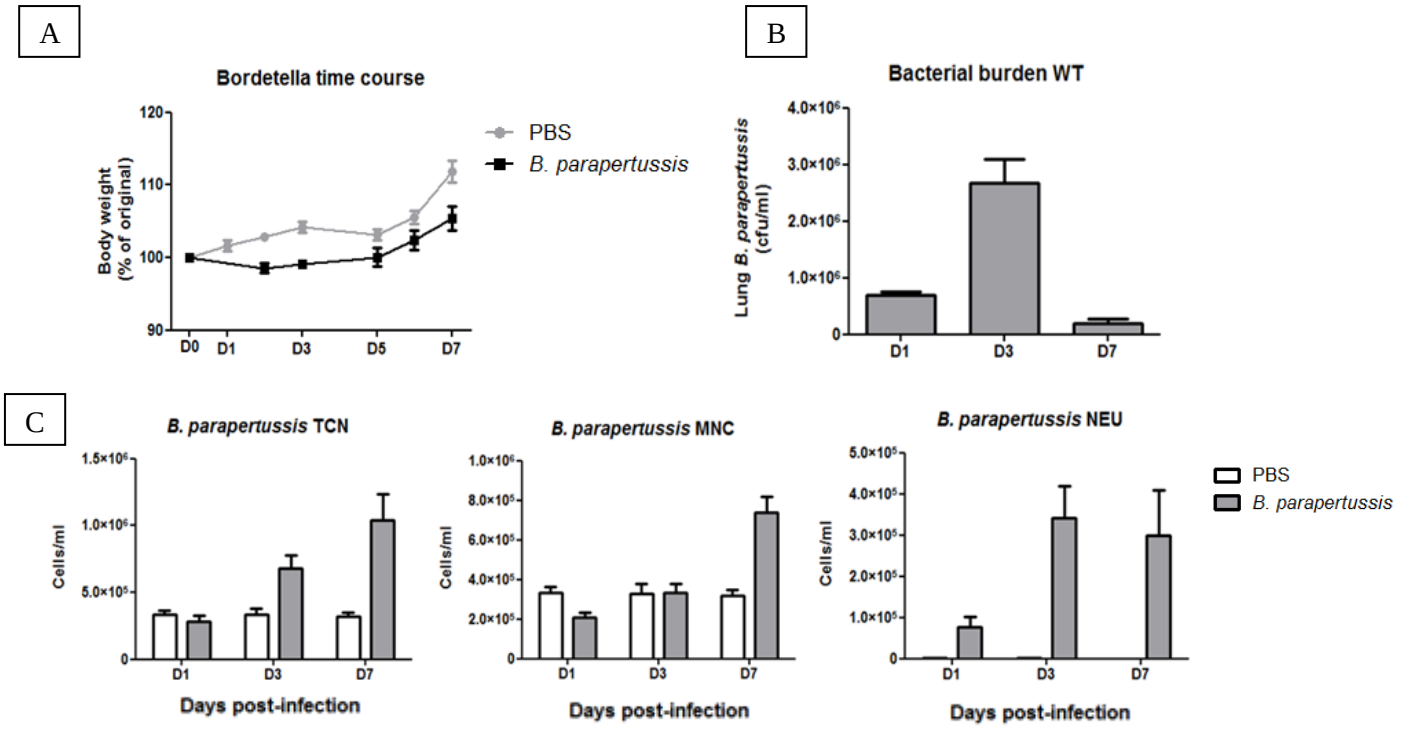
A
Bordetella time course
Body weight (% of original)
120
110
100
90
D0
D1
D3
D5
D7
PBS
B. parapertussis
B
Bacterial burden WT
Lung B. parapertussis (cfu/ml)
4.0×10⁶
3.0×10⁶
2.0×10⁶
1.0×10⁶
0
D1
D3
D7
C
B. parapertussis TCN
B. parapertussis MNC
B. parapertussis NEU
Cells/ml
Days post-infection
PBS
B. parapertussis

Figure 11: Analysis of IL-1β production and quantification of the main chemokines in lung homogenates at day 1, 3 and 7 post-*B. parapertussis* infection. Mice were infected with PBS (open bars) or *B. parapertussis* (filled bars) at day 0 and sacrificed at the noted time points. n=5 mice/group.

(A) Quantification of IL-1β, CXCL1 and CXCL2 levels by ELISA. Lung lobes were homogenized in PBS and cytokine levels were quantified by ELISA. Data show the mean±SEM of the concentration (pg/ml) for each cytokine. Data were analyzed by unpaired t-test. * denotes a significant difference at $p<0.05$ compared to PBS-exposed mice.

(B) Analysis of IL-1β processing by western blot. Lung lobes were homogenized in lysis buffer containing a protease inhibitor cocktail. The protein concentration was quantified by a dye-binding assay. Samples from each experimental group were pooled together and lysis buffer and loading buffer were added to make a final concentration of 80µg protein/50µl volume. A prestain protein ladder and the samples were separated electrophoretically in a 15% polyacrylamide gel and transferred onto a nitrocellulose membrane. The membrane was blot at 4ºC overnight with goat anti-mouse IL-1β antibodies, followed by incubation with secondary IRDye®-conjugated donkey anti-goat IgG antibodies. The membrane was finally scanned by infrared light to reveal the presence of the IRDye® using a Li-Cor Odyssey® infrared detector.

A

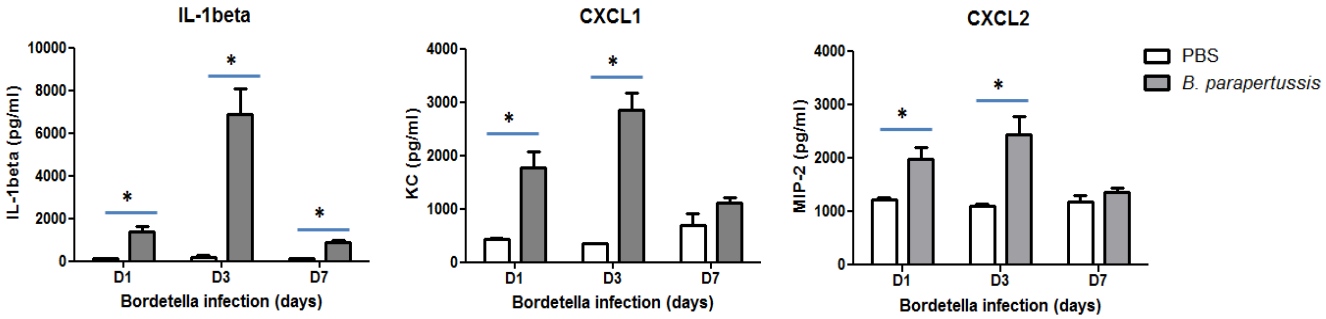
IL-1beta
IL-1beta (pg/ml)
10000
8000
6000
4000
2000
0
D1
D3
D7
Bordetella infection (days)
CXCL1
KC (pg/ml)
4000
3000
2000
1000
0
D1
D3
D7
Bordetella infection (days)
CXCL2
MIP-2 (pg/ml)
4000
3000
2000
1000
0
D1
D3
D7
Bordetella infection (days)
PBS
B. parapertussis

B

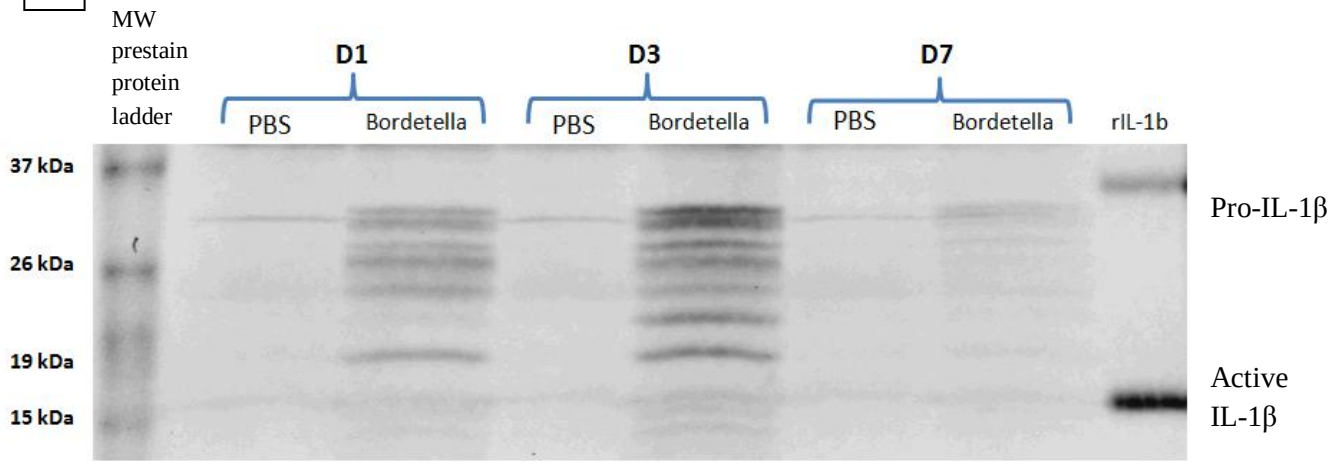
MW prestain protein ladder
D1
D3
D7
PBS
Bordetella
PBS
Bordetella
PBS
Bordetella
rIL-1b
37 kDa
26 kDa
19 kDa
15 kDa
Pro-IL-1β
Active IL-1β

Figure 12: Analysis of caspase-1 expression post-*B. parapertussis* infection. Mice were infected with PBS (open bars) or *B. parapertussis* (filled bars) at day 0 and sacrificed at the specified time points. n=5 mice/group

(A) **Caspase-1 western blot**. Lung lobes were homogenized in lysis buffer containing protease inhibitor cocktail. The protein concentration was quantified by a dye-binding assay. Samples from each experimental group were pooled together and lysis buffer and loading buffer were added to make a final concentration of 80µg protein/50µl volume. A prestain protein ladder and the samples were separated electrophoretically in a 15% polyacrylamide gel and transferred onto a nitrocellulose membrane. The membrane was blot at 4ºC overnight with rat anti-mouse caspase-1 antibodies, followed by incubation with secondary IRDye®-conjugated goat anti-rat IgG antibodies. The membrane was finally scanned by infrared light to reveal the presence of the IRDye® using a Li-Cor Odyssey® infrared detector.

(B) **Analysis of caspase-1 activity.** Lung lobes were homogenized in lysis buffer without protease inhibitor cocktail. The protein concentration was quantified by a dye-binding assay. Samples from each experimental group were pooled together containing the same amount of protein (32µg/50µl). 100µl of lung homogenates were mixed with reaction buffer, DTT, and the substrate YVAD-AFC. The plate was placed in a microplate reader at 37ºC. Samples containing active caspase-1 cleaved the substrate and free fluorescent AFC was measured every 10 minutes over a 2 hour period. The slope of the kinetic curve for each experimental group was extracted and compared to the vehicle-treated group.

A

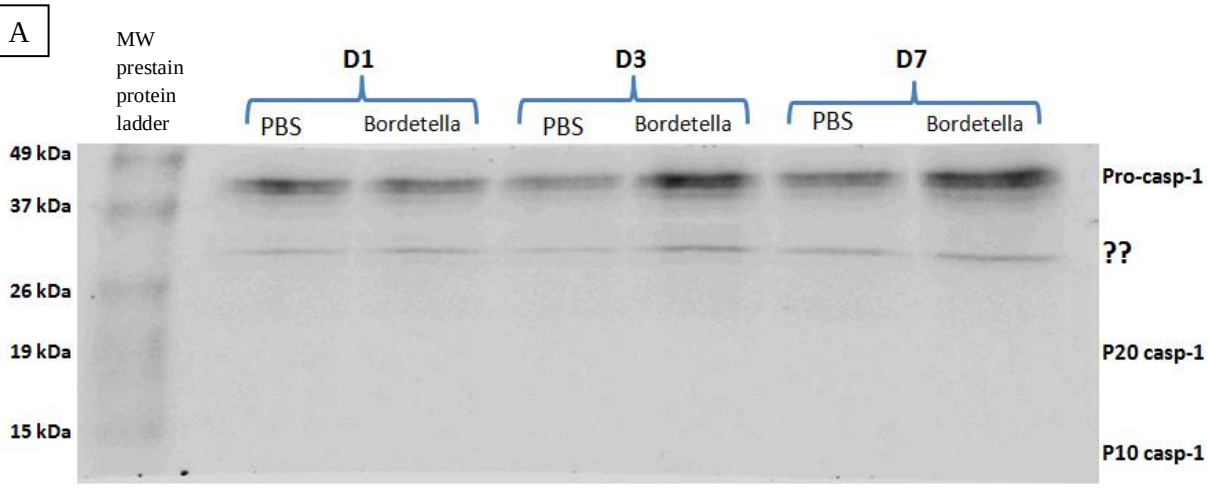
MW
prestain
protein
ladder
D1
D3
D7
PBS
Bordetella
PBS
Bordetella
PBS
Bordetella
49 kDa
37 kDa
26 kDa
19 kDa
15 kDa
Pro-casp-1
??
P20 casp-1
P10 casp-1

B

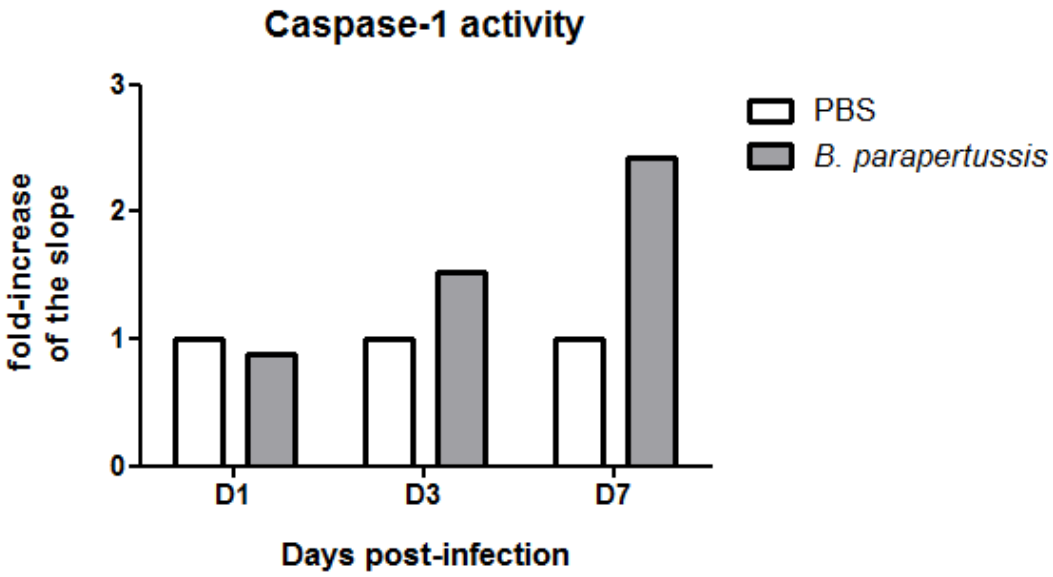
Caspase-1 activity
fold-increase of the slope
0
1
2
3
D1
D3
D7
Days post-infection
PBS
B. parapertussis

Figure 13: Analysis of IL-1β production and quantification of the main chemokines in lung homogenates at day 1, 3 and 7 post-heterologous infection. Mice were infected with PBS or IAV at day 0, and co-infected with PBS or *B. parapertussis* at day 5. Mice were sacrificed at D5+1, D5+3, and D5+7 post-infection. Each experimental group at each time point consisted of an n=5 mice.

(A) Quantification of IL-1β, CXCL1 and CXCL2 levels by ELISA. Lung lobes were homogenized in PBS and cytokine levels were quantified by ELISA. Graphs show the mean±SEM of the concentration (pg/ml) for each cytokine. Data were analyzed by 2-way ANOVA. *, †, ‡ denote a significant difference at $p<0.05$ compared to PBS, *B. parapertussis*, and IAV-exposed mice, respectively.

(B) Analysis of IL-1β processing by western blot. Lung lobes were homogenized in lysis buffer containing a protease inhibitor cocktail. The protein concentration was quantified by a dye-binding assay. Samples from each experimental group were pooled together and lysis buffer and loading buffer were added to make a final concentration of 80µg protein/50µl volume. A prestain protein ladder and the samples were separated electrophoretically in a 15% polyacrylamide gel and transferred onto a nitrocellulose membrane. The membrane was blot at 4ºC overnight with goat anti-mouse IL-1β antibodies, followed by incubation with secondary IRDye®-conjugated donkey anti-goat IgG antibodies. The membrane was finally scanned by infrared light to reveal the presence of the IRDye® using a Li-Cor Odyssey® infrared detector.

A

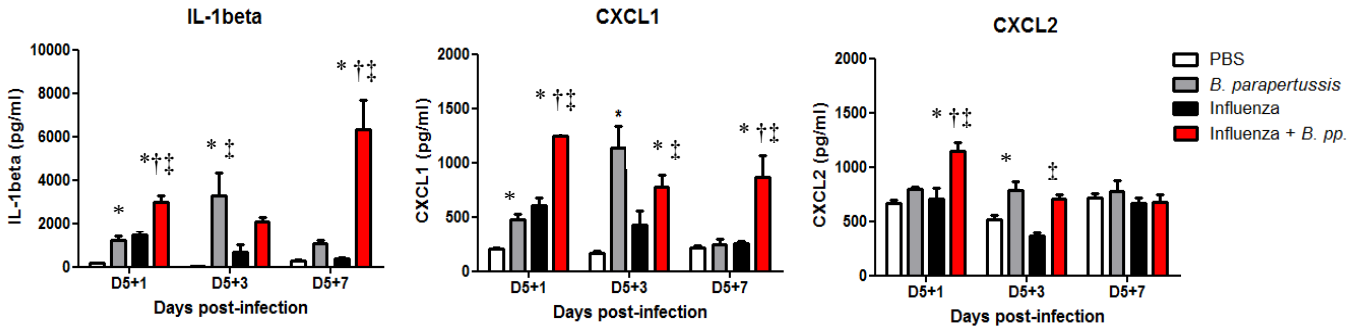
IL-1beta
IL-1beta (pg/ml)
10000
8000
6000
4000
2000
0
D5+1
D5+3
D5+7
Days post-infection
CXCL1
CXCL1 (pg/ml)
2000
1500
1000
500
0
D5+1
D5+3
D5+7
Days post-infection
CXCL2
CXCL2 (pg/ml)
2000
1500
1000
500
0
D5+1
D5+3
D5+7
Days post-infection
PBS
B. parapertussis
Influenza
Influenza + B. pp.

B

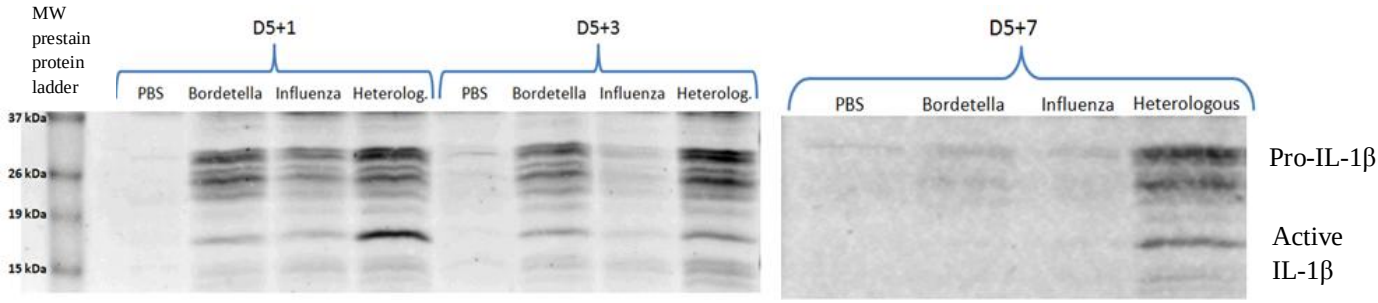
MW prestain protein ladder
D5+1
D5+3
D5+7
PBS
Bordetella
Influenza
Heterolog.
PBS
Bordetella
Influenza
Heterolog.
PBS
Bordetella
Influenza
Heterologous
37 kDa
26 kDa
19 kDa
15 kDa
Pro-IL-1β
Active IL-1β

Figure 14: Analysis of caspase-1 expression post-heterologous infection. Mice were inoculated intranasally with PBS or IAV at day 0, and superinfected with PBS or *B. parapertussis* at day 5. Mice were sacrificed at D5+1, D5+3, and D5+7 post-heterologous infection. Each experimental group at each time point consisted of an n=5 mice.

(A) Caspase-1 western blot. Lung lobes were homogenized in lysis buffer containing protease inhibitor cocktail. The protein concentration was quantified by a dye-binding assay. Samples from each experimental group were pooled together and lysis buffer and loading buffer were added to make a final concentration of 80µg protein/50µl volume. A prestain protein ladder and the samples were separated electrophoretically in a 15% polyacrylamide gel and transferred onto a nitrocellulose membrane. The membrane was blot at 4ºC overnight with rat anti-mouse caspase-1 antibodies, followed by incubation with secondary IRDye®-conjugated goat anti-rat IgG antibodies. The membrane was finally scanned by infrared light to reveal the presence of the IRDye® using a Li-Cor Odyssey® infrared detector.

(B) **Analysis of caspase-1 activity.** Lung lobes were homogenized in lysis buffer without protease inhibitor cocktail. The protein concentration was quantified by a dye-binding assay. Samples from each experimental group were pooled together containing the same amount of protein (50µg/50µl). Lung homogenates were mixed with reaction buffer, DTT, and the substrate YVAD-AFC. The plate was placed in a microplate reader at 37ºC. Free fluorescent AFC was measured every 10 minutes over a 2 hour period. The slope of the kinetic curve for each experimental group was extracted and compared to the vehicle-treated group.

A

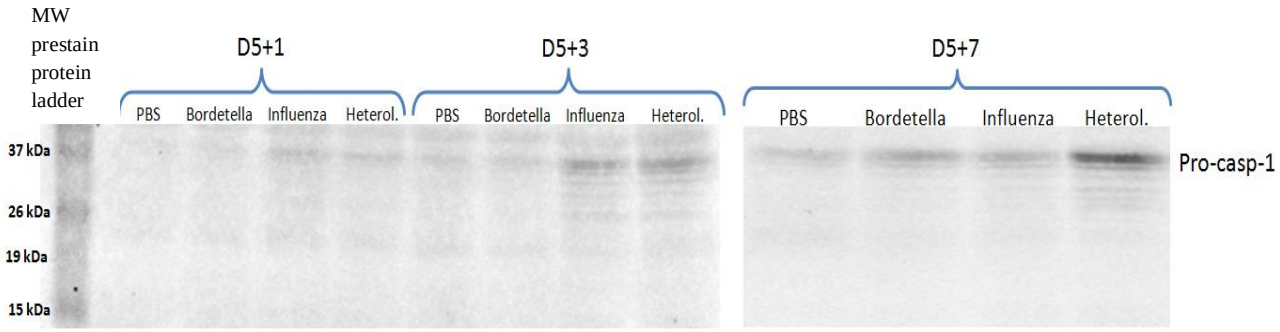
MW prestain protein ladder
D5+1
D5+3
D5+7
PBS
Bordetella
Influenza
Heterol.
37 kDa
26 kDa
19 kDa
15 kDa
Pro-casp-1

B

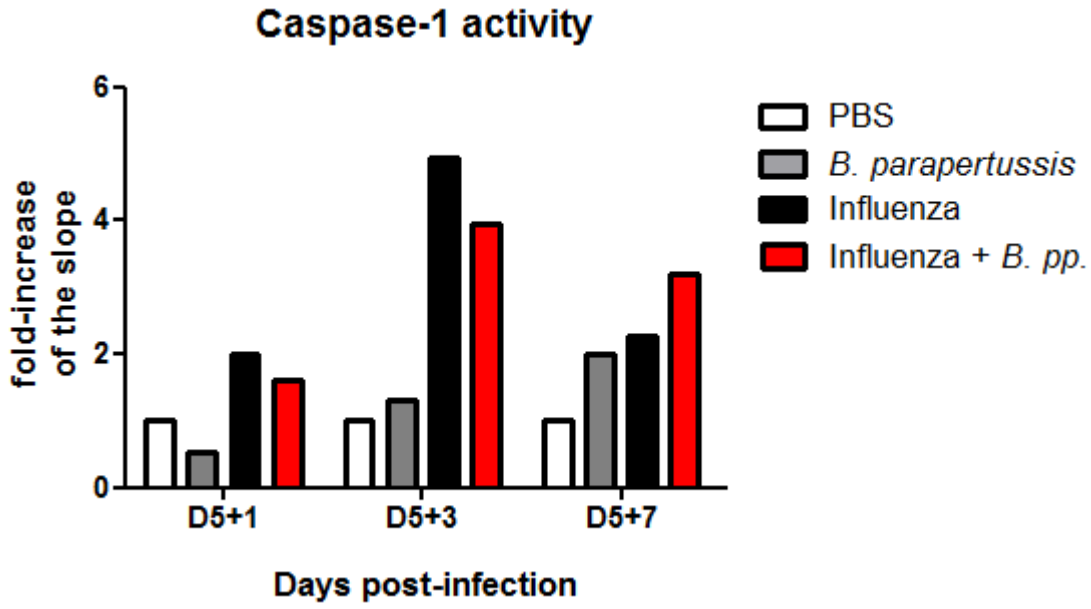
Caspase-1 activity
fold-increase of the slope
6
4
2
0
D5+1
D5+3
D5+7
Days post-infection
PBS
B. parapertussis
Influenza
Influenza + B. pp.

Figure 15: Localization of IL-1β production by immunohistochemistry.

Mice were infected with PBS or IAV at day 0, superinfected with PBS or *B. parapertussis* at day 5, and sacrificed at D5+7 post-infection. Lung lobes were dissected, inflated with 10% formalin and embedded in paraffin. 5µm-thick slices were cut. Tissue was sequentially washed in xylene and absolute ethanol. Endogenous peroxidase activity was blocked with methanolic hydrogen peroxide, and then tissue was rehydrated and rinsed in water, antigen retrieval with citrate buffer and washed with TBS-Tween 20. Tissue was then blocked and incubated with 4 µg/ml of either goat anti-mouse IL-1β IgG or an isotype control (goat IgG) overnight at 4ºC. After washing, a goat probe and a goat polymer were added and slices were placed in AEC buffer and in AEC chromogenic substrate solution to reveal the stain. Finally, slices were place in distilled water, Mayer's solution, rinsed again with tap water and washed in TBS before coverslip the slides with glycerin gelatin.

(A) Images were obtained from vehicle-infected mice (top) and heterologously-infected mice (bottom) at 100 diameters. IL-1β staining (left) is compared to its respective isotype control (right).

(B) Images were obtained from Influenza alone-infected mice (top) and *B. parapertussis* alone-infected mice (bottom) at 100 diameters. IL-1β staining (left) is compared to its respective isotype control (right).

A

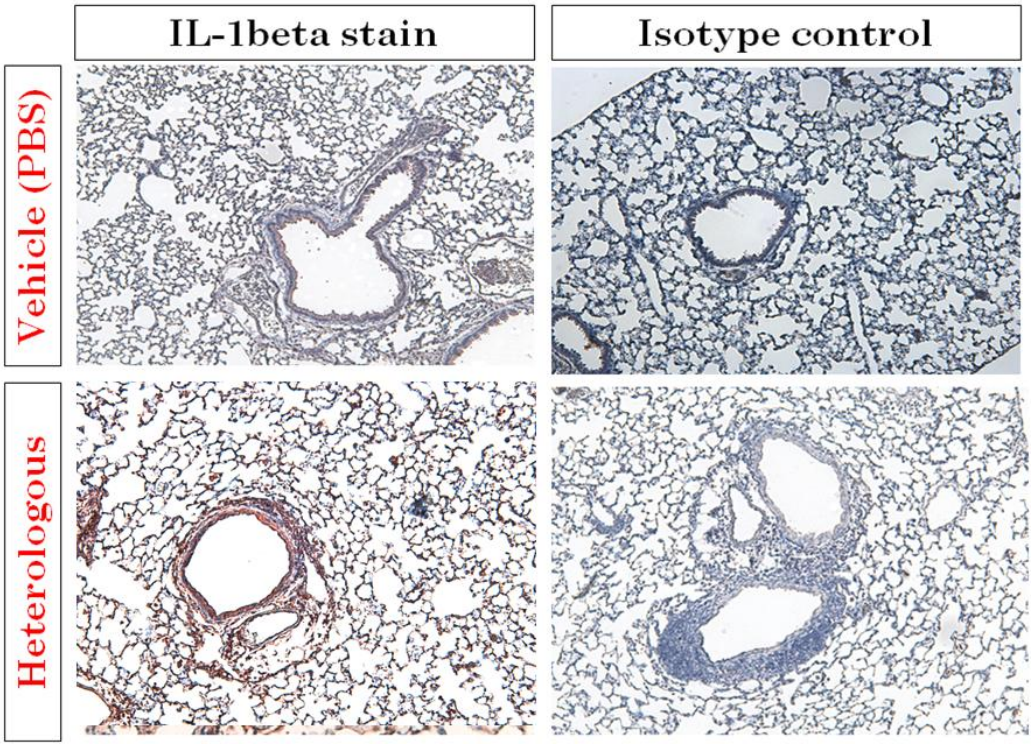
IL-1beta stain
Isotype control
Vehicle (PBS)
Heterologous

B

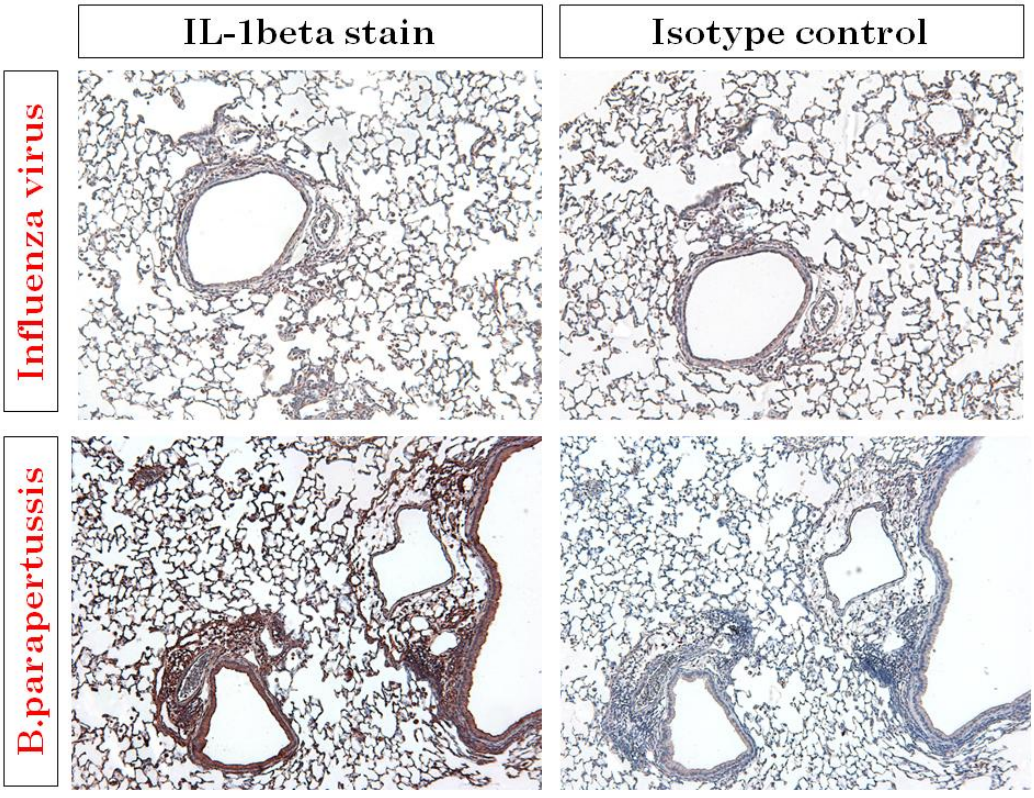
IL-1beta stain
Isotype control
Influenza virus
B.parapertussis

Figure 16: Comparison of the effect of heterologous infection on body weight and pulmonary inflammation in WT mice and ASC$^{-/-}$ mice for a twelve day period. WT (grey bars) and ASC$^{-/-}$ (black bars) mice were infected with IAV at day 0, superinfected with *B. parapertussis* at day 5 and sacrificed at D5+3 and D5+7 post-infection.

(A) Body weights recorded during the 12 days post infection.

(B) Bacterial burden in lung homogenates.

(C) Pulmonary cellular infiltration, measured by total cell number (TCN), mononuclear cells (MNC) and neutrophils (NEU) counted in the BAL at the mentioned time points.

Each experimental group at any time point contains an n=5-10 mice. Data are expressed as the mean±SEM and analyzed by unpaired t-test. ¥ denotes a significant difference at $p<0.05$ between WT and ASC$^{-/-}$ mice.

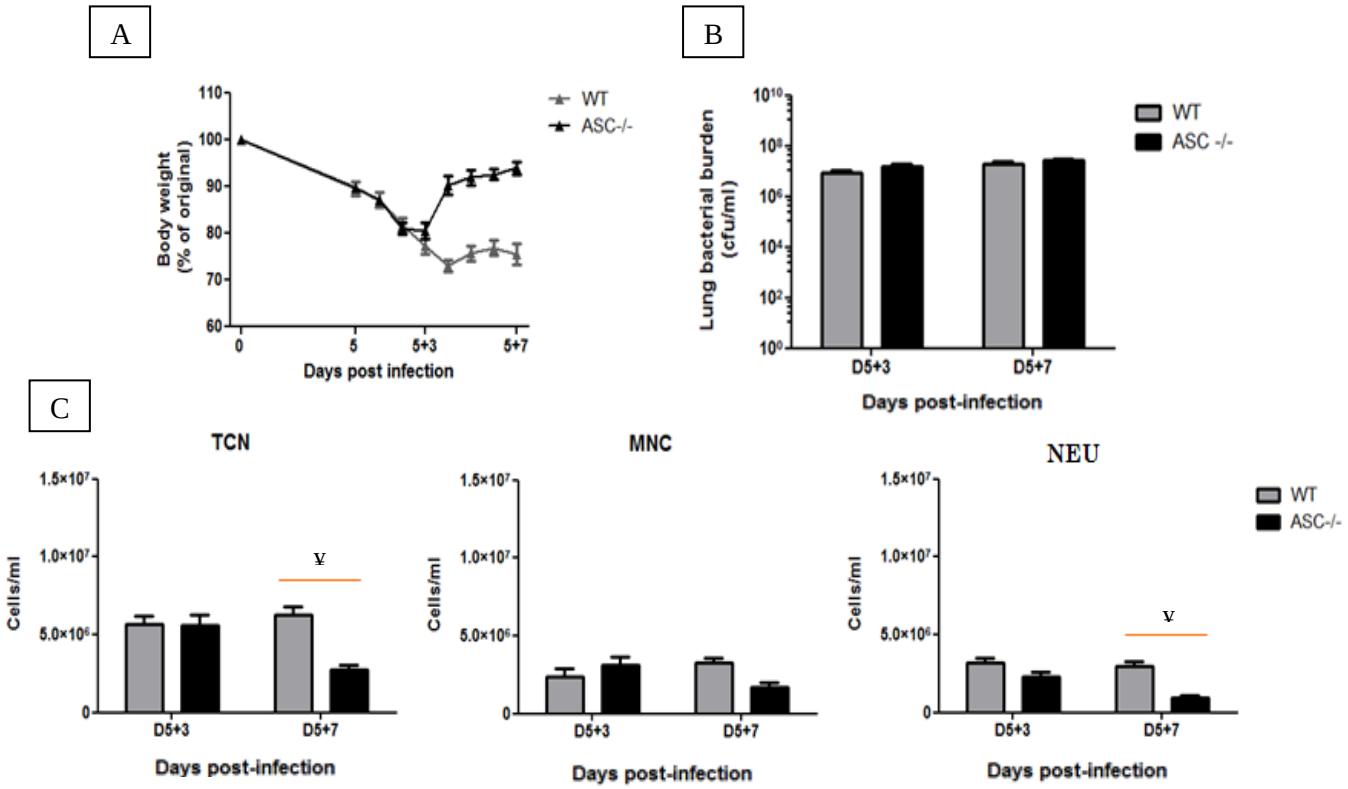
A
Body weight (% of original)
110
100
90
80
70
60
0
5
5+3
5+7
Days post infection
WT
ASC-/-
B
Lung bacterial burden (cfu/ml)
10^{10}
10^{8}
10^{6}
10^{4}
10^{2}
10^{0}
D5+3
D5+7
Days post-infection
WT
ASC -/-
C
TCN
MNC
NEU
Cells/ml
1.5×10⁷
1.0×10⁷
5.0×10⁶
0
D5+3
D5+7
Days post-infection
WT
ASC-/-

Figure 17: Assessment of the inflammation on lung slices from WT and ASC$^{-/-}$ heterologously-infected mice. WT and ASC$^{-/-}$ mice were infected were infected with IAV at day 0, superinfected with *B. parapertussis* at day 5 and sacrificed at D5+3 and D5+7 post-infection. Lung were inflated with 10% formalin, embedded in paraffin, cut in 5µm-thick slices and stained with H&E in order to analyze the pathology of heterologous infection in both types of mice. Each image is shown as 16 and 100 diameters.

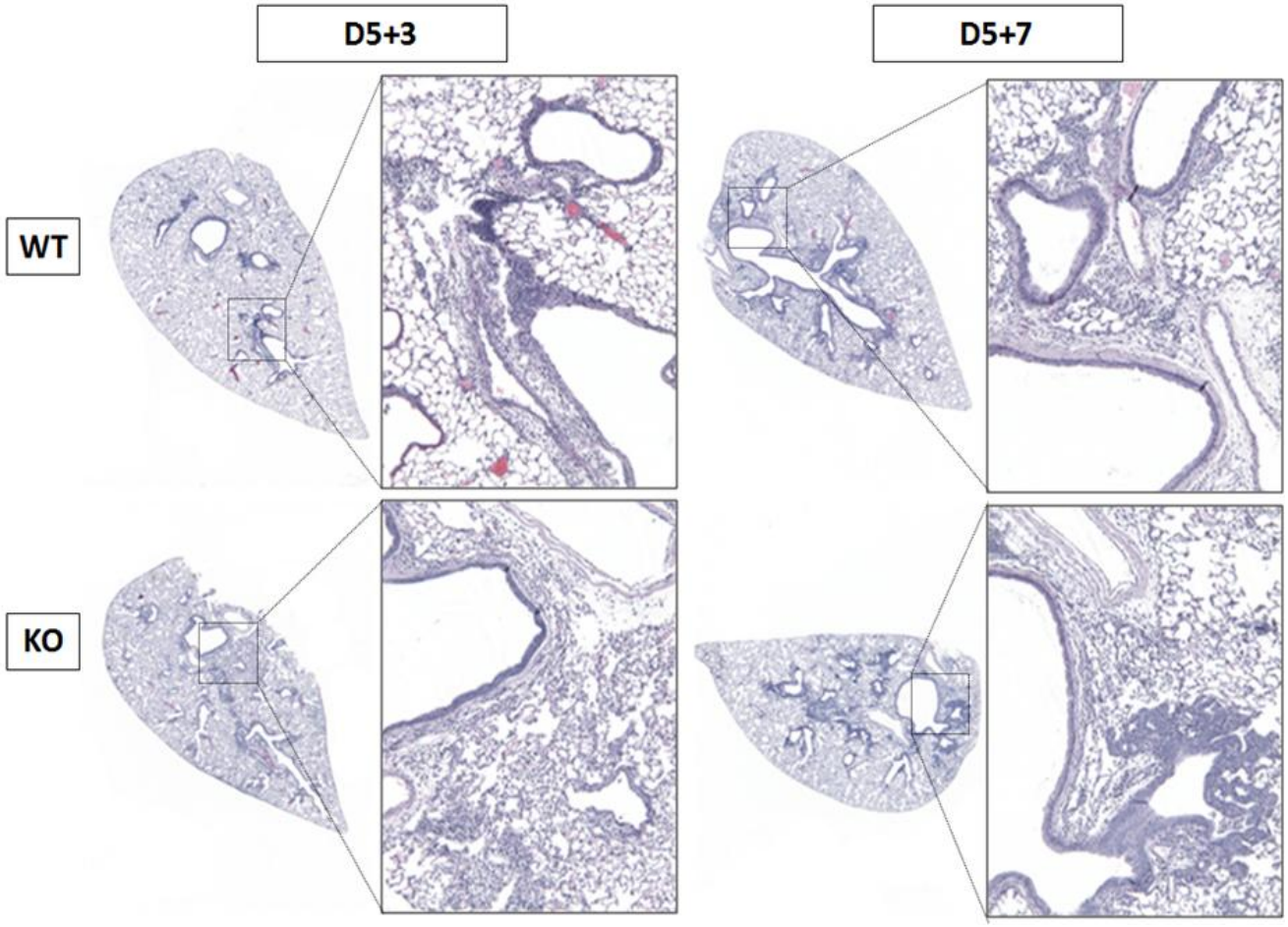
D5+3
D5+7
WT
KO

Figure 18: Assessment of epithelium damage in lung slices from WT and ASC$^{-/-}$ heterologously-infected mice. WT and ASC$^{-/-}$ mice were infected were infected with IAV at day 0, superinfected with *B. parapertussis* at day 5 and sacrificed at D5+3 and D5+7 post-infection. Lung were inflated with 10% formalin, embedded in paraffin, cut in 5µm-thick slices and stained with H&E in order to analyze the pathology of heterologous infection in both types of mice. Upper images correspond to WT mice whereas lower images correspond to ASC$^{-/-}$ mice. Images on the left correspond to D5+3 time point whereas images on the right correspond to D5+7 time point. Images represent 400x diameters.

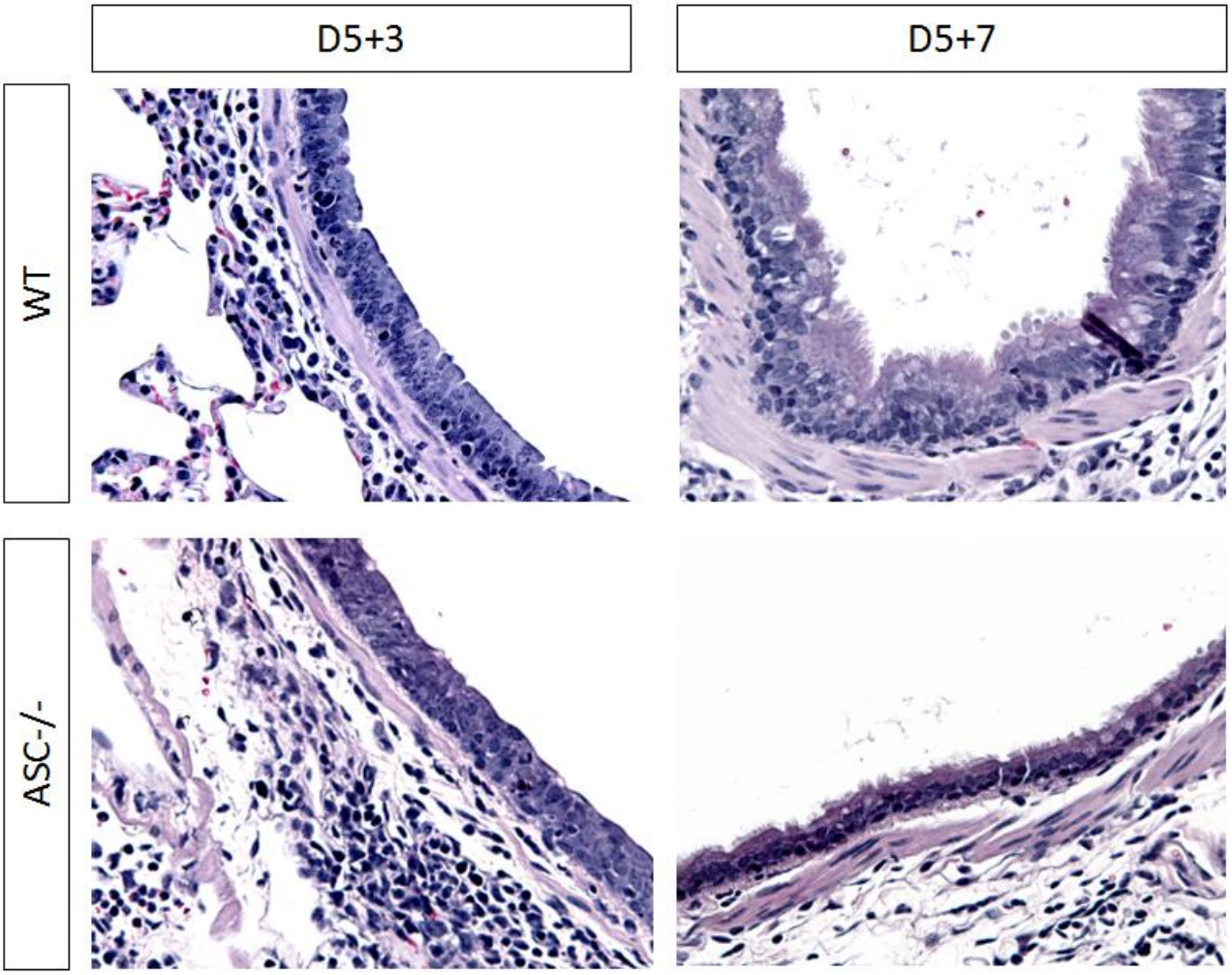
D5+3
D5+7
WT
ASC-/-

Figure 19: Quantification of IL-1β and CXCL2 in WT and ASC$^{-/-}$ mice upon heterologous infection. Mice were infected with IAV at day 0, superinfected with *B. parapertussis* at day 5 and sacrificed at D5+3 and D5+7 post infection. Levels of IL-1β and CXCL2 were quantified in lung homogenates by ELISA. Each experimental group at any time point contains an n=5-10 mice. Data are expressed as the mean±SEM and analyzed by unpaired t-test. ¥ denotes a significant difference at $p<0.05$ between WT and ASC$^{-/-}$ mice.

IL-1β expression

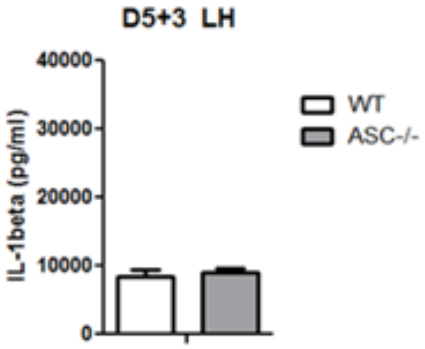

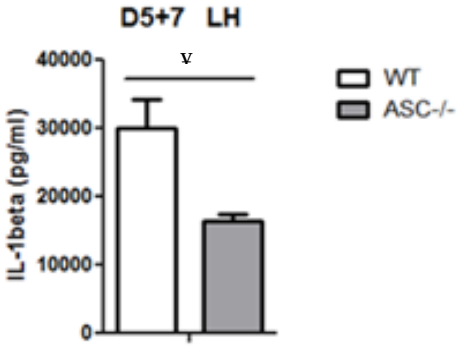

MIP-2 expression

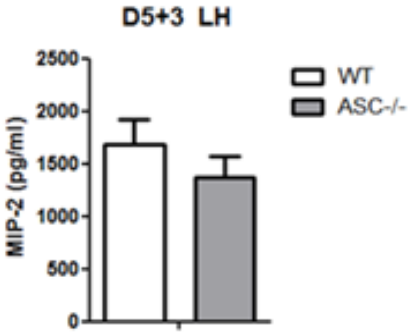

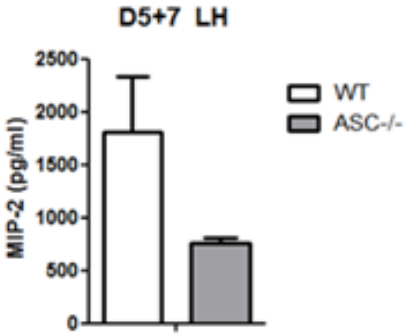

Figure 20: Comparison of the effect of heterologous infection on body weight and pulmonary inflammation in WT mice and ASC$^{-/-}$ mice for a twelve day period. WT and ASC$^{-/-}$ mice were infected with IAV at day 0, superinfected with *B. parapertussis* at day 5 and sacrificed at D5(+0), D5+3 and D5+7 post-infection.

(A) Body weights recorded during the 12 days post infection.

(B) Bacterial burden in lung homogenates.

(C) Pulmonary cellular infiltration, measured by total cell number (TCN), mononuclear cells (MNC) and neutrophils (NEU) counted in the BAL at the mentioned time points.

The D5+0 is a representation of one experiment containing an n of 5 WT mice and 4 ASC$^{-/-}$ mice. The D5+3 data is a representation of two separate experiments containing an n of 5 and 4 WT mice and 8 and 5 ASC$^{-/-}$ mice, respectively. The D5+7 data represents one experiment of 5 WT mice and 7 ASC$^{-/-}$ mice. Data are expressed as the mean±SEM and analyzed by unpaired t-test. NS denotes a not significant difference at $p<0.05$ between WT and ASC$^{-/-}$ mice. This experiment was a repeat of figure 16.

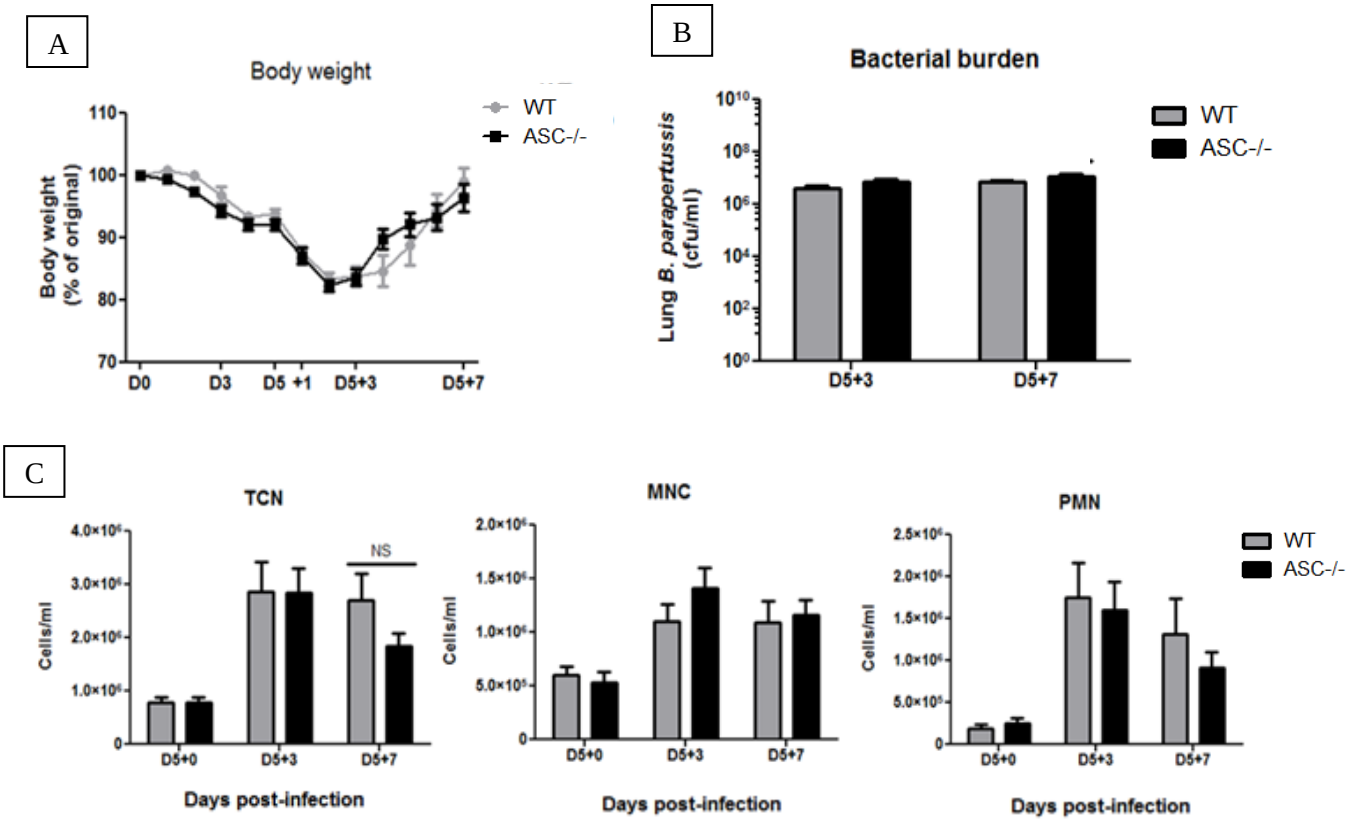
A
Body weight
WT
ASC-/-
Body weight (% of original)
110
100
90
80
70
D0
D3
D5 +1
D5+3
D5+7
B
Bacterial burden
WT
ASC-/-
Lung B. parapertussis (cfu/ml)
10^{10}
10^{8}
10^{6}
10^{4}
10^{2}
10^{0}
D5+3
D5+7
C
TCN
NS
Cells/ml
4.0×10⁶
3.0×10⁶
2.0×10⁶
1.0×10⁶
0
D5+0
D5+3
D5+7
Days post-infection
MNC
Cells/ml
2.0×10⁶
1.5×10⁶
1.0×10⁶
5.0×10⁵
0
D5+0
D5+3
D5+7
Days post-infection
PMN
WT
ASC-/-
Cells/ml
2.5×10⁶
2.0×10⁶
1.5×10⁶
1.0×10⁶
5.0×10⁵
0
D5+0
D5+3
D5+7
Days post-infection

Figure 21: Analysis of IL-1β production and quantification of the main chemokines in lung homogenates of WT and ASC$^{-/-}$ mice at day 0, 3 and 7 post-heterologous infection. WT (grey bars) and ASC$^{-/-}$ (black bars) mice were infected with IAV at day 0, superinfected with *B. parapertussis* at day 5 and sacrificed at D5(+0), D5+3, and D5+7 post-infection. Each experimental group consisted of an n = 5-7 mice.

(A) Quantification of IL-1β, CXCL1 and CXCL2 levels by ELISA. Lung lobes were homogenized in PBS and cytokine levels were quantified by ELISA. Data represent the mean±SEM of the concentration (pg/ml) for each cytokine. Data were analyzed by unpaired t-test. NS = not statistically significant.

(B) Analysis of IL-1β processing by western blot. Lung lobes were homogenized in lysis buffer containing a protease inhibitor cocktail. The protein concentration was quantified by a dye-binding assay. Samples from each experimental group were pooled together and lysis buffer and loading buffer were added to make a final concentration of 80µg protein/50µl volume. A prestain protein ladder and the samples were separated electrophoretically in a 15% polyacrylamide gel and transferred onto a nitrocellulose membrane. The membrane was blot at 4ºC overnight with goat anti-mouse IL-1β antibodies, followed by incubation with secondary IRDye®-conjugated donkey anti-goat IgG antibodies. The membrane was finally scanned by infrared light to reveal the presence of the IRDye® using a Li-Cor Odyssey® infrared detector.

A

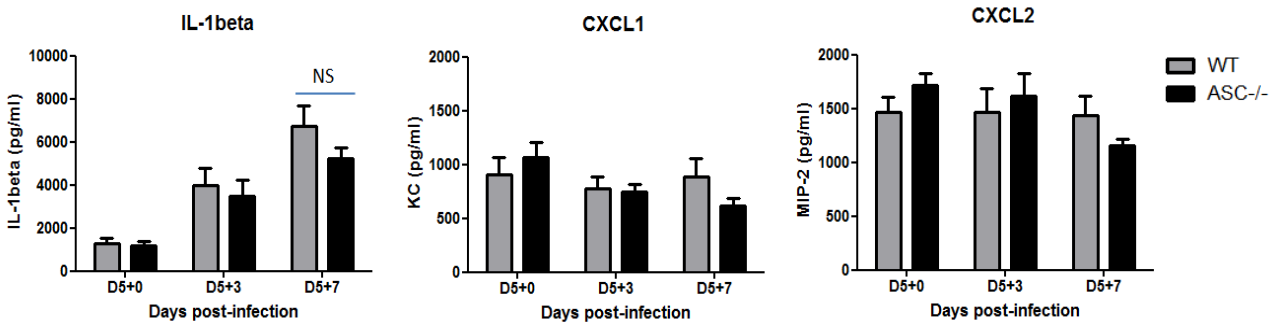
IL-1beta
IL-1beta (pg/ml)
10000
8000
6000
4000
2000
0
NS
D5+0
D5+3
D5+7
Days post-infection
CXCL1
KC (pg/ml)
2000
1500
1000
500
0
D5+0
D5+3
D5+7
Days post-infection
CXCL2
MIP-2 (pg/ml)
2000
1500
1000
500
0
D5+0
D5+3
D5+7
Days post-infection
WT
ASC-/-

B

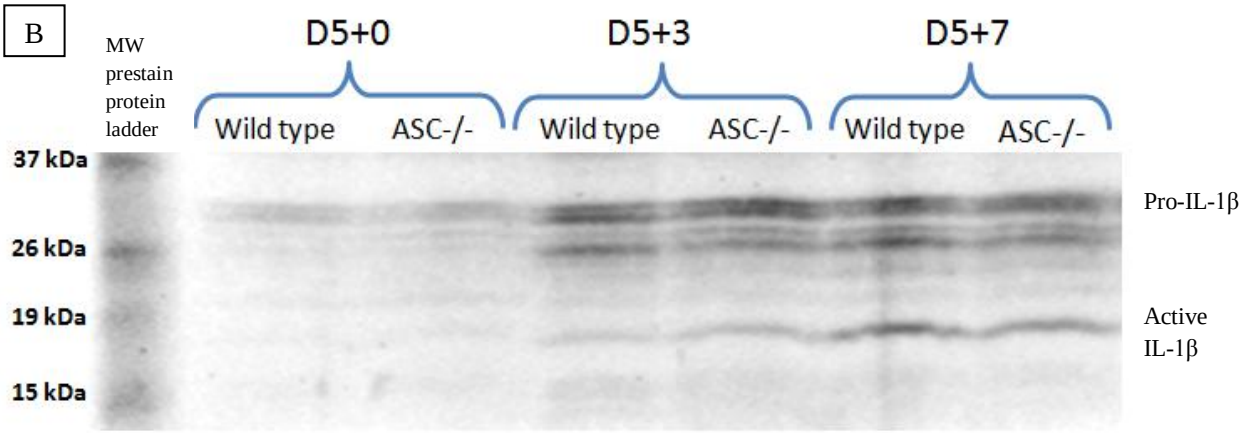
MW prestain protein ladder
D5+0
D5+3
D5+7
Wild type
ASC-/-
Wild type
ASC-/-
Wild type
ASC-/-
37 kDa
26 kDa
19 kDa
15 kDa
Pro-IL-1β
Active IL-1β

Figure 22: Analysis of caspase-1 expression in WT and ASC$^{-/-}$ mice post-heterologous infection. WT (grey bars) and ASC$^{-/-}$ (black bars) mice were infected with IAV at day 0, super-infected with *B. parapertussis* at day 5 and sacrificed at D5(+0), D5+3, and D5+7 post-infection. Each experimental group consisted of an n= 5-7 mice.

(C) **Caspase-1 western blot**. Lung lobes were homogenized in lysis buffer containing protease inhibitor cocktail. The protein concentration was quantified by a dye-binding assay. Samples from each experimental group were pooled together and lysis buffer and loading buffer were added to make a final concentration of 80µg protein/50µl volume. A prestain protein ladder and the samples were separated electrophoretically in a 15% polyacrylamide gel and transferred onto a nitrocellulose membrane. The membrane was blot at 4ºC overnight with rat anti-mouse caspase-1 antibodies, followed by incubation with secondary IRDye®-conjugated goat anti-rat IgG antibodies. The membrane was finally scanned by infrared light to reveal the presence of the IRDye® using a Li-Cor Odyssey® infrared detector.

(D) **Analysis of caspase-1 activity.** Lung lobes were homogenized in lysis buffer without protease inhibitor cocktail. The protein concentration was quantified by a dye-binding assay. Samples from each experimental group were pooled together containing the same amount of protein (50µg/50µl). Lung homogenates were mixed with reaction buffer, DTT, and the substrate YVAD-AFC. The plate was placed in a microplate reader at 37ºC. Free fluorescent AFC was measured every 10 minutes over a 2 hour period. The slope of the kinetic curve for each experimental group was extracted and compared to the vehicle-treated group.

A

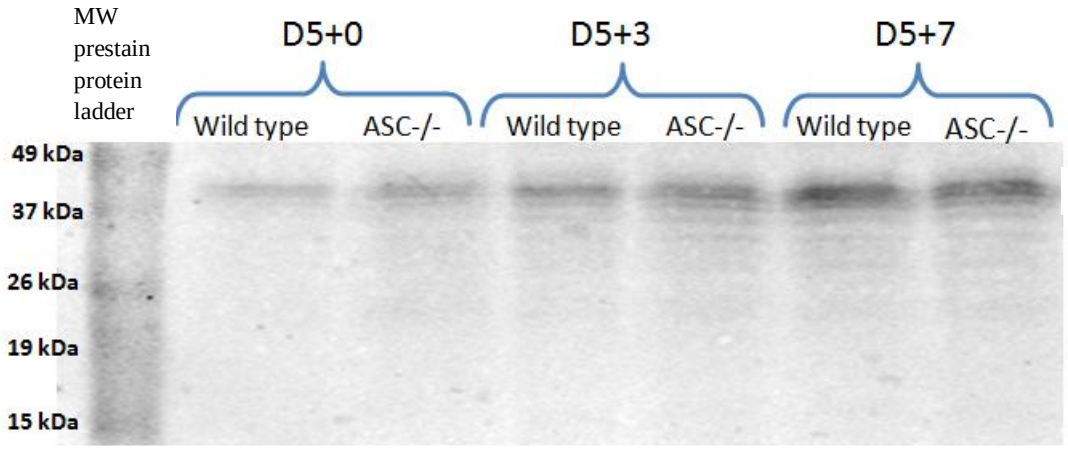
MW prestain protein ladder
D5+0
D5+3
D5+7
Wild type
ASC-/-
Wild type
ASC-/-
Wild type
ASC-/-
49 kDa
37 kDa
26 kDa
19 kDa
15 kDa
Pro-caspase-1

B

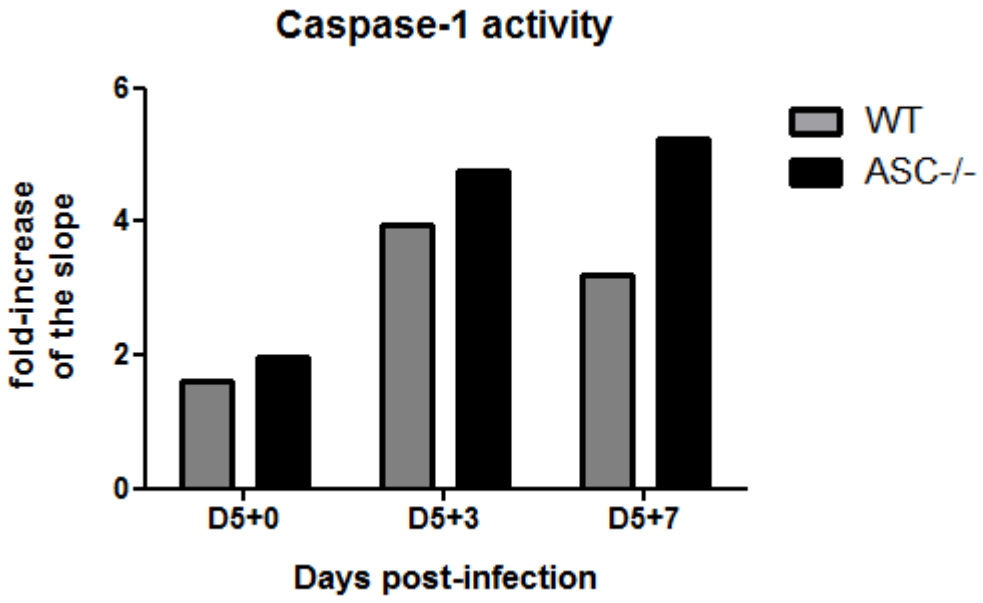
Caspase-1 activity
fold-increase of the slope
6
4
2
0
D5+0
D5+3
D5+7
Days post-infection
WT
ASC-/-

Chapter 6: References

1. Holt, P. G., D. H. Strickland, M. E. Wikström, and F. L. Jahnsen. 2008. Regulation of immunological homeostasis in the respiratory tract. *Nat Rev Immunol* 8: 142-152.
2. Layton, D. W. 1993. Metabolically consistent breathing rates for use in dose assessments. *Health Phys* 64: 23-36.
3. Nicas, M., W. W. Nazaroff, and A. Hubbard. 2005. Toward understanding the risk of secondary airborne infection: emission of respirable pathogens. *J Occup Environ Hyg* 2: 143-154.
4. Zhang, P., W. R. Summer, G. J. Bagby, and S. Nelson. 2000. Innate immunity and pulmonary host defense. *Immunol Rev* 173: 39-51.
5. Bartlett, J. A., A. J. Fischer, and P. B. McCray. 2008. Innate immune functions of the airway epithelium. *Contrib Microbiol* 15: 147-163.
6. Tamura, S., and T. Kurata. 2004. Defense mechanisms against influenza virus infection in the respiratory tract mucosa. *Jpn J Infect Dis* 57: 236-247.
7. Message, S. D., and S. L. Johnston. 2004. Host defense function of the airway epithelium in health and disease: clinical background. *J Leukoc Biol* 75: 5-17.
8. Singhera, G. K., T. S. Chan, J. Y. Cheng, T. Z. Vitalis, K. J. Hamann, and D. R. Dorscheid. 2006. Apoptosis of viral-infected airway epithelial cells limit viral production and is altered by corticosteroid exposure. *Respir Res* 7: 78.
9. Schnapp, D., and A. Harris. 1998. Antibacterial peptides in bronchoalveolar lavage fluid. *Am J Respir Cell Mol Biol* 19: 352-356.
10. Crouch, E., K. Hartshorn, and I. Ofek. 2000. Collectins and pulmonary innate immunity. *Immunol Rev* 173: 52-65.
11. Goerke, J. 1998. Pulmonary surfactant: functions and molecular composition. *Biochim Biophys Acta* 1408: 79-89.
12. Wright, J. R. 1997. Immunomodulatory functions of surfactant. *Physiol Rev* 77: 931-962.
13. Crouch, E., and J. R. Wright. 2001. Surfactant proteins a and d and pulmonary host defense. *Annu Rev Physiol* 63: 521-554.
14. Wu, H., A. Kuzmenko, S. Wan, L. Schaffer, A. Weiss, J. H. Fisher, K. S. Kim, and F. X. McCormack. 2003. Surfactant proteins A and D inhibit the growth of Gram-negative bacteria by increasing membrane permeability. *J Clin Invest* 111: 1589-1602.
15. Blander, J. M., and R. Medzhitov. 2004. Regulation of phagosome maturation by signals from toll-like receptors. *Science* 304: 1014-1018.
16. Nelson, S., and W. R. Summer. 1998. Innate immunity, cytokines, and pulmonary host defense. *Infect Dis Clin North Am* 12: 555-567, vii.
17. Marriott, H. M., and D. H. Dockrell. 2007. The role of the macrophage in lung disease mediated by bacteria. *Exp Lung Res* 33: 493-505.

18. Iwasaki, A. January 2011. Inflammasomes as mediators of immunity against influenza virus. *Trends in Immunology* 32: 8.
19. Kanneganti, T. D. 2010. Central roles of NLRs and inflammasomes in viral infection. *Nat Rev Immunol* 10: 688-698.
20. Franke-Ullmann, G., C. Pförtner, P. Walter, C. Steinmüller, M. L. Lohmann-Matthes, and L. Kobzik. 1996. Characterization of murine lung interstitial macrophages in comparison with alveolar macrophages in vitro. *J Immunol* 157: 3097-3104.
21. Sadik, C. D., N. D. Kim, and A. D. Luster. 2011. Neutrophils cascading their way to inflammation. *Trends Immunol* 32: 452-460.
22. Reynolds, H. Y. 1983. Lung inflammation: role of endogenous chemotactic factors in attracting polymorphonuclear granulocytes. *Am Rev Respir Dis* 127: S16-25.
23. Sibille, Y., and H. Y. Reynolds. 1990. Macrophages and polymorphonuclear neutrophils in lung defense and injury. *Am Rev Respir Dis* 141: 471-501.
24. Kunkel, S. L., T. Standiford, K. Kasahara, and R. M. Strieter. 1991. Interleukin-8 (IL-8): the major neutrophil chemotactic factor in the lung. *Exp Lung Res* 17: 17-23.
25. Calkins, C. M., D. D. Bensard, B. D. Shames, E. J. Pulido, E. Abraham, N. Fernandez, X. Meng, C. A. Dinarello, and R. C. McIntyre. 2002. IL-1 regulates in vivo C-X-C chemokine induction and neutrophil sequestration following endotoxemia. *J Endotoxin Res* 8: 59-67.
26. Standiford, T. J., S. L. Kunkel, M. J. Greenberger, L. L. Laichalk, and R. M. Strieter. 1996. Expression and regulation of chemokines in bacterial pneumonia. *J Leukoc Biol* 59: 24-28.
27. Gupta, S., L. Feng, T. Yoshimura, J. Redick, S. M. Fu, and C. E. Rose. 1996. Intra-alveolar macrophage-inflammatory peptide 2 induces rapid neutrophil localization in the lung. *Am J Respir Cell Mol Biol* 15: 656-663.
28. Zavitz, C. C., C. M. Bauer, G. J. Gaschler, K. M. Fraser, R. M. Strieter, C. M. Hogaboam, and M. R. Stampfli. 2010. Dysregulated macrophage-inflammatory protein-2 expression drives illness in bacterial superinfection of influenza. *J Immunol* 184: 2001-2013.
29. Frevert, C. W., S. Huang, H. Danaee, J. D. Paulauskis, and L. Kobzik. 1995. Functional characterization of the rat chemokine KC and its importance in neutrophil recruitment in a rat model of pulmonary inflammation. *J Immunol* 154: 335-344.
30. Frevert, C. W., A. Farone, H. Danaee, J. D. Paulauskis, and L. Kobzik. 1995. Functional characterization of rat chemokine macrophage inflammatory protein-2. *Inflammation* 19: 133-142.
31. Olson, T. S., and K. Ley. 2002. Chemokines and chemokine receptors in leukocyte trafficking. *Am J Physiol Regul Integr Comp Physiol* 283: R7-28.

32. Jeyaseelan, S., R. Manzer, S. K. Young, M. Yamamoto, S. Akira, R. J. Mason, and G. S. Worthen. 2005. Induction of CXCL5 during inflammation in the rodent lung involves activation of alveolar epithelium. *Am J Respir Cell Mol Biol* 32: 531-539.
33. Rossi, D. L., S. D. Hurst, Y. Xu, W. Wang, S. Menon, R. L. Coffman, and A. Zlotnik. 1999. Lungkine, a novel CXC chemokine, specifically expressed by lung bronchoepithelial cells. *J Immunol* 162: 5490-5497.
34. Chen, S. C., B. Mehrad, J. C. Deng, G. Vassileva, D. J. Manfra, D. N. Cook, M. T. Wiekowski, A. Zlotnik, T. J. Standiford, and S. A. Lira. 2001. Impaired pulmonary host defense in mice lacking expression of the CXC chemokine lungkine. *J Immunol* 166: 3362-3368.
35. Brandt, E., F. Petersen, A. Ludwig, J. E. Ehlert, L. Bock, and H. D. Flad. 2000. The beta-thromboglobulins and platelet factor 4: blood platelet-derived CXC chemokines with divergent roles in early neutrophil regulation. *J Leukoc Biol* 67: 471-478.
36. Johnson, Z., A. E. Proudfoot, and T. M. Handel. 2005. Interaction of chemokines and glycosaminoglycans: a new twist in the regulation of chemokine function with opportunities for therapeutic intervention. *Cytokine Growth Factor Rev* 16: 625-636.
37. Medeiros, A. I., C. H. Serezani, S. P. Lee, and M. Peters-Golden. 2009. Efferocytosis impairs pulmonary macrophage and lung antibacterial function via PGE2/EP2 signaling. *J Exp Med* 206: 61-68.
38. Pancer, Z., and M. D. Cooper. 2006. The evolution of adaptive immunity. *Annu Rev Immunol* 24: 497-518.
39. Flajnik, M. F., and M. Kasahara. 2010. Origin and evolution of the adaptive immune system: genetic events and selective pressures. *Nat Rev Genet* 11: 47-59.
40. Guermonprez, P., J. Valladeau, L. Zitvogel, C. Théry, and S. Amigorena. 2002. Antigen presentation and T cell stimulation by dendritic cells. *Annu Rev Immunol* 20: 621-667.
41. Palm, N. W., and R. Medzhitov. 2009. Pattern recognition receptors and control of adaptive immunity. *Immunol Rev* 227: 221-233.
42. Janeway, C. A. J., P. Travers, M. Walport, and M. J. Shlomchik. 2005. *Immunobiology: The immune system in health and disease*.
43. Goodnow, C. C. 1997. Chance encounters and organized rendezvous. *Immunol Rev* 156: 5-10.
44. Garside, P., E. Ingulli, R. R. Merica, J. G. Johnson, R. J. Noelle, and M. K. Jenkins. 1998. Visualization of specific B and T lymphocyte interactions in the lymph node. *Science* 281: 96-99.
45. Okada, T., M. J. Miller, I. Parker, M. F. Krummel, M. Neighbors, S. B. Hartley, A. O'Garra, M. D. Cahalan, and J. G. Cyster. 2005. Antigen-engaged B cells undergo

chemotaxis toward the T zone and form motile conjugates with helper T cells. *PLoS Biol* 3: e150.

46. Reif, K., E. H. Ekland, L. Ohl, H. Nakano, M. Lipp, R. Förster, and J. G. Cyster. 2002. Balanced responsiveness to chemoattractants from adjacent zones determines B-cell position. *Nature* 416: 94-99.
47. Jacob, J., R. Kassir, and G. Kelsoe. 1991. In situ studies of the primary immune response to (4-hydroxy-3-nitrophenyl)acetyl. I. The architecture and dynamics of responding cell populations. *J Exp Med* 173: 1165-1175.
48. MacLennan, I. C., A. Gulbranson-Judge, K. M. Toellner, M. Casamayor-Palleja, E. Chan, D. M. Sze, S. A. Luther, and H. A. Orbea. 1997. The changing preference of T and B cells for partners as T-dependent antibody responses develop. *Immunol Rev* 156: 53-66.
49. Pape, K. A., V. Kouskoff, D. Nemazee, H. L. Tang, J. G. Cyster, L. E. Tze, K. L. Hippen, T. W. Behrens, and M. K. Jenkins. 2003. Visualization of the genesis and fate of isotype-switched B cells during a primary immune response. *J Exp Med* 197: 1677-1687.
50. Kelsoe, G. 1996. Life and death in germinal centers (redux). *Immunity* 4: 107-111.
51. Vinuesa, C. G., S. G. Tangye, B. Moser, and C. R. Mackay. 2005. Follicular B helper T cells in antibody responses and autoimmunity. *Nat Rev Immunol* 5: 853-865.
52. Lopez, A. D., C. D. Mathers, M. Ezzati, D. T. Jamison, and C. J. Murray. 2006. Global and regional burden of disease and risk factors, 2001: systematic analysis of population health data. *Lancet* 367: 1747-1757.
53. http://www.cdc.gov/flu/about/viruses/types.htm.
54. Musher, D. M. 2003. How contagious are common respiratory tract infections? *N Engl J Med* 348: 1256-1266.
55. Longini, I. M., A. S. Monto, and J. S. Koopman. 1984. Statistical procedures for estimating the community probability of illness in family studies: rhinovirus and influenza. *Int J Epidemiol* 13: 99-106.
56. Viboud, C., W. J. Alonso, and L. Simonsen. 2006. Influenza in tropical regions. *PLoS Med* 3: e89.
57. Grijalva, C. G., A. S. Craig, W. D. Dupont, C. B. Bridges, S. J. Schrag, M. K. Iwane, W. Schaffner, K. M. Edwards, and M. R. Griffin. 2006. Estimating influenza hospitalizations among children. *Emerg Infect Dis* 12: 103-109.
58. Skehel, J. J., and D. C. Wiley. 2000. Receptor binding and membrane fusion in virus entry: the influenza hemagglutinin. *Annu Rev Biochem* 69: 531-569.
59. White, M. R., M. Doss, P. Boland, T. Tecle, and K. L. Hartshorn. 2008. Innate immunity to influenza virus: implications for future therapy. *Expert Rev Clin Immunol* 4: 497-514.
60. Johnson, N. P., and J. Mueller. 2002. Updating the accounts: global mortality of the 1918-1920 "Spanish" influenza pandemic. *Bull Hist Med* 76: 105-115.

61. Taubenberger, J. K., and D. M. Morens. 2006. 1918 Influenza: the mother of all pandemics. *Emerg Infect Dis* 12: 15-22.
62. Simonsen, L. 1999. The global impact of influenza on morbidity and mortality. *Vaccine* 17 Suppl 1: S3-10.
63. Morens, D. M., J. K. Taubenberger, and A. S. Fauci. 2008. Predominant role of bacterial pneumonia as a cause of death in pandemic influenza: implications for pandemic influenza preparedness. *J Infect Dis* 198: 962-970.
64. Brundage, J. F., and G. D. Shanks. 2008. Deaths from bacterial pneumonia during 1918-19 influenza pandemic. *Emerg Infect Dis* 14: 1193-1199.
65. Simonsen, L., M. J. Clarke, L. B. Schonberger, N. H. Arden, N. J. Cox, and K. Fukuda. 1998. Pandemic versus epidemic influenza mortality: a pattern of changing age distribution. *J Infect Dis* 178: 53-60.
66. Heikkinen, T., O. Ruuskanen, M. Waris, T. Ziegler, M. Arola, and P. Halonen. 1991. Influenza vaccination in the prevention of acute otitis media in children. *Am J Dis Child* 145: 445-448.
67. McCullers, J. A. 2006. Insights into the interaction between influenza virus and pneumococcus. *Clin Microbiol Rev* 19: 571-582.
68. McCullers, J. A. 2004. Effect of antiviral treatment on the outcome of secondary bacterial pneumonia after influenza. *J Infect Dis* 190: 519-526.
69. Spiller, S., G. Elson, R. Ferstl, S. Dreher, T. Mueller, M. Freudenberg, B. Daubeuf, H. Wagner, and C. J. Kirschning. 2008. TLR4-induced IFN-gamma production increases TLR2 sensitivity and drives Gram-negative sepsis in mice. *J Exp Med* 205: 1747-1754.
70. Pound, M. W., and D. B. May. 2005. Proposed mechanisms and preventative options of Jarisch-Herxheimer reactions. *J Clin Pharm Ther* 30: 291-295.
71. Glezen, W. P. 1982. Serious morbidity and mortality associated with influenza epidemics. *Epidemiol Rev* 4: 25-44.
72. Hament, J. M., J. L. Kimpen, A. Fleer, and T. F. Wolfs. 1999. Respiratory viral infection predisposing for bacterial disease: a concise review. *FEMS Immunol Med Microbiol* 26: 189-195.
73. Smith, M. W., J. E. Schmidt, J. E. Rehg, C. J. Orihuela, and J. A. McCullers. 2007. Induction of pro- and anti-inflammatory molecules in a mouse model of pneumococcal pneumonia after influenza. *Comp Med* 57: 82-89.
74. Lee, L. N., P. Dias, D. Han, S. Yoon, A. Shea, V. Zakharov, D. Parham, and S. R. Sarawar. 2010. A mouse model of lethal synergism between influenza virus and Haemophilus influenzae. *Am J Pathol* 176: 800-811.
75. Small, C. L., C. R. Shaler, S. McCormick, M. Jeyanathan, D. Damjanovic, E. G. Brown, P. Arck, M. Jordana, C. Kaushic, A. A. Ashkar, and Z. Xing. 2010. Influenza infection leads to increased susceptibility to subsequent bacterial superinfection by impairing NK cell responses in the lung. *J Immunol* 184: 2048-2056.

76. Alonso, J. M., A. Guiyoule, M. L. Zarantonelli, F. Ramisse, R. Pires, A. Antignac, A. E. Deghmane, M. Huerre, S. van der Werf, and M. K. Taha. 2003. A model of meningococcal bacteremia after respiratory superinfection in influenza A virus-infected mice. *FEMS Microbiol Lett* 222: 99-106.
77. Dinarello, C. A. 2009. Immunological and inflammatory functions of the interleukin-1 family. *Annu Rev Immunol* 27: 519-550.
78. Schroder, K., and J. Tschopp. 2010. The inflammasomes. *Cell* 140: 821-832.
79. Dunne, A., P. J. Ross, E. Pospisilova, J. Masin, A. Meaney, C. E. Sutton, Y. Iwakura, J. Tschopp, P. Sebo, and K. H. Mills. 2010. Inflammasome activation by adenylate cyclase toxin directs Th17 responses and protection against Bordetella pertussis. *J Immunol* 185: 1711-1719.
80. Netea, M. G., A. Simon, F. van de Veerdonk, B. J. Kullberg, J. W. Van der Meer, and L. A. Joosten. 2010. IL-1beta processing in host defense: beyond the inflammasomes. *PLoS Pathog* 6: e1000661.
81. Hartshorn, K. L., L. S. Liou, M. R. White, M. M. Kazhdan, J. L. Tauber, and A. I. Tauber. 1995. Neutrophil deactivation by influenza A virus. Role of hemagglutinin binding to specific sialic acid-bearing cellular proteins. *J Immunol* 154: 3952-3960.
82. Zhang, W. J., S. Sarawar, P. Nguyen, K. Daly, J. E. Rehg, P. C. Doherty, D. L. Woodland, and M. A. Blackman. 1996. Lethal synergism between influenza infection and staphylococcal enterotoxin B in mice. *J Immunol* 157: 5049-5060.
83. Muir, R., and G. H. Wilson. 1919. Observations ON INFLUENZA AND ITS COMPLICATIONS. *Br Med J* 1: 3-5.
84. MARTIN, C. M., C. M. KUNIN, L. S. GOTTLIEB, M. W. BARNES, C. LIU, and M. FINLAND. 1959. Asian influenza A in Boston, 1957-1958. I. Observations in thirty-two influenza-associated fatal cases. *AMA Arch Intern Med* 103: 515-531.
85. MARTIN, C. M., C. M. KUNIN, L. S. GOTTLIEB, and M. FINLAND. 1959. Asian influenza A in Boston, 1957-1958. II. Severe staphylococcal pneumonia complicating influenza. *AMA Arch Intern Med* 103: 532-542.
86. Avadhanula, V., C. A. Rodriguez, J. P. Devincenzo, Y. Wang, R. J. Webby, G. C. Ulett, and E. E. Adderson. 2006. Respiratory viruses augment the adhesion of bacterial pathogens to respiratory epithelium in a viral species- and cell type-dependent manner. *J Virol* 80: 1629-1636.
87. Didierlaurent, A., J. Goulding, S. Patel, R. Snelgrove, L. Low, M. Bebien, T. Lawrence, L. S. van Rijt, B. N. Lambrecht, J. C. Sirard, and T. Hussell. 2008. Sustained desensitization to bacterial Toll-like receptor ligands after resolution of respiratory influenza infection. *J Exp Med* 205: 323-329.
88. Jakab, G. J., and G. M. Green. 1976. Defect in intracellular killing of Staphylococcus aureus within alveolar macrophages in Sendai virus-infected murine lungs. *J Clin Invest* 57: 1533-1539.

89. Jakab, G. J., and G. M. Green. 1972. The effect of Sendai virus infection on bactericidal and transport mechanisms of the murine lung. *J Clin Invest* 51: 1989-1998.
90. Park, K., L. O. Bakaletz, J. M. Coticchia, and D. J. Lim. 1993. Effect of influenza A virus on ciliary activity and dye transport function in the chinchilla eustachian tube. *Ann Otol Rhinol Laryngol* 102: 551-558.
91. Kudva, A., E. V. Scheller, K. M. Robinson, C. R. Crowe, S. M. Choi, S. R. Slight, S. A. Khader, P. J. Dubin, R. I. Enelow, J. K. Kolls, and J. F. Alcorn. 2011. Influenza A inhibits Th17-mediated host defense against bacterial pneumonia in mice. *J Immunol* 186: 1666-1674.
92. Kandel, R., and K. L. Hartshorn. 2005. Novel strategies for prevention and treatment of influenza. *Expert Opin Ther Targets* 9: 1-22.
93. Mattoo, S., and J. D. Cherry. 2005. Molecular pathogenesis, epidemiology, and clinical manifestations of respiratory infections due to Bordetella pertussis and other Bordetella subspecies. *Clin Microbiol Rev* 18: 326-382.
94. Celentano, L. P., M. Massari, D. Paramatti, S. Salmaso, A. E. Tozzi, and E.-N. Group. 2005. Resurgence of pertussis in Europe. *Pediatr Infect Dis J* 24: 761-765.
95. Ichinohe T, L. H. K., Ogura Y, Flavell R, Iwasaki A. 2009. Inflammasome recognition of influenza virus is essential for adaptive immune responses. *J.Exp. Med.* 206: 79-87.
96. Kozak, W., H. Zheng, C. A. Conn, D. Soszynski, L. H. van der Ploeg, and M. J. Kluger. 1995. Thermal and behavioral effects of lipopolysaccharide and influenza in interleukin-1 beta-deficient mice. *Am J Physiol* 269: R969-977.
97. Horino, T., T. Matsumoto, M. Uramatsu, M. Tanabe, K. Tateda, S. Miyazaki, A. Nakane, Y. Iwakura, and K. Yamaguchi. 2005. Interleukin-1-deficient mice exhibit high sensitivity to gut-derived sepsis caused by Pseudomonas aeruginosa. *Cytokine* 30: 339-346.
98. Mizgerd, J. P., M. M. Lupa, J. Hjoberg, J. C. Vallone, H. B. Warren, J. P. Butler, and E. S. Silverman. 2004. Roles for early response cytokines during Escherichia coli pneumonia revealed by mice with combined deficiencies of all signaling receptors for TNF and IL-1. *Am J Physiol Lung Cell Mol Physiol* 286: L1302-1310.
99. van Rossum, A. M., E. S. Lysenko, and J. N. Weiser. 2005. Host and bacterial factors contributing to the clearance of colonization by Streptococcus pneumoniae in a murine model. *Infect Immun* 73: 7718-7726.
100. van der Poll, T., and S. J. van Deventer. 1999. Cytokines and anticytokines in the pathogenesis of sepsis. *Infect Dis Clin North Am* 13: 413-426, ix.
101. Si-Tahar, M., L. Touqui, and M. Chignard. 2009. Innate immunity and inflammation--two facets of the same anti-infectious reaction. *Clin Exp Immunol* 156: 194-198.

102. Brown, E. G., and J. E. Bailly. 1999. Genetic analysis of mouse-adapted influenza A virus identifies roles for the NA, PB1, and PB2 genes in virulence. *Virus Res* 61: 63-76.
103. Robbins, C. S., C. M. Bauer, N. Vujicic, G. J. Gaschler, B. D. Lichty, E. G. Brown, and M. R. Stämpfli. 2006. Cigarette smoke impacts immune inflammatory responses to influenza in mice. *Am J Respir Crit Care Med* 174: 1342-1351.
104. Parkhill, J., M. Sebaihia, A. Preston, L. D. Murphy, N. Thomson, D. E. Harris, M. T. Holden, C. M. Churcher, S. D. Bentley, K. L. Mungall, A. M. Cerdeño-Tárraga, L. Temple, K. James, B. Harris, M. A. Quail, M. Achtman, R. Atkin, S. Baker, D. Basham, N. Bason, I. Cherevach, T. Chillingworth, M. Collins, A. Cronin, P. Davis, J. Doggett, T. Feltwell, A. Goble, N. Hamlin, H. Hauser, S. Holroyd, K. Jagels, S. Leather, S. Moule, H. Norberczak, S. O'Neil, D. Ormond, C. Price, E. Rabbinowitsch, S. Rutter, M. Sanders, D. Saunders, K. Seeger, S. Sharp, M. Simmonds, J. Skelton, R. Squares, S. Squares, K. Stevens, L. Unwin, S. Whitehead, B. G. Barrell, and D. J. Maskell. 2003. Comparative analysis of the genome sequences of Bordetella pertussis, Bordetella parapertussis and Bordetella bronchiseptica. *Nat Genet* 35: 32-40.
105. Heininger, U., P. A. Cotter, H. W. Fescemyer, G. Martinez de Tejada, M. H. Yuk, J. F. Miller, and E. T. Harvill. 2002. Comparative phenotypic analysis of the Bordetella parapertussis isolate chosen for genomic sequencing. *Infect Immun* 70: 3777-3784.
106. Wolfe, D. N., G. S. Kirimanjeswara, and E. T. Harvill. 2005. Clearance of Bordetella parapertussis from the lower respiratory tract requires humoral and cellular immunity. *Infect Immun* 73: 6508-6513.
107. Stainer, D. W., and M. J. Scholte. 1970. A simple chemically defined medium for the production of phase I Bordetella pertussis. *J Gen Microbiol* 63: 211-220.
108. Lappalainen, U., J. A. Whitsett, S. E. Wert, J. W. Tichelaar, and K. Bry. 2005. Interleukin-1beta causes pulmonary inflammation, emphysema, and airway remodeling in the adult murine lung. *Am J Respir Cell Mol Biol* 32: 311-318.
109. Hussell, T., E. Wissinger, and J. Goulding. 2009. Bacterial complications during pandemic influenza infection. *Future Microbiol* 4: 269-272.
110. McCullers, J. A., and J. E. Rehg. 2002. Lethal synergism between influenza virus and Streptococcus pneumoniae: characterization of a mouse model and the role of platelet-activating factor receptor. *J Infect Dis* 186: 341-350.
111. McNamee, L. A., and A. G. Harmsen. 2006. Both influenza-induced neutrophil dysfunction and neutrophil-independent mechanisms contribute to increased susceptibility to a secondary Streptococcus pneumoniae infection. *Infect Immun* 74: 6707-6721.
112. Sun, K., and D. W. Metzger. 2008. Inhibition of pulmonary antibacterial defense by interferon-gamma during recovery from influenza infection. *Nat Med* 14: 558-564.

113. van der Sluijs, K. F., L. J. van Elden, M. Nijhuis, R. Schuurman, J. M. Pater, S. Florquin, M. Goldman, H. M. Jansen, R. Lutter, and T. van der Poll. 2004. IL-10 is an important mediator of the enhanced susceptibility to pneumococcal pneumonia after influenza infection. *J Immunol* 172: 7603-7609.
114. Bouvier, N. M., and A. C. Lowen. 2010. Animal Models for Influenza Virus Pathogenesis and Transmission. *Viruses* 2: 1530-1563.
115. Franchi, L., N. Warner, K. Viani, and G. Nuñez. 2009. Function of Nod-like receptors in microbial recognition and host defense. *Immunol Rev* 227: 106-128.
116. Franchi, L., R. Muñoz-Planillo, and G. Núñez. 2012. Sensing and reacting to microbes through the inflammasomes. *Nat Immunol* 13: 325-332.
117. Guma, M., L. Ronacher, R. Liu-Bryan, S. Takai, M. Karin, and M. Corr. 2009. Caspase 1-independent activation of interleukin-1beta in neutrophil-predominant inflammation. *Arthritis Rheum* 60: 3642-3650.
118. Joosten, L. A., M. G. Netea, G. Fantuzzi, M. I. Koenders, M. M. Helsen, H. Sparrer, C. T. Pham, J. W. van der Meer, C. A. Dinarello, and W. B. van den Berg. 2009. Inflammatory arthritis in caspase 1 gene-deficient mice: contribution of proteinase 3 to caspase 1-independent production of bioactive interleukin-1beta. *Arthritis Rheum* 60: 3651-3662.
119. Kawasaki, Y., Z. Z. Xu, X. Wang, J. Y. Park, Z. Y. Zhuang, P. H. Tan, Y. J. Gao, K. Roy, G. Corfas, E. H. Lo, and R. R. Ji. 2008. Distinct roles of matrix metalloproteases in the early- and late-phase development of neuropathic pain. *Nat Med* 14: 331-336.
120. Greten, F. R., M. C. Arkan, J. Bollrath, L. C. Hsu, J. Goode, C. Miething, S. I. Göktuna, M. Neuenhahn, J. Fierer, S. Paxian, N. Van Rooijen, Y. Xu, T. O'Cain, B. B. Jaffee, D. H. Busch, J. Duyster, R. M. Schmid, L. Eckmann, and M. Karin. 2007. NF-kappaB is a negative regulator of IL-1beta secretion as revealed by genetic and pharmacological inhibition of IKKbeta. *Cell* 130: 918-931.
121. Watkins, L. R., M. K. Hansen, K. T. Nguyen, J. E. Lee, and S. F. Maier. 1999. Dynamic regulation of the proinflammatory cytokine, interleukin-1beta: molecular biology for non-molecular biologists. *Life Sci* 65: 449-481.
122. Davis, B. K., H. Wen, and J. P. Ting. 2011. The inflammasome NLRs in immunity, inflammation, and associated diseases. *Annu Rev Immunol* 29: 707-735.
123. Yu, X., T. Tsibane, P. A. McGraw, F. S. House, C. J. Keefer, M. D. Hicar, T. M. Tumpey, C. Pappas, L. A. Perrone, O. Martinez, J. Stevens, I. A. Wilson, P. V. Aguilar, E. L. Altschuler, C. F. Basler, and J. E. Crowe. 2008. Neutralizing antibodies derived from the B cells of 1918 influenza pandemic survivors. *Nature* 455: 532-536.
124. Dinarello, C. A. 2011. Blocking interleukin-1β in acute and chronic autoinflammatory diseases. *J Intern Med* 269: 16-28.
125. Feist, E., and G. R. Burmester. 2010. Canakinumab for treatment of cryopyrin-associated periodic syndrome. *Expert Opin Biol Ther* 10: 1631-1636.

126. McAuley, J. L., F. Hornung, K. L. Boyd, A. M. Smith, R. McKeon, J. Bennink, J. W. Yewdell, and J. A. McCullers. 2007. Expression of the 1918 influenza A virus PB1-F2 enhances the pathogenesis of viral and secondary bacterial pneumonia. *Cell Host Microbe* 2: 240-249.
127. Ramphal, R., W. Fischlschweiger, J. W. Shands, and P. A. Small. 1979. Murine influenzal tracheitis: a model for the study of influenza and tracheal epithelial repair. *Am Rev Respir Dis* 120: 1313-1324.
128. Plotkowski, M. C., E. Puchelle, G. Beck, J. Jacquot, and C. Hannoun. 1986. Adherence of type I Streptococcus pneumoniae to tracheal epithelium of mice infected with influenza A/PR8 virus. *Am Rev Respir Dis* 134: 1040-1044.
129. Pittet, L. A., L. Hall-Stoodley, M. R. Rutkowski, and A. G. Harmsen. 2010. Influenza virus infection decreases tracheal mucociliary velocity and clearance of Streptococcus pneumoniae. *Am J Respir Cell Mol Biol* 42: 450-460.
130. LeVine, A. M., V. Koeningsknecht, and J. M. Stark. 2001. Decreased pulmonary clearance of S. pneumoniae following influenza A infection in mice. *J Virol Methods* 94: 173-186.
131. Seki, M., Y. Higashiyama, K. Tomono, K. Yanagihara, H. Ohno, Y. Kaneko, K. Izumikawa, Y. Miyazaki, Y. Hirakata, Y. Mizuta, T. Tashiro, and S. Kohno. 2004. Acute infection with influenza virus enhances susceptibility to fatal pneumonia following Streptococcus pneumoniae infection in mice with chronic pulmonary colonization with Pseudomonas aeruginosa. *Clin Exp Immunol* 137: 35-40.
132. Engelich, G., M. White, and K. L. Hartshorn. 2001. Neutrophil survival is markedly reduced by incubation with influenza virus and Streptococcus pneumoniae: role of respiratory burst. *J Leukoc Biol* 69: 50-56.
133. Hashimoto, Y., T. Moki, T. Takizawa, A. Shiratsuchi, and Y. Nakanishi. 2007. Evidence for phagocytosis of influenza virus-infected, apoptotic cells by neutrophils and macrophages in mice. *J Immunol* 178: 2448-2457.
134. Shahangian, A., E. K. Chow, X. Tian, J. R. Kang, A. Ghaffari, S. Y. Liu, J. A. Belperio, G. Cheng, and J. C. Deng. 2009. Type I IFNs mediate development of postinfluenza bacterial pneumonia in mice. *J Clin Invest* 119: 1910-1920.
135. Speshock, J. L., N. Doyon-Reale, R. Rabah, M. N. Neely, and P. C. Roberts. 2007. Filamentous influenza A virus infection predisposes mice to fatal septicemia following superinfection with Streptococcus pneumoniae serotype 3. *Infect Immun* 75: 3102-3111.
136. Wolfe, D. N., A. T. Karanikas, S. E. Hester, M. J. Kennett, and E. T. Harvill. 2010. IL-10 induction by Bordetella parapertussis limits a protective IFN-gamma response. *J Immunol* 184: 1392-1400.
137. Haye, K., S. Burmakina, T. Moran, A. García-Sastre, and A. Fernandez-Sesma. 2009. The NS1 protein of a human influenza virus inhibits type I interferon production and the induction of antiviral responses in primary human dendritic and respiratory epithelial cells. *J Virol* 83: 6849-6862.

138. Gaffen, S. L. 2008. An overview of IL-17 function and signaling. *Cytokine* 43: 402-407.
139. Littman, D. R., and A. Y. Rudensky. 2010. Th17 and regulatory T cells in mediating and restraining inflammation. *Cell* 140: 845-858.
140. Tilg, H., A. R. Moschen, and A. Kaser. 2009. Suppression of interleukin-17 by type I interferons: a contributing factor in virus-induced immunosuppression? *Eur Cytokine Netw* 20: 1-6.
141. Karlström, A., S. M. Heston, K. L. Boyd, E. I. Tuomanen, and J. A. McCullers. 2011. Toll-like receptor 2 mediates fatal immunopathology in mice during treatment of secondary pneumococcal pneumonia following influenza. *J Infect Dis* 204: 1358-1366.